

Serum Albumin Hydrogels

Characterization of Their Self-Assembled Structures, Nanoscopic and Macroscopic Properties

Dissertation

zur Erlangung des Doktorgrades der Naturwissenschaften
(Dr. rer. nat.)

Der

Naturwissenschaftlichen Fakultät II
Chemie, Physik und Mathematik

der Martin-Luther-Universität
Halle-Wittenberg

vorgelegt von

Herrn Seyed Hamidreza Arabi

Betreuer: Prof. Dr. Dariush Hinderberger

Gutachter:


Prof. Dr. Dariush Hinderberger

Prof. Dr. Oliver Ernst, Toronto

30.04.2024

Contents

1 Introduction and Objectives	5
2 Rheological Characterization and Viscoelasticity	7
2.1 Objectives:.....	7
2.2 Linear Viscoelastic Behaviour	7
2.2.1 Viscoelasticity.....	7
2.2.2 Linear Viscoelastic Behaviour	8
2.2.3 Mechanical Models	9
2.2.3.1 The Kelvin or Voigt Model	10
2.2.3.2 The Maxwell Model	11
2.3 Dynamical Mechanical Measurements: The Complex Modulus and Complex Compliance....	13
3 Principal Component Analysis (PCA)	16
3.1 Objectives:.....	16
3.2 Maximum Variance Perspective	17
3.2.1 M-dimensional Subspace with Maximal Variance	19
3.3 Projection Perspective	20
3.4 Practical Aspects.....	22
4 Continuous Wave Electron Paramagnetic Resonance Spectroscopy (CW EPR)	22
4.1 Objectives:.....	22
4.2 CW EPR spectroscopy in Theory:	23
4.2.1 Electron spin and resonance condition	23
4.2.2 Relaxation Processes.....	26
4.2.3 The Nuclear Zeeman Interaction and Hyperfine Coupling	27
4.2.4 Physical State of the Sample.....	31
5 Abstract: The Thesis Objective	32
5.1 Motivation and Concept:	32
6 Contribution Statements	38
6.1 Publication A: Publication in Biomaterials Science (2018), vol. 6, 478-492	38
6.2 Publication B: Publication in MDPI Molecules (2020), vol. 25, 1927.....	38
6.3 Publication C: Publication in Protein Science (2020), vol. 29, 2459-2467 73	38
7 Appendix: Publications	39

7.1 Publication A: Publication in Biomaterials Science (2018), vol. 6, 478-492	39
Introduction	41
Materials and methods	43
Conclusions	57
Conflicts of interest.....	57
Acknowledgements	57
References	57
7.2 Publication B: Publication in MDPI Molecules (2020), vol. 25, 1927	61
<i>Communication</i>	61
Seyed Hamidreza Arabi  , David Haselberger and Dariush Hinderberger * 	61
1. Introduction	61
2. Results	62
2.1. General Gelation Properties	63
2.2. Rheological Characterization	64
2.3. Infrared Spectroscopy (IR)	65
2.4. Electron Paramagnetic Resonance (EPR) Spectroscopy	66
3. Discussion.....	67
4. Materials and Methods.....	68
4.1. Materials and Gel Preparation.....	68
4.2. Gel Formation	68
4.3. Loading Stearic Acid (SA) into Gels	69
4.4. Rheology	69
4.5. Infrared Spectroscopy (IR)	69
4.6. Electron Paramagnetic Resonance (EPR) Spectroscopy	69
Appendix A.....	70
References	75
7.3 Publication C: Publication in Protein Science (2020), vol. 29, 2459-2467	76
Seyed Hamidreza Arabi Behdad Aghelnejad ² Jonas Volmer ¹ Dariush Hinderberger ¹	76
1 INTRODUCTION	78
2 RESULTS AND DISCUSSION.....	79
3 CONCLUSIONS	86
4 MATERIALS AND METHODS	87

ACKNOWLEDGMENTS.....	87
AUTHOR CONTRIBUTIONS	87
ORCID.....	88
REFERENCES.....	88
SUPPORTING INFORMATION	89
8 References	90
9 Eidesstattliche Erklärung.....	92

1 | Introduction and Objectives

In recent years there has been revolutionary advances in the fields of structured and intelligent materials science and nanomaterials properties [1]. Beside the variety of chemical structures, the power of precise control of the molecular architecture and morphology, paved the road of utilization of polymers in high-technology and biological and medical applications [1]. The need to improve patient care has always been a challenging task in medical diagnostics and therapeutics; hence, there is a continuous effort to enhance methods, materials, and devices. The development of novel biomaterials and their application to medical problems have shown great potential in the treatment of many diseases [2].

Despite the extensive use of materials in medicine, many biomaterials lack the desired functional properties to be associated with biological systems and have not been engineered for optimized performance. Consequently, there is an increasing need to develop new materials to address such problems in medicine and biology. Hydrogels, are a class of biomaterials that have demonstrated new possibilities for biological and medical applications [2].

Hydrogels are cross-linked networks made up of hydrophilic polymers, capable of retaining large amounts of water but yet remaining insoluble and maintaining their three-dimensional structures. The reason behind this insolubility is that the polymer is physically and/or chemically cross-linked [3-5].

Due to their unique biocompatibility, various methods of synthesis and desirable physical characteristics, hydrogels are good candidates and have been the material of choice for different tasks in medical applications. Furthermore, hydrogels mimic native tissue microenvironment due to their porous and hydrated molecular structure [6, 7]. Their high water content and soft nature make them similar to natural extracellular matrices and minimize tissue irritation and cell adherence [8]. In addition, their capacity to embed biologically active agents in their water-swollen network makes them very attractive for controlled release of therapeutics [9].

Serum Albumin, the most abundant plasma protein in mammals with the concentration of 40 to 50 mg.ml⁻¹ in plasma, is a versatile and easily obtainable biomaterial. It is temperature and pH responsive, dissolvable in high concentrations and gels readily in well-defined conditions. This flexibility, together with its inexpensiveness and biocompatibility, makes albumin an attractive biomaterial for biomedical research and therapeutics [10-12].

Serum albumin serves as a transporting agent for various endogenous compounds and drug molecules. Its capability to bind and transport multiple fatty acids (FA), in particular, has been studied extensively in the past [13, 14]. Human serum albumin (HSA) is a 66.5 kDa (585 amino acids) heliocidal protein, consisting of three structurally similar domains I, II, and III), each of them formed by two subdomains (A and B) [15]. It represents about 60 % of the total protein content in the blood serum [15]. HSA has the ability to bind insoluble substances such as fatty acids, porphyrins, and a wide variety of drugs. The pharmacokinetics and pharmacodynamics of any drug is strongly dependent on its interaction with HSA [16, 17]. Our model proteins are both Bovine Serum Albumin (BSA) and HSA. Both albumins share 76% sequence homology [18].

To obtain hydrogels from albumin different synthesis methods have been developed [19, 20]. Moreover, there are different techniques to study different characteristics of these gels. Figure 1 illustrates the various methods and tools used in this research.

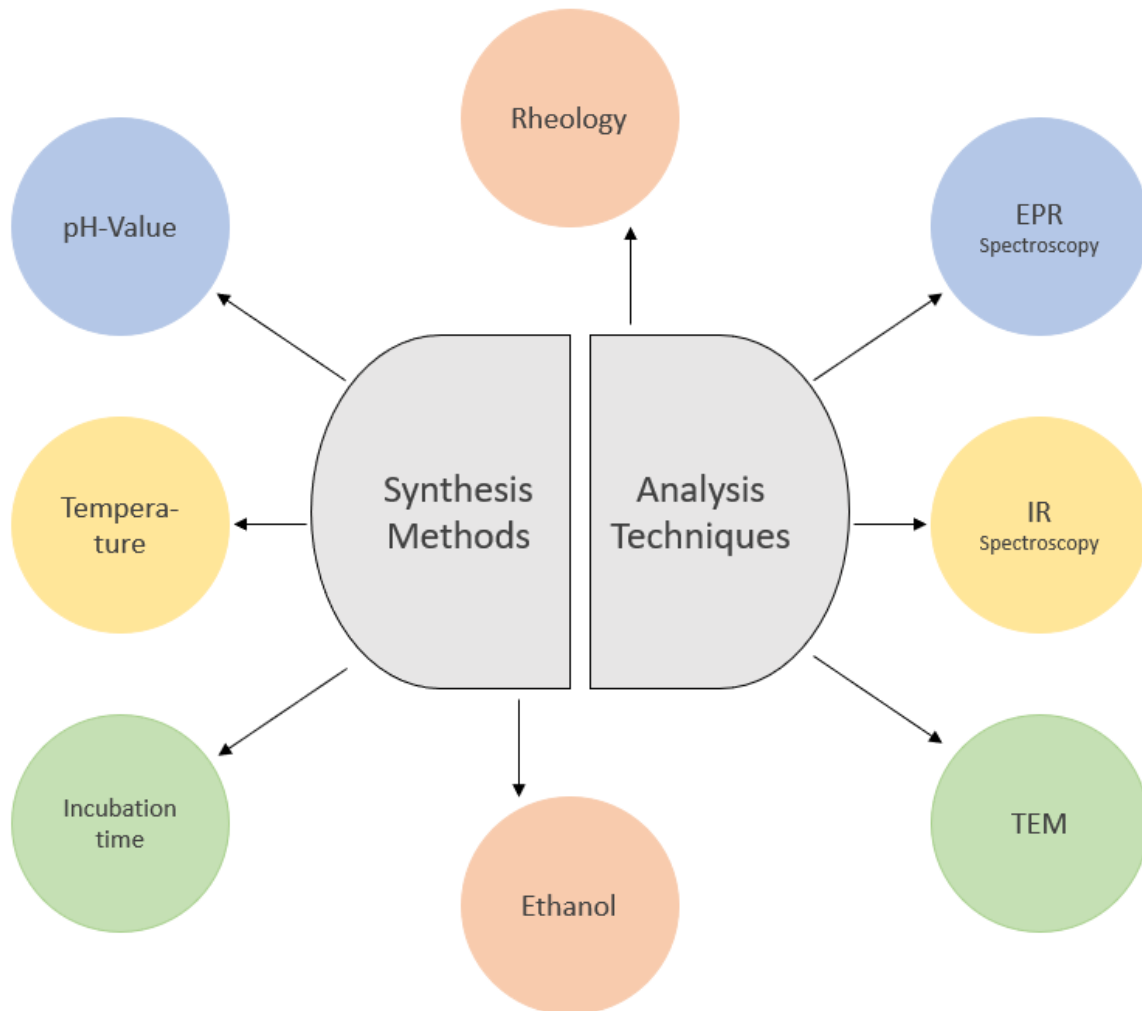


Figure 1: Different synthesis methods and techniques to obtain and study hydrogels from serum albumin.

2 | Rheological Characterization and Viscoelasticity

2.1 Objectives:

The main two inter-related goals of the discussions of the mechanical properties of polymeric materials are [21]:

1. to obtain an adequate macroscopic description of the specific facet of polymer behaviour under consideration.
2. To seek an explanation of this behaviour in molecular terms, which may include details of the chemical composition and physical structure.

2.2 Linear Viscoelastic Behaviour

2.2.1 Viscoelasticity

The behaviour of materials is usually discussed in terms of two main types of ideal material: the elastic solid and the viscous liquid [21].

- Elastic solid
 - Has a definite shape and deforms under external forces
 - Stores all energy that is obtained from external forces
 - Stored energy restores the original shape once the force is removed
- Viscous liquid
 - No definite shape
 - Flows irreversibly under the action of external forces

One of the most fascinating features of polymers is that a given polymer can exhibit all the intermediate range of properties between an elastic solid and a viscous liquid depending on the temperature and the experimentally chosen timescale [22]. Material response which combines both liquid and solid like features is termed viscoelasticity, it implies that the mechanical properties are a

function of time due to intrinsic nature of the material and material possess a memory (fading) of past events [22].

2.2.2 Linear Viscoelastic Behaviour

Mechanical behaviour is, in most general terms, defined as the deformations which occur under loading. In a more specific case, the deformations is dependent on details such as the geometrical shape of the specimen or the way in which the load is applied [22]. One of the simplest constitutive relations is Hooke's law, which illustrate the relation between the stress σ to the strain e for the uniaxial deformation of an ideal elastic isotropic solid [23].

Equation (1)

$$\sigma = Ee$$

Where E is the Young's modulus. For elastic behaviour $(\sigma_{xy})E = Ge_{xy}$, where G is the shear modulus.

On the other hand, Newton's law of viscosity defines viscosity η as:

Equation (2)¹

$$\sigma = \eta \frac{\partial V}{\partial y}$$

Where σ is stress, V is the velocity, and y is the direction of the velocity gradient.

Hooke's law describes the behaviour of a linear elastic solid and Newton's law that of a linear viscous liquid. It can be deduced that the shear stress σ is directly proportional to the rate of change of shear strain with time. This formulation makes the analogy between Hooke's law for elastic solids and Newton's law for viscous liquids apparent. In the former, the stress is linearly related to the strain, in the latter the stress is linearly related to the strain rate.

A simple constitutive relation for the behaviour of a linear viscoelastic solid is obtained by combining these two laws.

Equation (3)

$$\sigma_{xy} = Ge_{xy} + \eta \frac{\partial e_{xy}}{\partial t}$$

1. For velocity gradient in xy plane:

$$\sigma_{xy} = \eta \left(\frac{\partial V_x}{\partial y} + \frac{\partial V_y}{\partial x} \right)$$

$$V_x = \frac{\partial u}{\partial y} \quad V_y = \frac{\partial v}{\partial x}$$

$$\sigma_{xy} = \eta \left[\frac{\partial}{\partial t} \left(\frac{\partial u}{\partial y} + \frac{\partial v}{\partial x} \right) \right]$$

$$\sigma_{xy} = \eta \frac{\partial e_{xy}}{\partial t}$$

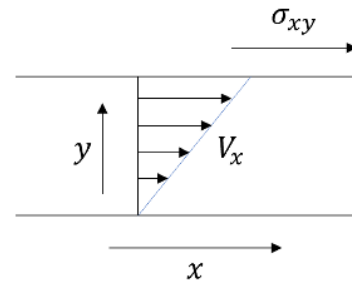


Figure 2: The velocity gradient.

The Equation (3) represents the Kelvin or Voigt model for linear viscoelastic solid [21]. Two main phenomena observed in materials as a result of viscoelastic deformation are [24]:

1. Creep
2. Stress Relaxation

Creep displays the tendency of a solid material to move slowly or deform under the influence of mechanical stresses [24]. It Occurs as a result of long-term exposure to high levels of stress that are still below the yield strength of the material. On the other hand, Stress relaxation is a time-dependent decrease in stress under a constant strain. For a linear viscoelastic solid, the instantaneous stress will be proportional to applied strain and will decrease with time [24].

2.2.3 Mechanical Models

Viscoelastic behaviour can be described by mechanical models constructed using elastic springs obeying Hooke's law and viscous dashpots obeying Newton's law of viscosity. By an arrangement of the element's spring, dashpot, and an element for friction, nearly all polymers can be modelled. The arrangement of these elements is based on a serial or parallel connection or a combination of these [22, 25].

Elastic springs follow Hooke's law:

$$\sigma = Ee$$



Figure 3: Elastic spring.

Viscous dashpots follow Newton’s law of viscosity:

$$\sigma_{xy} = \eta \frac{\partial e_{xy}}{\partial t}$$



Figure 4: Viscous dashpot.

2.2.3.1 The Kelvin or Voigt Model

This model (illustrated in Figure 5a) consists of a spring of modulus E_K , in parallel with a dashpot of viscosity η_K . If a constant stress σ is applied at time $t = 0$, there can be no instantaneous extension of the spring, since it is the dashpot which prevents it. Deformation then occurs at a changing rate, with the stress shared between the two components until, after a time dependent on the dashpot viscosity, the spring reaches a finite maximum extension. By removing the stress the reverse process occurs: there is no instantaneous retraction, but the initial unstretched length is eventually recovered (Figure 5.b).

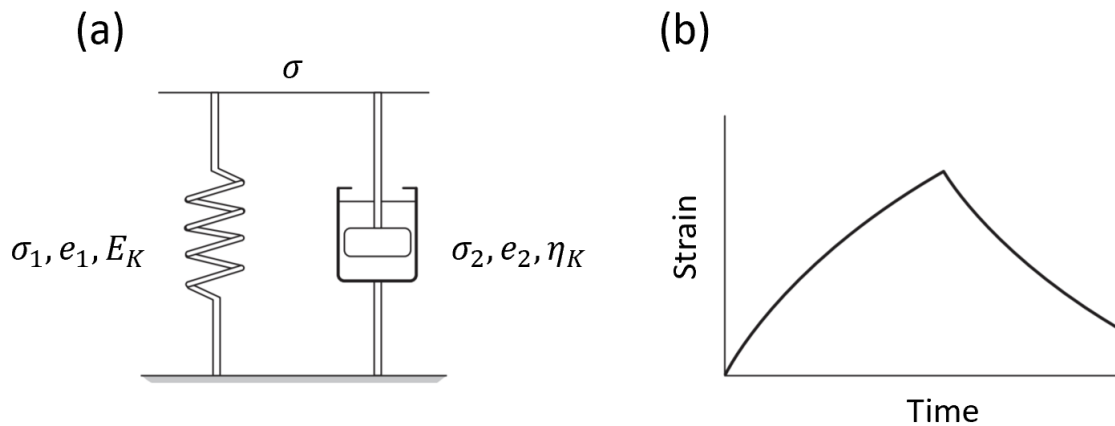


Figure 5: (a) The Kelvin, or Voigt, unit; (b) creep and recovery behaviour.

The model represents the time-dependent component of creep to a first approximation [25]. The stress–strain relations are, for the spring, $\sigma_1 = E_K e_1$ and for the dashpot $\sigma_2 = \eta_K \frac{de_2}{dt}$. The total stress σ is shared between spring and dashpot: $\sigma = \sigma_1 + \sigma_2$; but the strain in each component is the total strain: $e = e_1 = e_2$.

Equation (4)

$$\sigma = E_K e + \eta_K \frac{de}{dt}$$

Solving for $0 < t < t_1$, when the stress is σ

$$\frac{E_K}{\eta_K} \int_0^t dt = \int_0^e \frac{de}{\sigma/E_K - 1}$$

where η_K/E_K has the dimensions of time, and represents the rate at which the deformation occurs: it is the retardation time τ' . Hereafter by integration

$$\frac{t}{\tau'} = \ln \left(\frac{\sigma/E_K}{\sigma/E_K - 1} \right)$$

Giving

$$\frac{\sigma}{E_K} = \left(\frac{\sigma}{E_K} - e \right) \exp \left(\frac{t}{\tau'} \right)$$

By rearranging

Equation (5)

$$e = \frac{\sigma}{E_K} \left[1 - \exp \left(\frac{-t}{\tau'} \right) \right]$$

The main limitation of Kelvin model is that it is unable to describe stress relaxation.

2.2.3.2 The Maxwell Model

The Maxwell model consists of a spring and dashpot in series as shown in Figure 6(a). The equations for the stress-strain relations are $\sigma_1 = E_m e_1$ relating the stress σ_1 and the strain e_1 in the spring, and $\sigma_2 = \eta_m \frac{de_2}{dt}$ relating the stress σ_2 and the strain e_2 in the dashpot. Since the stress is identical for the spring and the dashpot, the total stress $\sigma = \sigma_1 = \sigma_2$. The total strain e is the sum of the strain in the spring and the dashpot, that is $e = e_1 + e_2$ [21].

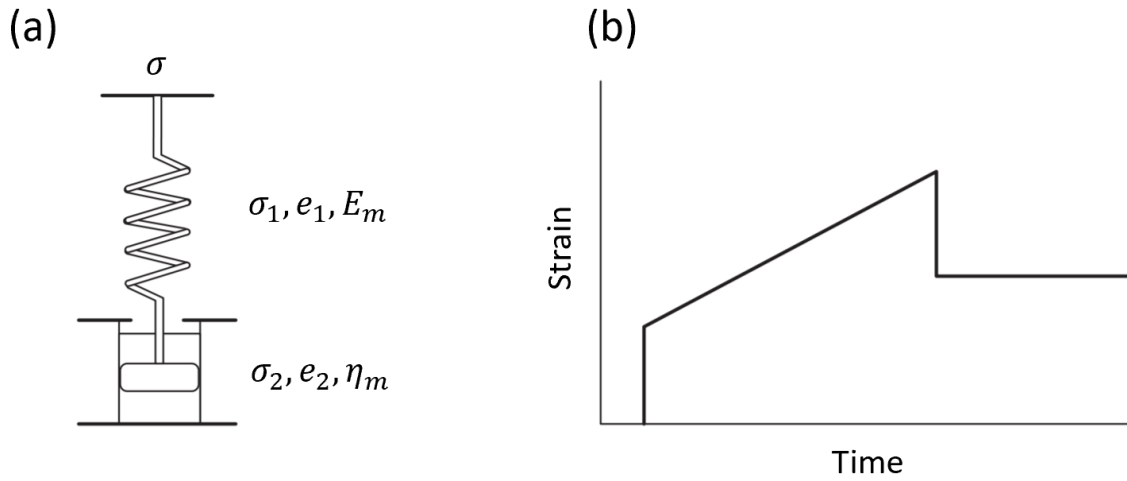


Figure 6: (a) The Maxwell unit and (b) creep and recovery behaviour

Stress can be written as $\sigma_1 = E_m e_1 \rightarrow \frac{d\sigma_1}{dt} = E_m \frac{de_1}{dt}$

Equation (6)

$$\frac{d\sigma_1}{dt} = E_m \frac{de_1}{dt}$$

Hence, total strain rate

Equation (7)

$$\frac{de}{dt} = \frac{1}{E_m} \frac{d\sigma}{dt} + \frac{\sigma}{\eta_m}$$

The Maxwell model is of great importance in considering a stress relaxation experiment [22]. In this case,

$$\frac{de}{dt} = 0 \rightarrow \frac{1}{E_m} \frac{d\sigma}{dt} + \frac{\sigma}{\eta_m} = 0$$

Thus,

$$\frac{d\sigma}{dt} = -E_m \frac{\sigma}{\eta_m}$$

At time $t = 0$, $\sigma = \sigma_0$, the initial stress, and integrating results in:

Equation (8)

$$\sigma = \sigma_0 \exp\left(\frac{-E_m}{\eta_m}t\right)$$

This equation shows that the stress decays exponentially with a characteristic time constant

$$\tau = \frac{\eta_m}{E_m}$$

where τ is called the “relaxation time” [21]. Equation (8) can be written as:

$$\sigma = \sigma_0 \exp\left(\frac{-t}{\tau}\right)$$

Limitations of Maxwell model [22]:

- Under constant stress (creep)

$$\frac{d\sigma}{dt} = 0 \rightarrow \frac{de}{dt} = \frac{\sigma}{\eta_m}$$

where Newtonian flow is observed which is generally not true for viscoelastic materials.

- Stress relaxation behaviour cannot be usually represented by a single exponential decay term

2.3 Dynamical Mechanical Measurements: The Complex Modulus and Complex Compliance

An alternative experimental procedure to investigate creep and stress relaxation is to subject the specimen to an alternating strain and simultaneously measure the stress [22]. For linear viscoelastic behaviour, when equilibrium is reached, both stress and strain will fluctuate sinusoidally; however,

the strain lags behind the stress [22]. To characterise the viscoelastic behaviour, material is sinusoidally deformed and resulting stress is recorded:

Equation (9)

$$\text{strain: } e = e_0 \sin(\omega t)$$

Equation (10)

$$\text{stress: } \sigma = \sigma_0 \sin(\omega t + \delta)$$

where ω is the angular frequency and δ is the phase lag.

For an ideal elastic material, stress and strain are in phase i.e. phase shift $\delta = 0$ and for an ideal viscous material, stress and strain are 90° out of phase $\delta = 90$ [21]. So stress can be written as:

Equation (11)

$$\sigma = \sigma_0 \cos(\delta) \sin(\omega t) + \sigma_0 \sin(\delta) \cos(\omega t)$$

For viscoelastic material, stress has two components [22]:

First of magnitude $\sigma_0 \cos(\delta)$ in phase with strain

Second of magnitude $\sigma_0 \sin(\delta)$ which is 90° out of phase with strain

The stress-strain relationship can therefore be defined by a quantity G' in phase with the strain and by a quantity G'' 90° out of phase with the strain, i.e.

Equation (12)

$$\sigma = e_0 G' \sin(\omega t) + e_0 G'' \cos(\omega t)$$

where

$$G' = \frac{\sigma_0}{e_0} \cos(\delta) \quad \text{and} \quad G'' = \frac{\sigma_0}{e_0} \sin(\delta)$$

A phasor diagram indicates that G' and G'' define a complex modulus G^* , shown in Figure (7).

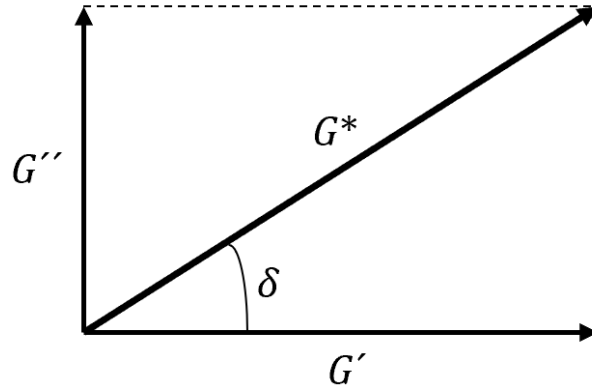


Figure 7: Phasor diagram for complex modulus $G^* = G' + iG''$.

If $e = e_0 \exp(i\omega t)$ and $\sigma = \sigma_0 \exp[i(\omega t + \delta)]$, thus:

Equation (13)

$$G^* = \frac{\sigma}{e} = \frac{\sigma_0}{e_0} \exp(i\delta) = \frac{\sigma_0}{e_0} (\cos\delta + i \sin\delta) = G' + iG''$$

where G' , which is in phase with the strain, is called the **storage modulus** since it defines the energy stored in the specimen due to the applied strain, and G'' , which is 90° out of phase with the strain, defines the dissipation of energy and is called the **loss modulus** [22].

To calculate the energy dissipated per cycle, ΔE :

Equation (14)

$$\Delta E = \oint \sigma de = \int_0^{2\pi/\omega} \sigma \frac{de}{dt} dt$$

Substituting for σ and e ,

Equation (15)

$$\Delta E = \omega e_0^2 \int_0^{2\pi/\omega} (G' \sin(\omega t) \cos(\omega t) + G'' \cos^2(\omega t)) dt$$

The integral is solved by using $\sin(\omega t) \cos(\omega t) = \frac{1}{2} \sin(2\omega t)$ and $\cos^2(\omega t) = \frac{1}{2}(1 + \cos 2\omega t)$ to give:

Equation (16)

$$\Delta E = \pi G'' e_0^2$$

If integral for ΔE is evaluated over a quarter cycle rather than over the complete period, the first term

$$G' \omega e_0^2 \int_0^{2\pi/\omega} \sin(\omega t) \cos(\omega t) dt$$

gives the maximum stored elastic energy, E , $E = \frac{1}{2} G' e_0^2$

The ratio of loss modulus to storage modulus can be written as:

Equation (17)

$$\frac{G''}{G'} = \tan \delta = \frac{\Delta E}{2\pi E}$$

Where ΔE is energy dissipated per cycle and E is maximum stored elastic energy [22]

3 | Principal Component Analysis (PCA)

3.1 Objectives:

Analyzing high-dimensional data, such as wide range spectra of an IR measurement, comes with some difficulties and data interpretation is difficult is nearly impossible. However, high-dimensional data often has properties that we can exploit. For example, high-dimensional

data is often overcomplete, i.e., many dimensions are redundant and can be explained by a combination of other dimensions. Furthermore, dimensions in high-dimensional data are often correlated so that the data possesses an intrinsic lower-dimensional structure. Dimensionality reduction exploits structure and correlation and allows us to work with a more compact representation of the data, ideally without losing information. We can think of dimensionality reduction as a compression technique [26].

Principal Component Analysis (PCA) is an algorithm for linear dimensionality reduction. PCA is one of the most commonly used techniques for data compression and data visualization. It is also used for the identification of simple patterns, latent factors, and structures of high-dimensional data [27]. In PCA, we are interested in finding projections \tilde{x}_n of data points x_n that are as similar to the original data points as possible, but which have a significantly lower intrinsic dimensionality [27]. Figure 8 gives an illustration of what this could look like.

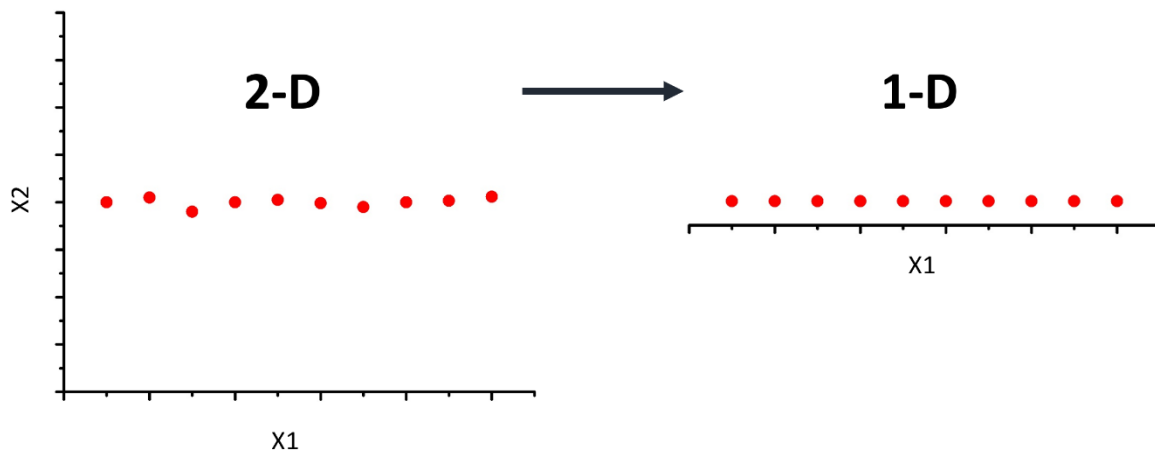


Figure 8: (a) Dataset with x_1 and x_2 coordinates. (b) Compressed dataset where only the x_1 coordinate is relevant.

3.2 Maximum Variance Perspective

Figure 8 is an example of how a two-dimensional dataset can be represented using a single coordinate. In Figure 8 (b), the X2-coordinate of the data is ignored due to the fact that it did not add too much information, so that the compressed data is similar to the original data in Figure 8 (a). On the other hand, When the X1-coordinate is ignored, then the compressed data had been very dissimilar from the original data, and much information in the data would have been lost.

The information contained in the data can be described by looking at the spread of the data. The variance is an indicator of the spread of the data, and we can derive PCA as a

dimensionality reduction algorithm that maximizes the variance in the low-dimensional representation of the data to retain as much information as possible. Figure 9 illustrates this.

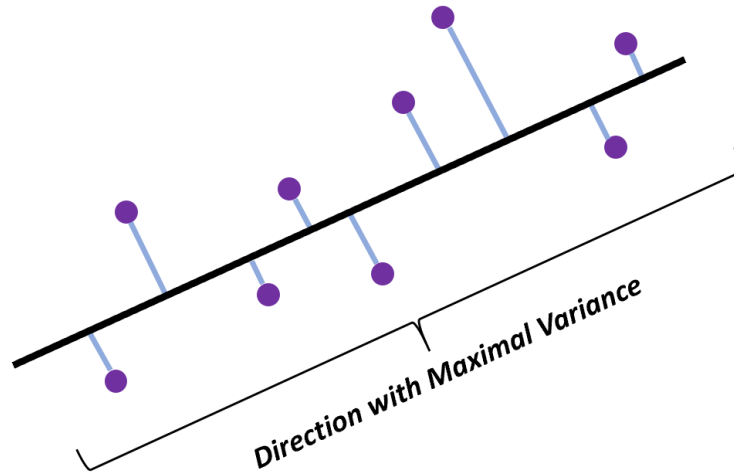


Figure 9: PCA finds a lower-dimensional subspace (black line) that maintains as much variance (spread of the data) as possible when the data (Violet) is projected onto this subspace (blue).

The goal is to find a matrix \mathbf{B} that retains as much information as possible when compressing data by projecting it onto the subspace spanned by the columns $\mathbf{b}_1, \mathbf{b}_2, \dots, \mathbf{b}_M$ of \mathbf{B} . Retaining most information after data compression is equivalent to capturing the largest amount of variance in the low-dimensional code [27]. Considering that $\boldsymbol{\mu}$ is the mean of the data and using the properties of the variance, we obtain:

Equation (18)

$$V_z[Z] = V_x[B^T(x - \boldsymbol{\mu})] = V_x[B^T x - B^T \boldsymbol{\mu}] = V_x[B^T x]$$

That means, the variance of the low-dimensional code does not depend on the mean of the data.

The approach to maximize the variance of the low-dimensional code is sequential approach. The starting point is to find a single vector $\mathbf{b}_1 \in \mathbb{R}^D$ that maximizes the variance of the projected data, i.e., the aim is to maximize the variance of the first coordinate \mathbf{z}_1 of $\mathbf{z} \in \mathbb{R}^M$ \mathbf{z}_1 of \mathbf{z}_2 RM so that

Equation (19)

$$V_1 := V[\mathbf{z}_1] = \frac{1}{N} \sum_{n=1}^N z_{1n}^2$$

is maximized. The first component of z_n is given by $z_{1n} = b_1^T x_n$, i.e., it is the coordinate of the orthogonal projection of x_n onto the one dimensional subspace spanned by b_1 . By substitution:

Equation (20)

$$V_1 = \frac{1}{N} \sum_{n=1}^N (b_1^T x_n)^2 = \frac{1}{N} \sum_{n=1}^N b_1^T x_n x_n^T b_1 = b_1^T \left(\frac{1}{N} \sum_{n=1}^N x_n x_n^T \right) b_1 = b_1^T S b_1$$

Where S is the data covariance matrix. All solutions are restricted to $\|b_1\|^2 = 1$, where the direction along which the data varies most is sought.

With the restriction of the solution space to unit vectors the vector b_1 that points in the direction of maximum variance can be found by the constrained optimization problem

$$\max b_1^T S b_1$$

By comparing this with the definition of an eigenvalue decomposition, it can be seen that b_1 is an eigenvector of the data covariance matrix S , and the Lagrange multiplier λ_1 plays the role of the corresponding eigenvalue.

Equation (21)

$$V_1 = b_1^T S b_1 = \lambda_1 b_1^T b_1 = \lambda_1$$

i.e., the variance of the data projected onto a one-dimensional subspace equals the eigenvalue that is associated with the basis vector b_1 that spans this subspace. Therefore, to maximize the variance of the low-dimensional code, the basis vector associated with the largest eigenvalue of the data covariance matrix is chosen. This eigenvector is called the **first principal component**.

The effect/contribution of the principal component b_1 in the original data space can be determined by mapping the coordinate z_{1n} back into data space, which gives the projected data point in the original data space.

Equation (22)

$$\tilde{x}_n = b_1 z_{1n} = b_1 b_1^T x_n \in \mathbb{R}^D$$

Although \tilde{x}_n is a D -dimensional vector, it only requires a single coordinate z_{1n} to represent it with respect to the basis vector $b_1 \in \mathbb{R}^D$.

3.2.1 M -dimensional Subspace with Maximal Variance

Based on spectral theorem [28], if the first $m - 1$ principal components as the $m - 1$ eigenvectors of S that are associated with the largest $m - 1$ eigenvalues, then Since S is

symmetric, these eigenvectors can be used to construct an orthonormal eigenbasis of an $(m - 1) - \text{dimensional}$ subspace of \mathbb{R}^D . The m th principal component can be found by subtracting the effect of the first $m - 1$ principal components b_1, b_2, \dots, b_{m-1} from the data, thereby finding the principal components that compress the remaining information [29].

Equation (23)

$$\hat{X} = X - \sum_{i=1}^{m-1} b_i b_i^T X = X - B_{m-1} X$$

Where $X = [x_1, x_2, \dots, x_N] \in \mathbb{R}^{D \times N}$ contains the data points as column vectors and $B_{m-1} = \sum_{i=1}^{m-1} b_i b_i^T$ is a projection matrix that projects onto the subspace spanned by b_1, b_2, \dots, b_{m-1} .

To find the m th principal component, the variance should be maximized [29].

Equation (24)

$$V_m = \mathbb{V}[z_m] = \frac{1}{N} \sum_{n=1}^N z_{mn}^2 = \frac{1}{N} \sum_{n=1}^N (b_m^T \hat{x}_n)^2 = b_m^T \hat{S} b_m$$

subject to $\|b_m\|^2 = 1$ and \hat{S} as the data covariance matrix of the transformed dataset $\hat{X} :=$
Error! Bookmark not defined..

3.3 Projection Perspective

In the following, PCA is derived as an algorithm that directly minimizes the average reconstruction error. This perspective allows to interpret PCA as implementing an optimal linear auto-encoder. PCA has been derived by maximizing the variance in the projected space to retain as much information as possible. In the following, the difference vectors between the original data x_n and their reconstruction \tilde{x}_n is taken into consideration as well as minimizing this distance so that x_n and \tilde{x}_n are as close as possible [29, 30].

By assuming an (ordered) orthonormal basis (ONB) $B = (b_1, b_2, \dots, b_D)$ of \mathbb{R}^D , i.e., $b_i^T b_j = 1$ if and only if $i = j$ and 0 otherwise. Moreover, for a basis (b_1, b_2, \dots, b_S) of \mathbb{R}^D any $x \in \mathbb{R}^D$ can be written as a linear combination of the basis vectors of \mathbb{R}^D , i.e.,

Equation (25)

$$x = \sum_{d=1}^D \zeta_d b_d = \sum_{m=1}^M \zeta_m b_m + \sum_{j=M+1}^D \zeta_j b_j$$

for suitable coordinates $\zeta_d \in \mathbb{R}$. The goal is to find vectors $\tilde{x} \in \mathbb{R}^D$, which live in lower dimensional subspace $U \subseteq \mathbb{R}^D$, $\dim(U) = M$, so that

Equation (26)

$$\tilde{x} = \sum_{m=1}^M z_m \mathbf{b}_m \in U \subseteq \mathbb{R}^D$$

is as similar to x as possible [31]. The premise is that the coordinates z_m of \tilde{x} and ζ_m of x are not identical. Using this kind of representation of \tilde{x} helps to find optimal coordinates z and basis vectors b_1, b_2, \dots, b_M such that \tilde{x} is as similar to the original data point x as possible. The objective is to minimize the (Euclidean) distance $\|x - \tilde{x}\|$. Without loss of generality, the assumption is that the dataset $X = (x_1, x_2, \dots, x_N)$, $x_n \in \mathbb{R}^D$, is centered at 0, i.e., $E[X] = 0$. Without the zero-mean assumption, the solution could be derived, but the notation would be substantially more cluttered. The objective is to find the best linear projection of X onto a lower dimensional subspace U of \mathbb{R}^D , $\dim(U) = M$ and orthonormal basis vectors (b_1, b_2, \dots, b_M) . This subspace is called U the principal subspace [29-31].

The projections of the data points are denoted by

Equation (27)

$$\tilde{x}_n := \sum_{m=1}^M z_{mn} \mathbf{b}_m = \mathbf{B} \mathbf{z}_n \in \mathbb{R}^D$$

where $\mathbf{z}_n := [z_{1n}, \dots, z_{Mn}]^T \in \mathbb{R}^M$ is the coordinate vector of \tilde{x}_n with respect to the basis (b_1, b_2, \dots, b_M) . More specifically, There is a need for the \tilde{x}_n to be as similar to x_n as possible.

The similarity measure used in the following is the squared distance (Euclidean norm) $\|x - \tilde{x}\|^2$ between x and \tilde{x} . Thus, the objective is to minimize the average squared Euclidean distance (reconstruction error)

Equation (28)

$$J_m := \frac{1}{N} \sum_{n=1}^N \|x_n - \tilde{x}_n\|^2$$

The subspace onto which we project the data is projected is M . A linear projection is found by finding the orthonormal basis of the principal subspace and the projection coordinates $z_n \in \mathbb{R}^M$ with respect to this basis. To find the coordinates z_n and the ONB of the principal subspace, a two-step approach will be followed. First, optimizing the coordinates z_n for a given ONB (b_1, b_2, \dots, b_M) ; second, finding the optimal ONB [31].

3.4 Practical Aspects

PCA is one example where only a few eigenvectors are needed. Completing the full decomposition and discarding all eigenvectors with eigenvalues that are beyond the first few would be wasteful. The iterative process, which directly optimizes the first few eigenvectors (with the largest eigenvalues), is computationally more efficient than an eigendecomposition (or SVD), if we are interested in only the first few eigenvectors [32].

In the extreme case of only needing the first eigenvector, a simple method called the power iteration is very efficient. Power iteration chooses a random vector x_0 that is not in the null space of S and follows the iteration

Equation (29)

$$x_{k+1} = \frac{Sx_k}{\|Sx_k\|} \quad k = 0, 1, \dots$$

This means the vector x_k is multiplied by S in every iteration and then normalized, in other words, it will always be the case that $\|x_k\| = 1$. This sequence of vectors converges to the eigenvector associated with the largest eigenvalue of S . The original Google PageRank algorithm uses such an algorithm for ranking web pages based on their hyperlinks [33].

4 | Continuous Wave Electron Paramagnetic Resonance Spectroscopy (CW EPR)

4.1 Objectives:

CW EPR Spectroscopy is used to evaluate the structure of the protein and its interactions with smaller molecules, such as fatty acids, on a nanometer scale. Electron paramagnetic resonance (EPR) spectroscopy involves measuring the resonance frequency of unpaired

electrons inside an external magnetic field. Using EPR spectroscopy methods, one can determine (i) nuclear spin transition frequencies or (ii) electron spin couplings via resonance excitation of electron spins. Depending on the system, one can gain information about the structure, dynamics, and spatial distribution of paramagnetic centers [34].

4.2 CW EPR spectroscopy in Theory:

4.2.1 Electron spin and resonance condition

EPR (also known as electron spin resonance, ESR) spectroscopy dates back to 1944, when E. K. Zavoisky observed the first EPR signal [35]. EPR spectroscopy was originally used to study the electronic structure of inorganic or organic paramagnetic samples. An EPR spectrometer uses microwaves to irradiate samples containing unpaired electrons while exposing them to a relatively homogeneous magnetic field [17].

The electron is a negatively charged particle which possesses orbital angular momentum as it moves around the nucleus. The electron also possesses spin angular momentum S as it spins about its own axis. These are intrinsic property of the electron [34]. The magnitude of S is given

Equation (30)

$$S = \left(\frac{h}{2\pi}\right)[s(s + 1)]^{1/2}$$

where S is the spin quantum number and h is the Planck 's constant. The component of spin angular momentum can only take two values if the dimension is restricted to one direction, usually assigned the z direction.

Equation (31)

$$S_z = \frac{M_S h}{2\pi}$$

The term M_S can have $(2S + 1)$ different values: $+S$, $(S - 1)$, $(S - 2)$ and so on. If the possible values of S differ by one and range from $-S$ to $+S$ then the only two possible values for M_S are $+1/2$ and $-1/2$ for a single unpaired electron.

An electron's spin has an important physical consequence: its magnetic moment μ_e . This magnetic moment is directly proportional to the spin angular momentum and one may therefore write

Equation (32)

$$\mu_e = -g_e \mu_B S$$

The negative sign arises from the fact that the magnetic momentum of the electron is collinear but antiparallel to the spin itself [34]. The factor $(g_e\mu_B)$ is referred to as the magnetogyric ratio and is composed of two important factors. The Bohr magneton, μ_B , is the magnetic moment for one unit of quantum mechanical angular momentum

Equation (33)

$$\mu_B = \frac{e\hbar}{2m_e}$$

where e is the electron charge, m_e is the electron mass and $\hbar = \frac{h}{2\pi}$. The factor, g_e , is known as the free electron g-factor with a value of 2.002 319 304 386 (one of the most accurately known physical constants) [36].

This magnetic moment interacts with the applied magnetic field. In classical terms the energy of the interaction between the magnetic moment μ and the field B is described by

Equation (34)

$$E = -\mu \cdot B$$

For a quantum mechanical system one must substitute μ by the corresponding operator, giving the following simple spin Hamiltonian for a free electron in a magnetic field [34, 37].

Equation (35)

$$\hat{H} = g_e\mu_B\hat{S} \cdot B$$

If the field is defined along the z direction, then the scalar product simplifies to the following Hamiltonian

Equation (35.2)

$$\hat{H} = g_e\mu_B\hat{S}_z \cdot B$$

The S_z value in the equation 35.2 can then be replaced by M_S , giving

Equation (36)

$$E = g_e\mu_B B M_S$$

Since $M_S = \pm 1/2$ only two energy states are available, which are degenerate in the absence of a magnetic field [38]. However, as B increases this degeneracy is lifted linearly as shown in **Figure 1.1**.

The separation of the two levels (Zeeman levels) can be matched to a quantum of radiation through the Bohr frequency condition [38].

Equation (37)

$$\Delta E = h\nu = g\mu_B B$$

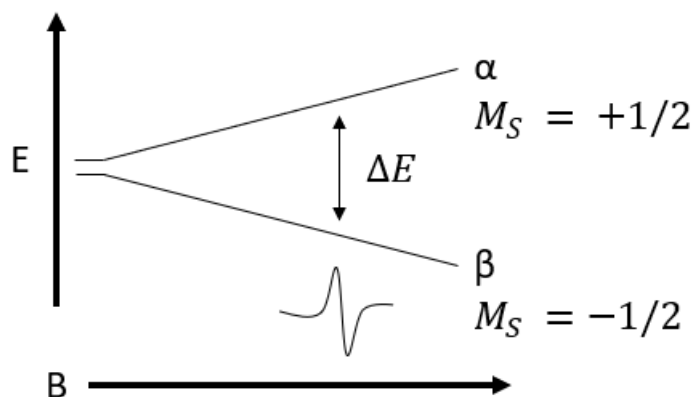


Figure 10: Energy levels for an electron spin ($S = \pm 1/2$) in an applied magnetic field B

The EPR spectroscopy is based on the existence of two Zeeman levels, and the possibility of inducing transitions between them [38]. Historical perspectives have divided resonance frequencies corresponding to external magnetic fields into separate bands. There are three main bands commonly used by commercially available spectrometers: X-band (9.4 GHz), Q-band (34 GHz), and W-band (94 GHz). The resonance experiment can be conducted in two ways; either the magnetic field is kept constant and the applied frequency varied, or the applied frequency is held constant and the magnetic field is varied. EPR spectroscopy generally uses the latter case since it is easier to change magnetic field over a wide range than to change frequency [37].

From Equation 37 it can be seen that the frequency required for the transition to occur is about 2.8 MHz per Gauss of applied field. This means that for the magnetic field usually employed in the laboratory, the radiation required belongs to the microwave region. For organic radicals the magnetic field used is in the region of 3400 Gauss and the corresponding applied frequency is in the microwave region of the electromagnetic spectrum (9 – 10 GHz). This corresponds to a wavelength of about 3.4 cm and is known as the X - band frequency. Higher and lower frequencies have different advantages, depending on the paramagnetic system, but X-band provides the best balance of resolution, intensity, and simplicity.

The SI units of magnetic field strength are Tesla, T, and millitesla, mT, though many people, for historical reasons, still use the older Gauss unit, G, which equates to 1 mT = 10 G.

There are two fundamental differences between EPR and NMR (Nuclear Magnetic Resonance) and other spectroscopic techniques. Firstly, the magnetic component of the applied electromagnetic radiation (microwave) interacts with permanent magnetic moments created by the electron (or nucleus in the case of NMR). In many other spectroscopic techniques, permanent or fluctuating electric dipole moments in the sample interact with the electric field component of the electromagnetic radiation. Secondly, a distinguishing feature of EPR is the experimental setup, which is based on a monochromatic radiation source coupled with a variable magnetic field. EPR spectra are basically plots of microwave absorption (at constant frequency) in response to applied magnetic fields [37].

The Maxwell-Boltzmann law states that the spin population at thermal equilibrium and under external magnetic fields is divided into two Zeeman levels (Figure 10) [34].

Equation (38)

$$\frac{n_1}{n_2} = e^{\frac{-\Delta E}{kT}}$$

where k is the Boltzmann constant, T the absolute temperature and n_1 and n_2 the spin populations characterized by the M_S values of $+1/2$ and $-1/2$ respectively. At 298 K in a field of about 3000 G the distribution shows that:

Equation (39)

$$\frac{n_1}{n_2} = e^{\frac{-\Delta E}{kT}} = e^{\frac{-g_e \mu_e B}{kT}}$$

This gives a value of $\frac{n_1}{n_2} = 0.9986$.

Thus, the populations of the two Zeeman levels are almost equal, but the slight excess in the lower level causes a net absorption. This would, however, very quickly result in the disappearance of the EPR signal since energy absorption would equalize these two states. It is therefore necessary to have a mechanism for releasing energy. Such mechanisms exist and are known as relaxation processes [37].

4.2.2 Relaxation Processes

A continuous promotion to a high energy level of electrons would result in the populations of the two energies balancing out and no net radiation absorption would occur [37]. In order to maintain a population excess in the lower level, the odd number of electrons from the upper level give up the $h\nu$ quantum to return to the lower level and satisfy the Maxwell – Boltzmann law. Spin relaxation releases this energy through two types of relaxation: spin-lattice relaxation and spin-spin relaxation [34, 37].

In the first case, known as spin–lattice relaxation, the energy is dissipated within the lattice as phonons, that is, vibrational, rotational and translational energy. It is characterized by an exponential decay of energy as a function of time. The exponential time constant is denoted T_{1e} and is called the spin–lattice relaxation time. The second case can also result in an initial equilibrium through a different process. Energy could be exchanged between spins without transferring to the lattice. This phenomenon, known as spin – spin relaxation is characterized by a time constant T_{2e} called the spin–spin relaxation time [37]. When both spin – spin and spin – lattice relaxations contribute to the EPR line, the resonance line width (ΔB) can be written as

Equation (40)

$$\Delta B \propto \frac{1}{T_{1e}} + \frac{1}{T_{2e}}$$

In general, $T_{1e} > T_{2e}$ and the line width depends mainly on spin–spin interactions. T_{2e} increases on decreasing the spin concentration, that is, the spin–spin distance in the system.

Conversely, if T_{1e} becomes very short, roughly below 10^{-7} seconds, its effect on the lifetime of a species in a given energy level makes an important contribution to the linewidth. T_{1e} is inversely proportional to the absolute temperature ($T_{1e} \propto T^{-n}$) with n depending on the precise relaxation mechanism [38].

As a result, cooling the sample increases T and usually produces lines that are detectable. Therefore, it is often the case that EPR experiments are conducted at liquid nitrogen (77 K) or liquid helium (4 K) temperatures [34]. On the other hand if the spin–lattice relaxation time is too long, electrons do not have time to return to the ground state. The populations of the two levels (n_1 and n_2) tend therefore to equalize and the intensity of the signal decreases, being no longer proportional to the number of spins in the sample itself. It is possible to avoid this saturation effect by using low incident microwave power on the sample.

4.2.3 The Nuclear Zeeman Interaction and Hyperfine Coupling

In the scenario that EPR could detect only electron interactions with an external magnetic field, all spectra would consist of a single line and would be of little significance to chemists. Though, the most valuable chemical information that can be derived from an EPR spectrum generally results from nuclear hyperfine structure. This hyperfine structure results from the interaction between magnetic nuclei and the unpaired electron magnetic moment within paramagnetic species [34, 37]. Many molecules contain nuclei that have a magnetic moment, and these can interact with the electron to cause hyperfine structure [37].

When neutrons and protons have uneven numbers, some nuclei also possess spin angular momentum. Spin quantum numbers, I , describe the spin of a nucleus. The angular momentum of a nucleus with spin I can be calculated by:

Equation (41)

$$|\mathbf{I}| = \hbar[I(I + 1)]^{1/2}$$

As with electron spin angular momentum (Equation 30), the orientation of the vector along an axis is quantized. The magnitude of the angular momentum along the z-axis is given by $M_I \hbar$, where M_I can have the values given by $M_I = +I, (I - 1), (I - 2)$, and so on. As nuclei possessing nuclear spin result in magnetic dipoles, the magnitude of this moment would be:

Equation (42)

$$\mu = \frac{g_n e_p \hbar}{4\pi m_p} [I(I + 1)]^{1/2}$$

where g_n is the nuclear g-factor, e_p is the proton charge and m_p is the mass of nucleus.

Several constants in Equation 42 can be substituted with the nuclear magneton (μ_N) to make it simpler [36].

Equation (43)

$$\mu_N = \frac{e_p \hbar}{2m_p} = 5.050 \times 10^{-29} \text{ J G}^{-1}$$

As a result:

Equation (44)

$$\mu_N = \gamma_N I$$

where the factor γ_N is referred to as the nuclear magnetogyric ratio. The simple spin Hamiltonian for a nuclear spin can therefore be given as

Equation (45)

$$\hat{H} = -\gamma_N \mathbf{B} \cdot \mathbf{I}$$

and the eigen state values for this are:

Equation (46)

$$E = -\gamma BM_I$$

Considering the case of a proton, which has $M_I = \pm 1/2$, then there are two spin states. In the absence of an external magnetic field the two spin states are degenerate. Though, if an applied external magnetic field is applied the degeneracy is lost and results in two states of different energy. In this circumstance, the lower energy state (the α state) has both the magnetic moment and the spin parallel to the applied field. The magnetic moment of an unpaired electron can now not only interact with the external applied field, but also with local nuclear magnetic moments. In the EPR spectrum, hyperfine structure results from this interaction between electron magnetic moments and nuclear magnetic moments [37, 38].

A unpaired electron's energy will no longer be determined solely by the interactions between the unpaired electron (Zeeman level) and the nucleus (Nuclear Zeeman level) with a magnetic field applied outside it, but will also be determined by its interaction with magnetic nuclei. For such a system the energy terms can be derived, for instance, for a simple two - spin system ($S = 1/2, I = 1/2$) by considering the simplified spin Hamiltonian for this two - spin system ($S = 1/2, I = 1/2$) in an external applied field B [38].

Equation (47)

$$\mathbf{H} = H_{EZ} + H_{NZ} + H_{HFS}$$

where EZ is the electron Zeeman term, NZ is the nuclear Zeeman term, and HFS is the hyperfine interaction. This equation can be rewritten as [38]:

Equation (48)

$$\hat{\mathbf{H}} = g\mu_B BS_Z - g_N\mu_N BI_Z + hSaI$$

taking a as the isotropic hyperfine coupling in Hertz. In the equation 48 it is also presumed that the g value is isotropic and the external magnetic field is aligned along the z axis. Neglecting second order terms, and in the high field approximation where the electron Zeeman interaction dominates all other interactions, the energy levels for the two - spin system ($S = 1/2, I = 1/2$) can be shown as [38]:

Equation (49)

$$\mathbf{E}(M_S, M_I) = g\mu_B BM_S - g_N\mu_N BM_I + haM_S M_I$$

To simplify the equation, the electron and nuclear Zeeman energy terms can be stated in frequency units giving:

Equation (50)

$$\mathbf{E}(M_S, M_I)/h = \nu_e M_S - \nu_N M_I + aM_S M_I$$

where $\nu_e = g\mu_B B/h$ and $\nu_N = g_N\mu_N B/h$. The four possible energy levels resulting from equation 50 can be expressed as follows

Equation (51.a)

$$E_a = -\frac{1}{2}g\mu_B B_0 + \frac{1}{2}g_N\mu_N B_0 + \frac{1}{4}ha - \frac{1}{2} + \frac{1}{2}$$

Equation (51.b)

$$E_a = +\frac{1}{2}g\mu_B B_0 + \frac{1}{2}g_N\mu_N B_0 + \frac{1}{4}ha + \frac{1}{2} + \frac{1}{2}$$

Equation (51.c)

$$E_a = +\frac{1}{2}g\mu_B B_0 - \frac{1}{2}g_N\mu_N B_0 + \frac{1}{4}ha + \frac{1}{2} - \frac{1}{2}$$

Equation (51.d)

$$E_a = -\frac{1}{2}g\mu_B B_0 - \frac{1}{2}g_N\mu_N B_0 - \frac{1}{4}ha - \frac{1}{2} - \frac{1}{2}$$

By application of the EPR selection rules ($\Delta M_I = 0$ and $\Delta M_S = \pm 1$), it is found that the two transitions give rise to two absorption peaks at different magnetic field positions and are separated by a , the isotropic hyperfine coupling. These frequencies are accessed in hyperfine techniques such as ENDOR and ESEEM, and are extremely important for measuring very small hyperfine couplings, particularly in cases when a is unresolved in the EPR spectrum [34, 37].

Figure 11 illustrates an example of energy level diagram of a nitroxide spin label in the presence of a static magnetic field (B_0). The inset traces show the corresponding electron paramagnetic resonance (EPR) spectrum in the absence and presence of a ^{14}N ($I = 1$) hyperfine interaction [39].

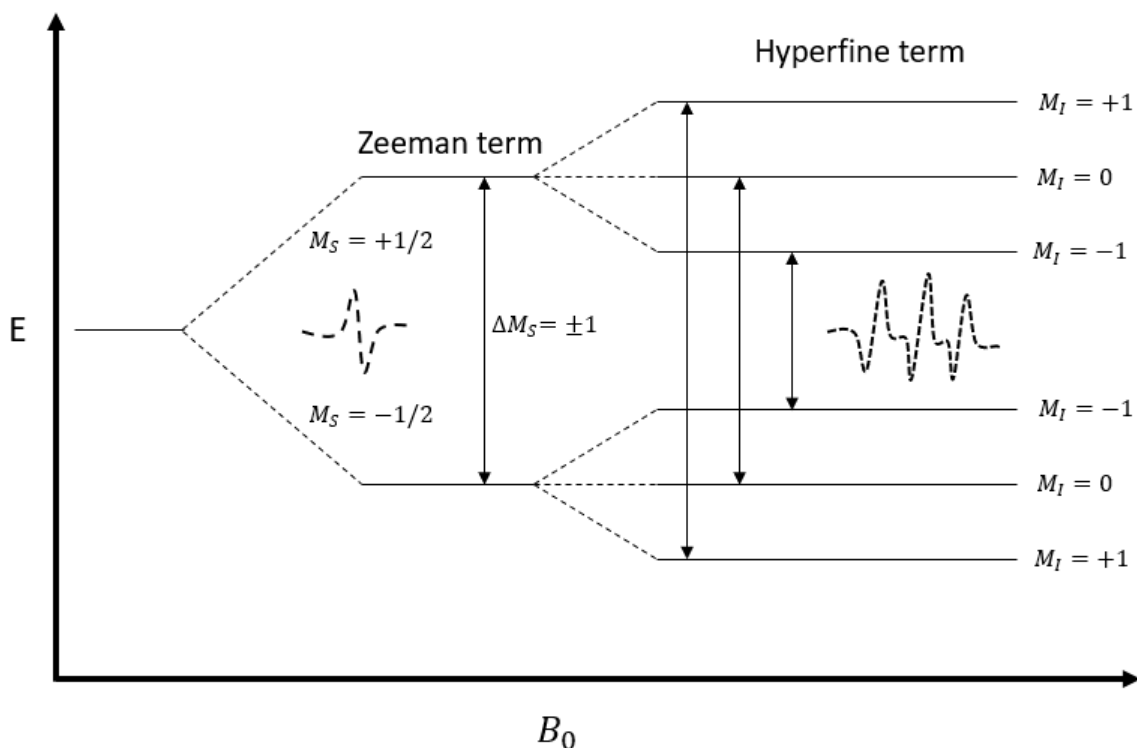


Figure 11: An energy level diagram of nitroxide spin labels in the presence of a static magnetic field (B_0). Inset traces show corresponding electron paramagnetic resonance (EPR) spectra without and with ^{14}N ($I = 1$) hyperfine interactions.

4.2.4 Physical State of the Sample

In EPR spectroscopy, it is possible to measure spectra of paramagnetic samples in a variety of forms, including fluid solution, frozen solution, powdered solid or single crystal. For polycrystalline heterogeneous systems, such as oxides, the problems of solvent choice, lossy samples, poor glass quality when frozen, etc., are all eliminated, facilitating the analysis of such heterogeneous systems. The dielectric loss of polycrystalline samples is usually not a problem, except for ionic compounds with large ionic charges and for large samples. With powdered solids it is important to grind the sample sufficiently to avoid any preferential orientation of the crystallites. Re-recording the spectrum after rotating the sample tube to give a different orientation with respect to the magnetic field may reveal preferential orientations of paramagnets in either powders or glasses. When the spectrum changes, there is some preference in the orientation of the paramagnet, and interpretation of the spectrum must then be taken with caution [40].

5 | Abstract: The Thesis Objective

5.1 Motivation and Concept:

In the following the main three publications, based on the theoretical part discussed in previous chapters, are presented in a nutshell. Full publications are included in the Appendix.

In our initial publication, our primary focus centered on unraveling the intricate relationships among pH, temperature, and incubation time in the synthesis of hydrogels. This comprehensive investigation spanned both the nanoscale and macroscale properties of hydrogels produced under a wide range of pH values, temperatures, and incubation durations. This systematic exploration provided a solid foundation for the exploration of these biomaterials, employing various gelation agents.

Our research then delved into the role of ethanol as a catalyst in the synthesis of serum albumin hydrogels. Ethanol emerged as a key influencer, notably affecting the secondary structure of proteins within these hydrogels. This influence led to a diverse array of synthesis possibilities, each imparting unique macroscopic and microscopic characteristics to the resulting hydrogels.

Furthermore, we conducted a thorough examination of the relationship between ethanol concentration and protein denaturation, a topic of significant relevance in molecular biophysics. Ethanol's impact on protein structure and stability yielded intriguing insights, shedding light on the complex interplay between solvent composition and macromolecular conformation.

The recent findings, combined with prior research on the molten globule (MG) state using electron paramagnetic resonance (EPR), have sparked a fascinating idea. We began to consider whether this unique MG state might persist even within a gel state. This concept led us to embark on our third major publication, where we successfully confirmed the presence of the MG state within the gel matrix. This discovery not only enhances our understanding of macromolecular behavior within gels but also sheds light on the significant impact of the MG state on gel properties, bridging the gap between physical chemistry and biomaterial characterization. Below, you'll find further elaboration on each publication and the methods employed for characterization.

In the first publication, "Serum albumin hydrogels in broad pH and temperature ranges: characterization of their self-assembled structures and nanoscopic and macroscopic properties" the key focus was to synthesis and characterize new biocompatible materials for smart drug delivery systems. The study was conducted to examine the materials and molecular properties of different types of hydrogels prepared from human and bovine serum

albumin, a major transport protein in mammals' blood. Three levels of properties of these hydrogels are described: (1) their viscoelastic (macroscopic) behaviour, (2) changes in protein secondary structures during gelation (via ATR-FTIR spectroscopy), and (3) the ability of hydrogels to bind fatty acids (FA) and derive from this the generalized tertiary structure through CW EPR spectroscopy. Hydrogels can be prepared from serum albumin under mild conditions such as low temperatures (notably below albumin's denaturation temperature) and neutral pH values. Consequently, most of the protein's secondary structure remains intact. In summary, all the combined data indicate that gelation occurs in two stages. Our phase diagrams for HSA and BSA gel states summarize these findings and their dependence on pH, temperature, concentration, and incubation time. In future, it will be possible to test gels for, e.g., drug delivery applications, which will have the desired nanoscopic and macroscopic properties.

To comprehensively understand the properties and behavior of serum albumin hydrogels, multiple characterization methods were employed. Rheological characterization using a rheometer provided insights into gelation kinetics, viscoelastic behavior, and mechanical properties by measuring the loss and storage modulus. This technique facilitated the determination of gelation start-time and evaluation of modulus changes during gelation. Transmission electron microscopy (TEM) allowed visualization and examination of the microstructure of albumin precursor solutions of hydrogels prepared under different conditions and shedding light on the impact of gel preparation methods on resulting structures. Attenuated total reflection infrared (ATR-IR) spectroscopy, specifically ATR-FTIR spectroscopy, analyzed secondary structure changes during hydrogel formation by examining characteristic IR bands like amide I and amide II, providing insights into conformational alterations, and assessing stability and behavior. Principal component analysis (PCA) of IR data enabled the evaluation of complex changes and correlated variations observed in the IR spectra, facilitating the identification of trends and patterns within large datasets. Plotting the scores on principal components over time aided in assessing gel transition kinetics. Continuous wave electron paramagnetic resonance (CW EPR) spectroscopy investigated the fatty acid binding capacity of hydrogels by monitoring the interaction between albumin and spin-labeled fatty acid derivatives. This technique revealed information on rotational motion immobilization upon fatty acid binding and changes in environmental polarity, offering insights into fatty acid binding sites' availability and chemical nature in the hydrogels.

Hydrogels can be formed at temperatures significantly lower than those necessary to denature the proteins. It is discussed explicitly how the gelation incubation time plays a critical role in protein aggregation and the gelation. Phase diagrams for HSA and BSA are

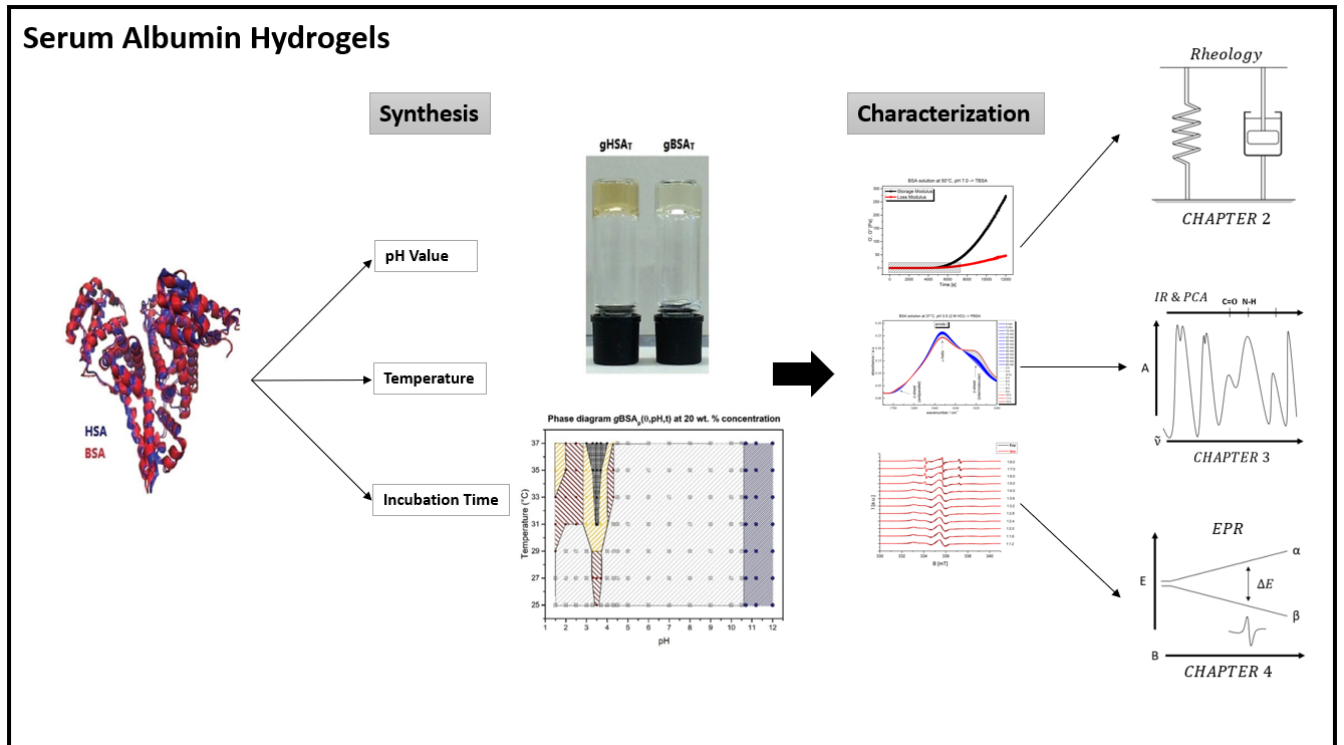


Figure 12: Schematic illustration of the experimental investigations in this work.

drawn to illustrate the phase spaces of thermally induced and electrostatically triggered gels based on temperature, concentration, pH, and time. We were able to provide additional details on the electrostatically triggered BSA hydrogel and its gelation mechanism. Partial denaturation of the protein is caused by changing the charge distribution on BSA by adjusting the pH value. A low-temperature hydrogel formation of BSA is facilitated by newly exposed hydrophobic areas and counter-ions. In addition to showing that the pH range is significantly broader than what was previously thought, this research has been extended to HSAs as well. Furthermore, the results of our experiments indicate that counterions not only affect the minimum protein concentration required for gelation, but they also affect the stability and gelation kinetics of the hydrogels, as well as their mechanical properties and, particularly, the ability of the gels to bind fatty acids (FA).

The focus of the “The Effect of Ethanol on Gelation, Nanoscopic, and Macroscopic Properties of Serum Albumin Hydrogels” publication is to investigate other factors which might cause change in the macroscopic and nanoscopic properties of the gels and give more insight to tailor the properties according to practical needs.

A chemical denaturant, ethanol, is used in this study to investigate the basic mechanisms of albumin gelation at 37°C. We showed that the denaturation of serum albumin and subsequent gelation can also be triggered by ethanol. This temperature corresponds to human body temperature, and albumin is in a non-denatured N conformation under physiological conditions. In this study, we investigated the conformational and physical properties of albumin hydrogels induced by ethanol, complementing our earlier findings on the effects of pH, temperature, and incubation time. Ethanol can be employed as a suitable agent to achieve desired gel properties at both nanoscopic and macroscopic scales. In order to characterize the gels, we combined spectroscopic data and mechanical data (rheology). The binding capacity of gels for fatty acids is studied with electron paramagnetic resonance (EPR) spectroscopy, which implies observing the effects of ethanol on binding sites of stearic acids in gel-form. The addition of ethanol to bovine serum albumin (BSA) hydrogels results in a significant reduction (by 52%) in the fraction of strongly bound fatty acids (FAs). This ethanol-induced effect leads to BSA hydrogels exhibiting relatively weak mechanical properties, as evidenced by a maximum storage modulus of 5000 Pa. The weak mechanical properties, besides the loosely bound FAs in ethanol-based hydrogels introduce interesting new materials for fast drug delivery systems.

The third publication “Hydrogels from serum albumin in a molten globule-like state” sheds light into persistence and/or formation of molten globule-like state in gel state.

In this study, the preservation of a molten globule-like state of BSA protein within self-assembled hydrogels adds complexity to the understanding of the nature and characteristics of these partially folded conformations. This research expands the knowledge on albumin hydrogels and their potential applications in drug delivery systems.

The presence of a molten globule state in human serum albumin (HSA) has been established under acidic conditions at pH 2.0, as confirmed by various techniques including circular dichroism and binding assays. Similarly, the existence of a first molten globule state in alkaline BSA solutions at pH 11.2 has been well-established through spectral analyses. Additionally, experimental evidence suggests a potential second molten globule state of BSA in the acidic pH range, supported by small-angle X-ray scattering and protein fluorescence studies.

Based on CW EPR, it has been demonstrated that basic molten globule states exist in the basic BSA hydrogels (but not in acidic hydrogels). In this method, hydrophobic patches in the MG state are more exposed than they are in the native or unfolded states, which can be detected using CW EPR spectroscopy on amphiphilic fatty acid derivatives (16-DSA). The findings indicate that albumin molecules persist in their MG state during and after gelation, allowing 16-DSA molecules to attach to exposed hydrophobic areas. Despite the strong intermolecular interactions in the gel state, the MG state of albumin remains robust. Other conventional methods for verifying the MG state, such as IR spectroscopy and rheological measurements, were not applicable due to the high protein concentration and rapid gelation process.

The present study is the first, to the best of our knowledge, to propose the presence of the molten globule state in a high-crowding hydrogel environment. Additionally, the MG-state was observed to be more stable (in independent measurements by different experimenters). It is clear from these results that experimental studies of MG states in proteins can be redirected to a "polymer under constraints" perspective, and since protein structures range from globally folded via MG to intrinsically disordered states, testing the persistence of many MG state proteins under high crowding conditions may be of interest. It is even possible to fine-tune the macroscopic gel properties by adding equimolar amounts of other amphiphilic molecules like long-chain fatty acids. Although BSA MG hydrogels require too high pH values for direct practical use, it is possible to envision new biocompatible materials (probably derived from proteins in MG states that are induced under milder conditions) with unique properties that can be used in biomaterials science, such as drug delivery. Biophysically, it is remarkable that the enigmatic molten globule state persists in a high concentration environment and dominates the nanoscopic and macroscopic properties of a hydrogel.

Collectively, these publications contribute to the advancement of serum albumin hydrogels as promising biomaterials for smart drug delivery systems. The hydrogels exhibit desirable properties, including biocompatibility, nanoscopic stability, and controlled drug release capabilities. The studies emphasize the significance of factors such as pH, temperature, concentration, and incubation time in tailoring hydrogels with specific properties. Furthermore, the utilization of ethanol as a denaturant and the exploration of the molten globule state offer avenues for manipulating the properties of hydrogels to meet practical requirements. These scientific advancements hold great potential for the development of novel biocompatible materials for drug delivery applications in the field of biomedicine.

To comprehensively understand the properties and behaviour of serum albumin hydrogels for drug delivery applications, various characterization methods were utilized. These methods provided insights into different aspects of the hydrogels, including gelation kinetics, viscoelastic behaviour, secondary structure changes, fatty acid binding capacity, and molecular dynamics. The following list highlights the key methods employed in this study:

1. Rheological characterization: Rheological characterization was performed using a rheometer to investigate the gelation kinetics and viscoelastic behaviour of the hydrogels. The measurement of loss and storage modulus provided valuable information on the stability, steady-state behaviour, and mechanical properties of the gels. This characterization method helped determine the gelation start-time and evaluate the changes in modulus during the gelation process.

2. Transmission electron microscopy (TEM): TEM was used to visualize and examine the microstructure of albumin precursor solutions of hydrogels prepared under different conditions. This technique allowed us to visualize the morphology and self-assembled

structures of the hydrogels and helped understand the impact of gel preparation methods on the resulting structures.

3. Attenuated total reflection (ATR) infrared (IR) spectroscopy: ATR-FTIR spectroscopy was utilized to analyse the secondary structure changes of serum albumin during hydrogel formation. By examining the characteristic IR bands of proteins, such as the amide I and amide II bands, the alterations in the protein's secondary structure could be determined. This method provided insights into the conformational changes occurring during gelation and helped assess the stability and behaviour of the hydrogels.

4. Principal component analysis (PCA) of IR data: PCA was employed to evaluate complex changes in peak intensities and correlated variations observed in the IR spectra. By transforming the data into orthogonal variables called principal components, this analysis method facilitated the identification of trends and patterns within the large datasets. Plotting the scores on the principal components over time helped assess the kinetics of the gel transition.

5. Continuous wave (CW) electron paramagnetic resonance (EPR) spectroscopy: CW EPR spectroscopy was utilized to investigate the fatty acid binding capacity of the hydrogels. By introducing spin-labeled fatty acid derivatives into the hydrogels, the interaction between albumin and fatty acids was monitored. This spectroscopic technique provided information on the immobilization of rotational motion upon fatty acid binding and changes in environmental polarity, enabling insights into the availability and chemical nature of fatty acid binding sites in the hydrogels.

The combination of rheological characterization, TEM, ATR-IR spectroscopy, PCA of IR data, and CW EPR spectroscopy provided valuable insights into gelation kinetics, mechanical properties, microstructure, secondary structure changes, and fatty acid binding capacity. This knowledge contributes to the development of efficient and controlled drug delivery systems using albumin hydrogels.

6 | Contribution Statements

The contributions of Seyed Hamidreza Arabi in the research presented in the following publications:

6.1 Publication A: Publication in Biomaterials Science (2018), vol. 6, 478-492

Prepared the samples. Performed the measurements, processed the experimental data, performed the analysis, drafted the manuscript and designed the figures. Characterized with EPR and IR spectroscopy. Performed the rheological characterization. Aided in interpreting.

6.2 Publication B: Publication in MDPI Molecules (2020), vol. 25, 1927

Prepared the samples and supervised the sample preparations. Aided and supervised the measurements, processed the experimental data, performed the analysis, drafted the manuscript and designed the figures. Characterized with EPR and IR spectroscopy. Performed the rheological characterization. Aided in interpreting.

6.3 Publication C: Publication in Protein Science (2020), vol. 29, 2459-2467 73

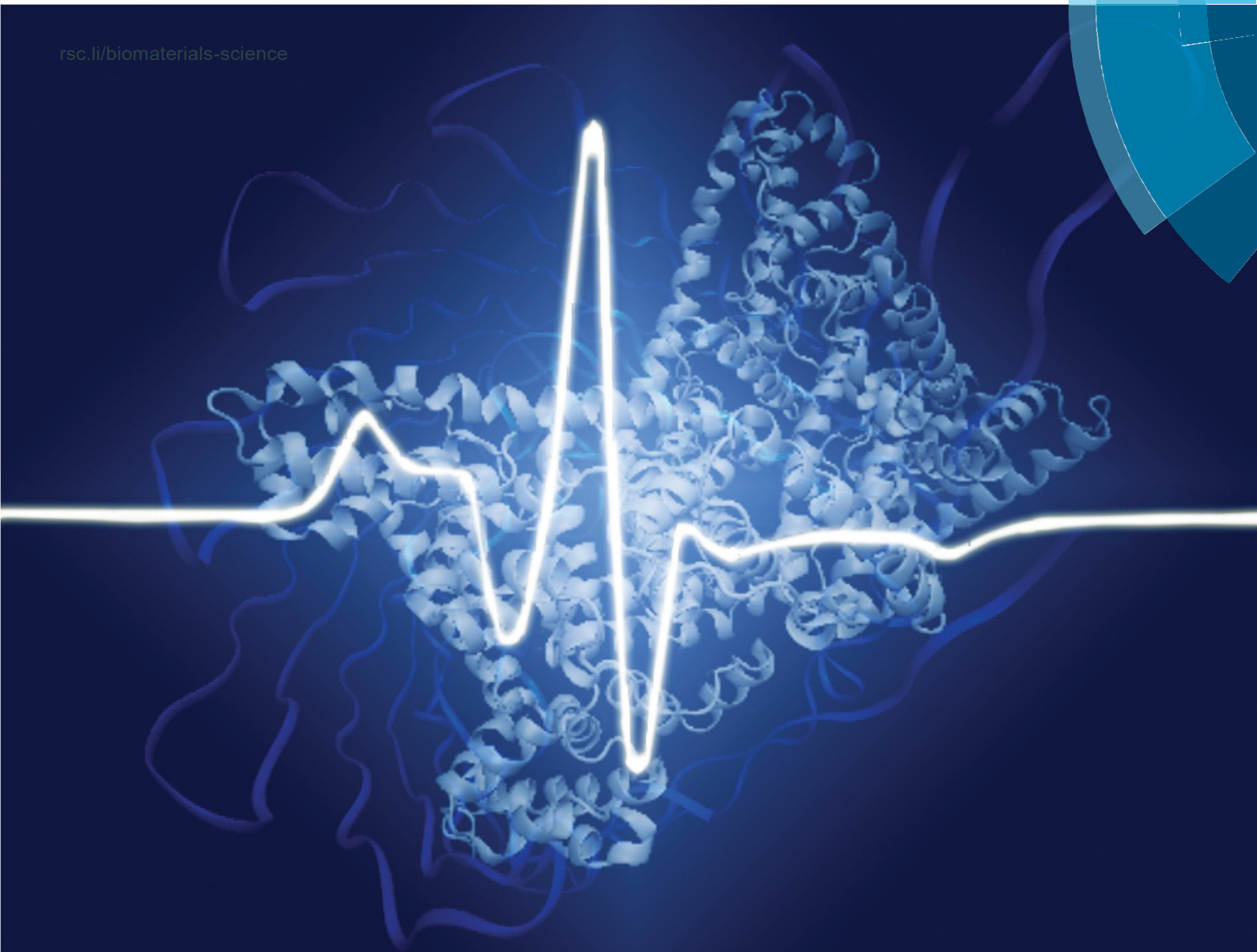
Prepared the samples and supervised the sample preparations. Performed the measurements, processed the experimental data, performed the analysis, drafted the manuscript and designed the figures. Characterized with EPR spectroscopy. Aided in interpreting.

7 | Appendix: Publications

7.1 Publication A: Publication in Biomaterials Science (2018), vol. 6, 478-492

Biomaterials Science

rsc.li/biomaterials-science



ISSN 2047-4849

PAPER

Dariusz Hinderberger *et al.*

Serum albumin hydrogels in broad pH and temperature ranges:
characterization of their self-assembled structures and nanoscopic and
macroscopic properties



Cite this: *Biomater. Sci.*, 2018, 6, 478

Serum albumin hydrogels in broad pH and temperature ranges: characterization of their self-assembled structures and nanoscopic and macroscopic properties†

S. Hamidreza Arabi,  Behdad Aghelnejad, Christian Schwieger,  Annette Meister, Andreas Kerth and Dariush Hinderberger *

We report extended pH- and temperature-induced preparation procedures and explore the materials and molecular properties of different types of hydrogels made from human and bovine serum albumin, the major transport protein in the blood of mammals. We describe the diverse range of properties of these hydrogels at three levels: (1) their viscoelastic (macroscopic) behavior, (2) protein secondary structure changes during the gelation process (*via* ATR-FTIR spectroscopy), and (3) the hydrogel fatty acid (FA)

binding capacity and derive from this the generalized tertiary structure through CW EPR spectroscopy. We describe the possibility of preparing hydrogels from serum albumin under mild conditions such as low temperatures (notably below albumin's denaturation temperature) and neutral pH value. As such, the proteins retain most of their native secondary structure. We find that all the combined data indicate a two-stage gelation process that is studied in detail. We summarize these findings and the explored dependences of the gels on pH, temperature, concentration, and incubation time by proposing phase diagrams for both HSA and BSA gel-states. As such, it has become possible to prepare gels that have the desired nanoscopic and macroscopic properties, which can, in future, be tested for, *e.g.*, drug delivery applications.

Received 5th September 2017,
Accepted 18th January 2018DOI: 10.1039/c7bm00820a
rsc.li/biomaterials-science

Introduction

Serum albumin is the most abundant protein in the blood plasma of mammals, reaching a concentration of 40 to 50 mg ml⁻¹ in plasma, and it is the primary carrier of various solutes in plasma.^{1,2} Its high abundance, stability and availability at high purity and low cost make serum albumin a model protein in many physicochemical and biomaterials science studies.^{3,4} We have, in the past, elucidated the structural versatility and flexibility especially of human (and bovine) serum albumin through an electron paramagnetic resonance (EPR) spectroscopy-based research platform.^{5–7}

Concurrently, in the biomedical sciences there is an increasing need to develop new materials which simultaneously have the desired affinities to biological and therapeutic materials and high biocompatibility. Hydrogels made from synthetic or bio-macromolecules have exhibited great

† Electronic supplementary information (ESI) available. See DOI: 10.1039/c7bm00820a

Institut für Chemie, Martin-Luther-Universität Halle-Wittenberg, Von-Danckelmann-Platz 4, 06120 Halle, Saale, Germany.

E-mail: dariush.hinderberger@chemie.uni-halle.de

478 | *Biomater. Sci.*, 2018, 6, 478–492

This journal is © The Royal Society of Chemistry 2018



potential for biological and medical applications.^{8–10} Among them, protein gels can be assumed to be cage-like unit structures forming a matrix in which the solvent (water in the case of hydrogels) and potentially releasable drugs and adjuvants are trapped.¹¹

There has been an ongoing endeavor to synthesize hydrogels from serum albumin in such a way that robust, biocompatible hydrogels are delivered while preserving protein functionality, *i.e.* the capability to bind, retain, and release a variety of molecules in a well-defined manner. So far, very few (considering the abundance and availability of albumin) different synthetic methods have been developed^{12–15} and so far only hydrogels from bovine serum albumin (BSA), which has a

primary sequence identity with human serum albumin (HSA) of ~76%,¹⁶ have been reported. Here, we report, to the best of our knowledge for the first time, gels made from HSA (as well

as from BSA, which have been described before), and we particularly focus on (i) systematically studying the conditions (temperature, pH and incubation time) under which gelation can take place, (ii) the characterization of the gels at the macroscopic level (mechanical properties as seen in rheological measurements) as well as (iii) the characterization of the accompanying changes in structure, dynamics, and functional-

ity at the molecular level as seen in ATR-IR and electron paramagnetic resonance (EPR) spectroscopy.

Thermally induced BSA hydrogels (see Fig. 1) are already well established and one finds long-standing work on the mechanism of thermally induced gelation of proteins such as BSA.^{17–19} Heating-induced gel formation consists of two sequential processes. First, unfolding of polypeptide segments induced by heating causes conformational changes and an altered tertiary structure in the protein. A subsequent phase of protein–protein (secondary structure element) interactions results in a progressive build-up of a network structure leading to the final gel.²⁰ The main disadvantage of this method is the extensive protein denaturation, with the risk of compromising protein functionality and biocompatibility.²¹ The currently accepted working hypothesis^{20,22–25} states that in order to obtain thermally induced albumin hydrogels at neutral pH, the temperature must be set above the denaturation temperature of the protein (at pH 7.4 the denaturation temperature of serum albumin is 62 °C (ref. 26)).

Another preparation method for albumin hydrogels has recently been introduced by Baler *et al.* (2014),²² which the authors called electrostatically triggered serum albumin hydrogels. In this method, the pH of the precursor solution (solution of serum albumin dissolved in water) is lowered to the value of 3.5 using 2 M HCl; consequently, the net charge on the protein (according to a theoretical PROPKA analysis)

changes from -16 at pH 7.4 to $+100$ at pH 3.5.²⁷ One effect of this charge inversion is that now positively charged protein domains repel each other, which causes partial denaturation of the protein and results in solvent exposure of the buried hydrophobic areas of the albumin. This then triggers intermolecular self-assembly of the proteins into a hydrogel at 37 °C. It has been suggested that hydrophobic interactions and counter-ion binding are the key drivers of protein aggregation in this system.²⁷ The gelation process takes place at much lower temperatures when the pH is adjusted. It has been reported that this mechanism works in the pH range of 3.0 to 4.0 for BSA with the optimum value of 3.5.²²

The incubation time t_i during gelation, *i.e.* the time after which the gelation process is quenched, is a critical factor that

has remarkably not been studied systematically thus far. As will be shown in the following, by changing t_i it is possible to obtain serum albumin hydrogels (from both HSA and BSA) at temperatures far below the denaturation temperature of the proteins at neutral pH. Furthermore, it will be shown that by varying t_i , also the pH range in which electrostatically triggered albumin hydrogels form is much broader than reported. Changing the incubation time t_i affects the mechanical properties of the hydrogels in a highly complex manner. Some gels harden with longer t_i , while others start to decompose again; the rise times of gelation can be very different, ranging from instantaneous to several hours, and many other non-trivial differences are observed. Herein, we report a systematic study of the combined effects of pH, temperature and incubation time on albumin hydrogel formation and its properties and provide explicit phase diagrams for both human and bovine serum albumin. Besides the mechanical properties as studied by rheology, the changes in secondary structure are characterized using their IR-spectroscopic signatures. Our investigation is complemented by a nanoscopic view on the fatty acid (FA) binding capacity in albumin hydrogels as seen by continuous wave (CW) electron paramagnetic resonance (EPR) spectroscopy, which on the one hand is of great importance with respect to the capability of these hydrogels for controlled drug release and on the other hand has been developed into a method of characterizing the proteins' tertiary structure in an experimental, "coarse-grained" manner.^{5–7}

Materials and methods

Bovine serum albumin (lyophilized powder, essentially fatty acid free, >96%, A6003, Sigma, St Louis, MO, USA) and albumin from human serum (lyophilized powder, essentially fatty acid free, A1887, Sigma, St Louis, MO, USA) were used in the experiments. In ref. 22 and 27, the authors introduced "TBSA" and "PBSA" as nomenclature for thermally and electrostatically (pH) triggered BSA hydrogels, respectively. Since we here extend the work to gels made from HSA and we wish to clearly discriminate the gel-state from the non-gelated precursor solutions, we introduce a notation as follows: $gXSA_i(\Theta, p, t)$, where g denotes the gel-state, $X = B, H$ clarifies the origin ($B =$ bovine, $H =$ human) and the index $i = T, p$ indicates the preparation method ($T =$ thermally induced or $p =$ electrostatically/pH-induced). Since we present a larger variety of different gels and their physical properties as a function of temperature (Θ), pH (p), and incubation time (t), these parameters can be specified in parentheses ($\Theta =$ temperature in °C, $p =$ pH, $t =$ incubation time in minutes). This means that, *e.g.*, $gHSA_p(65, 3.5, 60)$ denotes an HSA-based hydrogel that was electrostatically prepared at pH 3.5, 65 °C for 60 minutes.

Thermally induced human/bovine serum albumin hydrogels (gHSAT, gBSAT)

Serum Albumin (HSA/BSA) was added into a flask equipped with a magnetic stirrer. Then, according to the desired concen-

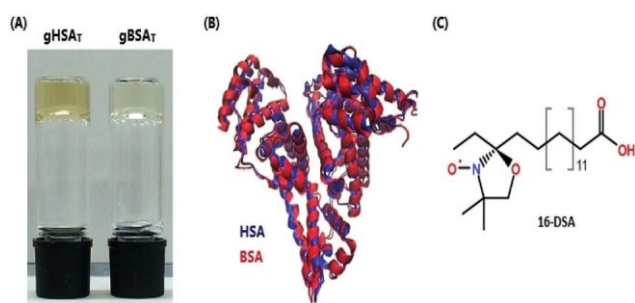


Fig. 1 (A) Bovine and human serum albumin hydrogels are formed at 50 °C and pH 7.0 and 7.2, respectively. (B) Superimposed three-dimensional structures of HSA and BSA are shown in blue and red. The protein topologies from pdb IDs 1BM0HSA⁴⁷ and 3v03BSA.⁴⁸ (C) Chemical structure of 16-DSA used as a spinprobe.



tration of HSA/BSA in water, deionized water was added into the flask with final concentrations in the range of 12 to 20 wt% (1.8 to 3.0 mM). The protein–water solution was stirred at a low rate, 100 rpm, until the dissolution of the albumin precursor solution in water was completed. The pH values of the solutions were 7.0 and 7.2 for BSA and HSA, respectively. The final solution was sterilized with a 0.2 μm nylon syringe filter into vials. The vials were kept at different temperatures (37 to 80 °C) in a thermomixer for different durations in order to yield gHSA_T and gBSA_T, respectively.

pH-Induced human/bovine serum albumin hydrogels (gHSA_p, gBSA_p)

gHSA_p and gBSA_p were prepared according to the procedure explained above for the gXSA_T analogues with some extra steps. After the preparation of the precursor solution, the pH was lowered or increased by addition of different acids or bases (2 M HCl, 0.1, 1, 2 M H₂SO₄, 2 M H₃PO₄, 2 M CH₂(COOH)₂, 2 M NaOH) to the solution. In contrast to the pH range reported by Baler *et al.* (pH 3.0–4.0)²² we obtained gBSA_p and gHSA_p at pH values of 4.3 or lower (down to 1.0) and even above pH 10.6. As shown below, at high pH, we obtained hydrogels at temperatures as low as room temperature. Again, the incubation time needed for the hydrogels to form depends on the temperature, the concentration of the protein solution and the used acid/base and varies from several seconds to several days.

Loading FAs into the hydrogels

Three different methods of loading FAs into the hydrogels were tested: (1) 16-DSA (the spin-labeled stearic acid, Fig. 1C) was first dissolved in 0.1 M KOH. Then, according to the desired albumin : FA molar ratio, the 16-DSA solution was added to the precursor solution of the hydrogel. Finally, the gel was synthesized by changing the temperature and/or pH to obtain FA-loaded hydrogels (gXSA_T and gXSA_p). (2) The solid powder 16-DSA was added directly to the precursor solution of the hydrogel. (3) Hydrogels were prepared as described above without fatty acid. At the desired stage in the formation process of the hydrogel, a solution of 16-DSA dissolved in 0.1 M KOH was simply poured onto the stable hydrogels.

Rheological characterization

The rheological characterization was performed to investigate the gelation kinetics as well as the viscoelastic behavior of the hydrogels. We define the gelation start-time as the time when loss and the storage modulus (G'' and G' , respectively) start to deviate, *i.e.* where the elastic behavior of the material is more pronounced than its viscous properties ($G' > G''$). Additionally, an evaluation of loss and storage modulus during this process has been recorded in order to obtain an insight into the stability of the hydrogels, the time they take to show steady state behavior and more generally the mechanical properties of the gels.

The experiments were performed using a Physica MCR 301 rheometer (Anton Paar, Graz, Austria) equipped with a CP50-2/

TG cone/plate measurement system. To avoid evaporation of water during the measurements the measuring gap was covered with silicon oil and the closing cap of the bracket was down. 0.5% oscillatory strain was applied throughout the experiment. The frequency of oscillations (ω) was set to 1 rad s⁻¹.

Transmission electron microscopy (TEM)

The samples of albumin precursor solutions (1 wt% (0.15 mM)) were prepared according to different gel preparation methods, explicitly, (1) incubated at 65 °C for 2 hours at neutral pH, (2) incubated at 50 °C for 24 hours at neutral pH, (3) incubated at 37 °C for 12 hours and the pH was set to 3.5 using 2 M HCl. The samples were prepared by spreading 5 μL of the dispersion onto a Cu grid coated with a Formvar-film (PLANO, Wetzlar, Germany). After 1 min, excess liquid was blotted off with filter paper and 5 μL of 1% aqueous uranyl acetate solution were placed onto the grid and drained off after 1 min. The dried specimens were examined with an EM 900 transmission electron microscope (Carl Zeiss Microscopy GmbH, Oberkochen, Germany). Micrographs were taken using an SSCCD SM-1k-120 camera (TRS, Moorenweis, Germany).

ATR IR spectroscopy

The secondary structure content of a protein sample can be characterized using vibrational (infrared and Raman) spectroscopy.²⁸ The characteristic IR bands of proteins are the amide I and amide II bands.^{29,30} While the amide I band is mainly due to the stretching vibration of C=O bonds of the amide group, the amide II band is primarily caused by bending vibrations of N–H bonds.^{30–32}

Attenuated Total Reflection (ATR) Fourier Transform Infrared Spectroscopy (FTIR) was used to examine how the secondary structure of serum albumin changes during hydrogel formation. A Bruker Tensor 27 FT-IR spectrometer equipped with a BioATRCeII and an LN-MCT photovoltaic detector and the OPUS Data Collection Program (all from Bruker, Ettlingen, Germany) were used for these experiments. 30 μL of an XSA precursor solution were pipetted onto the Si-crystal surface before heating the sample to the desired temperature by means of a circulating water bath using a HAAKE C25P thermostat. Spectral recording was started once the desired temperature was reached. The lag time due to heating was approx. 2 min. The spectra were obtained with the following parameters: resolution 4 cm⁻¹, scanning was conducted from 4000 to 900 cm⁻¹ (256 scans recorded), scanning velocity: 20 kHz, zero-filling factor: 4, apodization function: a Blackman-Harris 3-term. spectrometer and an ATR cell were purged with dry air. As a reference, an empty ATR cell was used. Each spectrum was corrected for water contributions by subtracting a spectrum of H₂O recorded at the same temperature and pH.

Principal component analysis (PCA) of IR data

PCA is a technique which transforms a number of possibly inter-correlated variables into a smaller number of orthogonal variables called principal components. In general terms, the



dimensionality of large datasets would be reduced by using a vector space transform. This way the user could spot trends and patterns in large datasets.³³ The goal is to de-correlate the original data by finding the directions along which the variance is maximized and then use these directions to define the new basis.³⁴ The first principal component (PC1) has the largest possible variance. The direction of the second largest variance in the data, which is orthogonal to PC1, is the second principal component (PC2). By using orthogonal projection of the data in the new principal component coordinate system onto PC1 or PC2, we achieve scores on PC1 and scores on PC2, respectively. The scores are plotted over time to assess the kinetics of the transition. Mathematically, the principal components are the eigenvalues of the covariance matrix of the data matrix X , where PC1 is the eigenvector with the highest eigenvalue, PC2 the eigenvector with the second highest eigenvalue, etc. X_{ij} contains the spectral intensities, where columns (j) represent the probed wavenumbers and rows (i) the different temperatures of measurement. After data transformation, $X_{ij} = S_{ij}P_{jj}$ where S_{ij} is the score matrix and P_{jj} contains

rows of PC1 to PC j . There is an extensive body of literature regarding PCA analysis and multivariate data analysis.^{34–36}

As our IR spectra contain several intricately linked and correlated changes in peak intensities,^{37,38} we evaluated them in a principal component analysis. The PCA was applied to the spectral range of 1600 to 1700 cm^{-1} after subtraction of a linear baseline and vector normalization of the spectra.

Principal component analysis was performed using the *prin-comp* function of MATLAB (MathWorks, Inc., USA).

Continuous wave (CW) EPR spectroscopy

CW EPR spectroscopy was used to investigate the fatty acid binding capacity of the hydrogels.³⁹

CW EPR spectroscopy as a magnetic resonance technique can be used to monitor and characterize the electronic and molecular structures, self-assembly, and dynamics of natively paramagnetic species and selectively introduced paramagnetic probe molecules under different conditions.^{40,41} To investigate the FA binding capacity of the serum albumin hydrogels, spin-labeled FAs were introduced into the hydrogels. Albumin–FA interactions can then be monitored by observing immobilization of rotational motion upon FA binding to albumin^{5,6} and according to changes in environmental polarity.^{42–44} We use spin-labeled stearic acid derivatives, which we have shown to be bound by albumin (both HSA and BSA) in solution and which report on the availability and chemical nature of long-chain fatty acid binding sites.^{5,16} The stearic acids are spin-labeled at position 16 from the carboxylic acid headgroup, hence called 16-DSA (16-doxyl stearic acid, free radical, 253596, ALDRICH), bearing a nitroxide doxyl group, Fig. 1C.

CW EPR spectra were recorded using a MiniScope MS400 (Magnetech, Berlin, Germany) spectrometer working at X-band (a microwave frequency of approximately $\nu = 9.4$ GHz and a magnetic field sweep of 15 mT centered at 340 mT). Temperatures were adjusted with a Temperature Controller H03 (Magnetech) with an accuracy of ~ 0.2 °C. The exact fre-

quency was recorded using a frequency counter (Racal Dana 2101, Neu-Isenburg, Germany). Absorption spectra were detected as first-derivative spectra through modulation⁵ and the simulations were performed using the EasySpin program package for MATLAB, in which the Schneider–Freed model of slow and intermediate rotational motion is implemented to solve the Schrödinger equation for slowly tumbling nitroxides.⁴⁵ The final simulated spectrum is the result of a linear (weighted) combination of three different components representing hydrophilic, hydrophobic and aggregated (micellized) spin probes.^{45,46}

Results & discussion

In general, hydrogels from serum albumin (HSA and BSA) are prepared from a precursor solution of HSA or BSA dissolved in deionized water. This precursor solution is converted into a gel during the incubation period, in which the temperature and/or pH of the solution as well as the incubation time are adjusted to obtain the desired hydrogels at certain stages of equilibration.

We found that by changing the pH value of the solution to the acidic range of 1.0 to 4.3 or the basic range of >10.6 , the pH induced hydrogels ($gXSA_p$) form at low temperatures. Moreover, a variety of different types of thermally induced hydrogels ($gXSA_T$) form at neutral pH of the precursor solution at different incubation times t_i and temperatures, even at temperatures much lower than the denaturation temperature of the respective protein. Fig. 1 shows $gXSA_T$ hydrogels, a plot of the crystal structures of HSA and BSA and the molecular structure of the EPR-active FA spin probe 16-DSA used in this study.

Viscoelastic behavior of the hydrogels

The rheological properties of protein solutions arise from intermolecular interactions between proteins that facilitate the formation of a cohesive continuous protein network. In viscoelastic protein solutions as they evolve during gelation, these noncovalent interactions include solvation, hydrophobic, van der Waals, electrostatic and dipolar interactions (like hydrogen bonding). The magnitude and number of these interactions as well as the interaction pattern/distribution determine the extent of conformational changes in the protein.⁴⁹ Fig. 2 depicts time-dependent rheological measurements of storage and loss moduli, G' and G'' , respectively, during the formation of $gXSA_{p/T}$ from 20 wt% precursor solutions at different temperatures. In Fig. 2(A) and (B), the temperature in HSA (A) and BSA (B) solutions at \sim pH 7 was increased to 65 °C (above the denaturation temperature). The storage modulus increases instantaneously above the loss modulus, suggesting that gelation starts immediately.

After the initially steep increase in the storage modulus curve in the first 15 minutes (900 s), the growth continues in a much slower manner. These results show that the storage modulus G' increases up to 20 000 Pa for BSA and 45 000 Pa for HSA after two hours, which are values typical of mechanically robust hydrogels (when the difference between G' and G''



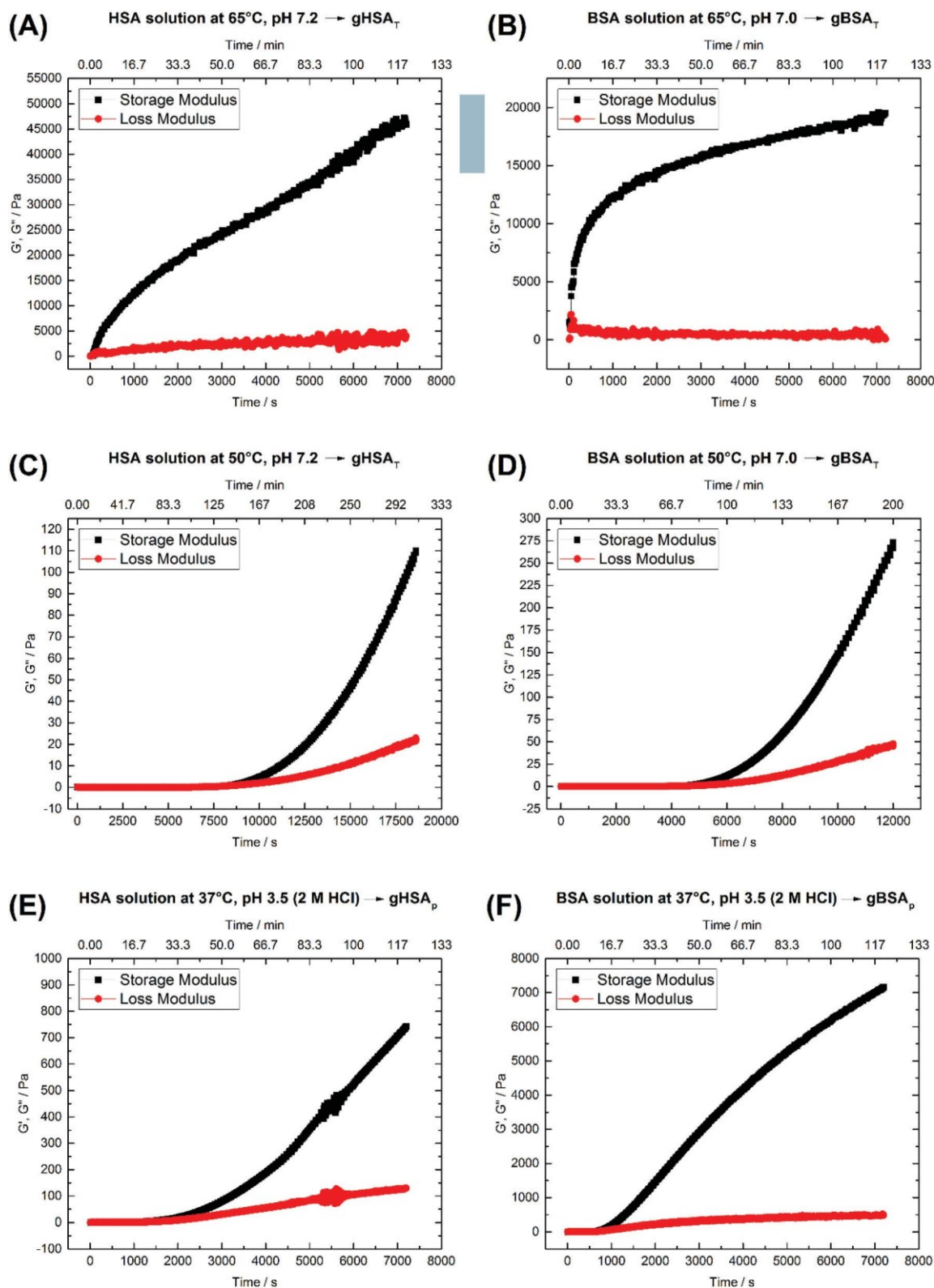


Fig. 2 Time-dependent storage (G') and loss (G'') moduli of 20 wt% (A) HSA precursor solution at 65 °C, pH 7.2 forming $gHSA_T(65,7.2,t)$, (B) BSA precursor solution at 65 °C, pH 7.0 forming $gBSA_T(65,7.0,t)$, (C) HSA precursor solution at 50 °C, pH 7.2 forming $gHSA_T(50,7.2,t)$, (D) BSA precursor solution at 50 °C, pH 7.2 forming $gBSA_T(50,7.2,t)$, (E) HSA precursor solution at 37 °C, pH 3.5 (2 M HCl used as an acid) forming $gHSA_p(37,3.5,t)$ and (F) BSA precursor solution at 37 °C, pH 3.5 (2 M HCl used as acid) forming $gBSA_p(37,3.5,t)$. See Table 1 for a comparison of the G' and G'' values at different time scales.



is more than 10 000 Pa after 1 hour, we assume the hydrogel to be mechanically robust). On the other hand, even longer incubation times do not necessarily lead to better mechanical properties, but in contrast may impair the water-holding capacity.

As one can see in Fig. 2(A) and (B), 45 minutes for the formation of gHSA_T(65,7.2,45) and 2 hours for gBSA_T(65,7.2,120) are good incubation times to achieve mechanically robust hydrogels at this temperature. In Fig. 2(C) and (D), we present the same experiments performed at 50 °C (12 degrees lower than the denaturation temperature of HSA and BSA). There was no sign of hydrogel formation after two hours, which can be expected under the assumption that gBSA_T does not form at temperatures below 62 °C.

However, on increasing the incubation time, the storage modulus increases above the loss modulus curve, indicating (at least weak) hydrogel formation. These low-temperature incubated hydrogels are mechanically much weaker than the ones formed above the denaturation temperature T_d of the protein. The storage modulus is two orders of magnitude smaller than that recorded at temperatures above T_d , see Fig. 2 (A–D), respectively. Moreover, the incubation time needed for gel formation is much longer and the hydrogel properties are strongly time dependent. Nonetheless, hydrogels with noticeable elastic behavior can be obtained at temperatures below T_d . Additionally, as the IR results suggest, see Fig. 4, serum albumin retains more of its native secondary structure during the gelation process as the temperature is lower. One may envision potential application of these hydrogels *e.g.* for fast small molecule (drug) release, but a study of the specific release profiles is outside the scope of this study.

Fig. 2(E) and (F) show the time-dependent results for gHSA_p(37,3.5, t) and gBSA_p(37,3.5, t) formation. In both cases the pH of the precursor solution of the hydrogel (20 wt%) was adjusted to 3.5 by adding 2 M HCl and time-dependent measurements of G' and G'' were performed at 37 °C. When inspecting Fig. 2(E) and (F), it appears that in these cases the deviation of G' from G'' commences considerably faster than for gHSA_T(50,7.2, t) and gBSA_T(50,7.2, t), namely at times below one hour. This is still not as fast as in the case of gHSA_T(65,7.2, t) and gBSA_T(65,7.2, t), though. Note that the exact time dependence is only valid for specified parameters *e.g.* the chosen frequency of ω (see Fig. S1†).

For probing the tertiary structure changes in the proteins constituting the hydrogels in an indirect and a “coarse grained manner”, we use our EPR-based platform for studying the capacity to bind long-chain fatty acids.^{5,6} Hence, we first examined how addition of fatty acids affects the gelation kinetics and the viscoelastic behavior of the hydrogels. It has been reported that SDS (Sodium Dodecyl Sulfate)²⁰ and long-chain fatty acids⁵⁰ increase the thermal stability of BSA and HSA in solution, respectively.

To analyze the potential effects of stearic acid (SA) on albumin gelation we repeated the gHSAT and gBSAT formation experiments in the presence of SAs at both 50 °C and 65 °C (HSA, BSA) during the formation of gXSAT and also at 37 °C for BSA. The results (see the ESI†) reveal that SAs lead to a

delayed onset of the gelation process and weaken the mechanical properties of the gels. Depending on the method of preparation and how the FAs are added to the solutions (see the EPR result part and the ESI†) gel formation is obstructed completely at certain molar ratios of albumin : FAs. It should be noted that 16-DSA and SA are EPR-spectroscopically shown to be interchangeable in their binding to HSA and BSA.^{5,6}

TEM images

With TEM, we can describe the morphological differences of albumin hydrogels prepared with different methods down to the scale of ~10 nm. Fig. 3 illustrates that in temperature-induced gXSA_T formation, protein fibrillation occurs more readily, even at 50 °C (Fig. 3(C)), compared to the pH-induced method, Fig. 3(D). On the other hand, TEM images, alongside other methods, reveal that protein aggregation is highly concentration dependent. To obtain TEM results, we had to dilute the precursor solution to 1 wt%, which is below the minimum concentration required for gel formation. Hence, the results can only give indications about the potential gelation processes taking place at higher precursor solution concentration (20 wt%). At very low concentration, very few protein fibrils are detected. Fig. 3(A) show the 1 wt% HSA solution and (B) 0.3 wt% HSA solution, incubated for 2 hours at 65 °C. While in (A) many smaller fibers in the length range of a few tens of nanometers are observable, in (B) fewer but longer and thicker fibers can be detected. This difference became more prominent when we lowered the temperature or when pH-induced gels and precursor solutions were used. In (C) and (D) it seems

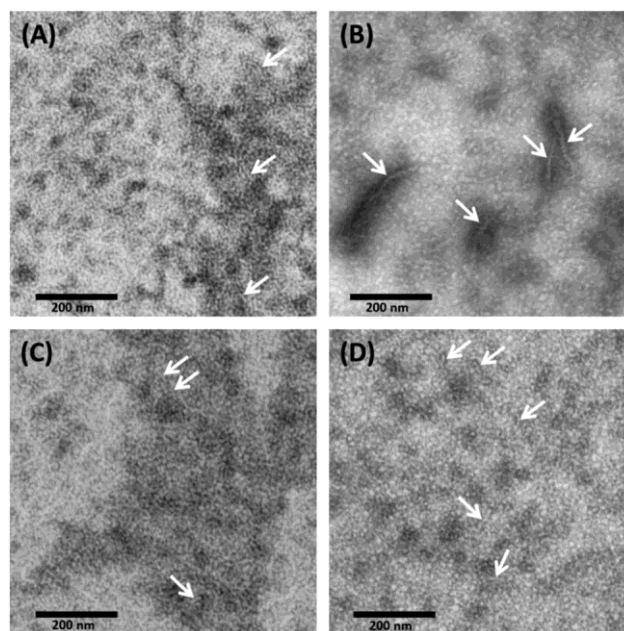


Fig. 3 TEM micrograph obtained from (A) 1 wt% HSA solution at neutral pH, incubated for 2 hours at 65 °C (B) 0.3 wt% HSA solution at neutral pH, incubated for 2 hours at 65 °C, (C) 1 wt% HSA solution at neutral pH, incubated for 24 hours at 50 °C and (D) 1 wt% HSA solution at pH 3.5 using 2 M HCl, incubated for 12 hours at 37 °C.



that a complex geometry of protein molecules is formed more than individual detectable fibers. However, some fibers (see the arrows in the TEM images) can also be spotted; these fibers are smaller in length and lower in abundance in comparison with (A). Due to the locally high concentration of protein in the samples used in TEM measurements, these results are helpful to obtain a deeper understanding of the results obtained by rheometry where the $gXSA_T(65,7,t)$ shows stronger mechanical properties and has a lower minimum concentration threshold for gel formation. At the same time, TEM results show that in $gXSA_T(65,7,t)$ fibers are longer and easier to detect. This correlation becomes clearer in the IR part.

In Fig. 3A, C and D, the average fiber diameter is 5 nm, whereas in B, fiber diameters of 5 and 10 nm were measured. The larger diameter is most probably due to aggregation of individual fibers.

The length of the fibers could not be determined since the flexible fibers are strongly intertwined so that the fiber ends could not be detected.

Secondary structure changes of serum albumin during gelation

According to its crystal structure, BSA contains 67% α -helices next to 10% β -turn and 23% extended chain configuration without any β -sheets. It is well known that changes in temperature, pH, ionic strength and other physical and chemical factors affect the secondary structure content.^{1,31,51} To study the changes in the secondary structure of the proteins, we performed time-dependent ATR-IR measurements during the gelation process (the hydrogels were formed on the ATR crystal of the spectrometer). As is known, hydrogel formation proceeds through the formation of β -sheets, which can include fibrillar morphologies as seen in TEM from our low concentration solutions.^{44,53} The bands at 1618 and 1684 cm^{-1} are attributed to the formation of intermolecular, hydrogen-bonded β -sheet structures that lead to protein aggregation or gel formation.⁵² As shown in Fig. 4, these bands increase during gelation in all cases, for $gXSA_p$ as well as $gXSA_T$ formation, at temperatures above or below the denaturation temperature. The β -sheet forms at the cost of native α -helical structure, suggesting that the intramolecular hydrogen bonds involved in α -helix formation become available for inter-molecular H-bonding, leading to three-dimensional network formation of the hydrogels. Hence, hydrogel formation and the accompanying secondary structure changes can be quantified through the ratio of α -helical to β -sheet content as reflected in the intensities of both bands ($I(\alpha\text{-helix})/I(\beta\text{-sheet})$).

The general trend shows a decrease in α -helix content while a new beta-sheet structure forms. However, the α -helix/ β -sheet ratio is different in each case, which can now be used to more quantitatively correlate the structural evolution with the differences in hydrogel properties prepared by the various methods described above. Fig. 4(A) and (B) shows the IR spectra of the gelation processes of $gHSA_T$ and $gBSA_T$ at 65 °C, respectively. When we compare these spectra with the respective spectra obtained at a gelation temperature of 50 °C (Fig. 4(C) and (D)),

we see that the α -helix/ β -sheet ratio is much higher for the latter (see the PCA evaluation part, Fig. 5 and the ESI, Fig. S3–S6†). This is an indication that the proteins experience notably less structural change during hydrogel formation when the temperature is below the denaturation temperature. Moreover, there is a dead time of ~ 2 minutes before T-equilibration is reached in the ATR-IR spectrometer. This is a critical time for gel formation in the case of $gHSA_T$ and $gBSA_T$ at 65 °C (see Fig. 2); hence, the first and potentially strongest decrease in the amount of α -helix content is hard to detect at this temperature. By comparing these results with those for the gelation of $gHSA_p$ and $gBSA_p$, shown in Fig. 4(E) and (F) alongside the rheological results, we can state the relations between the β -sheet/ α -helix ratio, gelation kinetics and mechanical properties, as listed in Table 2. For detailed information see the Discussion and the ESI.†

PCA evaluation

Fig. 5 shows the PC1 scores and the respective IR spectra for (a) $gBSA_T(50,7)$ and (b) $gBSA_p(37,3.5)$. In all cases (see also Fig. S3–S6†), more than 98% of changes can be comprised in one component (PC1), *i.e.* are strongly correlated. This principal component (red traces in Fig. 5C and D) describes a decrease in α -helical and random structure content and a concomitant increase in intermolecular β -sheet and turn content. However, PC1 is not identical for the different gels formed under different conditions. This indicates that the difference in ionic strength changes the gelation mechanism to some extent. In $gBSA_T(50,7)$ and in general the temperature-induced samples, hydrogel networks form by the formation of inter-molecular β -sheets at the cost of a reduction of α -helices (see Fig. S3–S5†). In the pH induced hydrogel formation $gXSA_p(37,3.5)$, see also Fig. S6,† PC1 is broader in the wavenumber region of 1640–1660 cm^{-1} than temperature induced ones. We speculate that this alteration can be explained since, in $gXSA_p(37,3.5)$, intermolecular β -sheets not only form by reduction of α -helix, but also by reduction of random coils, and this is why more α -helix content is preserved in the pH induced gelation mechanism.

To compare the kinetics of gelation at the molecular level with macroscopic results (see the Rheological characterization part), the PC1 scores *vs.* time are best fitted through a double exponential equation (1), revealing underlying fast and slow processes. The resulting time constants are summarized in Table 3. We can deduce that in all gelation mechanisms the majority of the changes at the molecular level occur during the fast process. This is decisively different from what one notices macroscopically by rheological measurements, especially in the case of $gXSA_T(50,7)$ and $gXSA_p(37,3.5)$, where there is a lag time before the transformation from a protein solution into a protein gel is observable. ATR-IR measurements show that in this lag time already secondary structure transitions occur. Precursor structures for the full gel state, such as XSA oligomers, might be formed in this faster process. After the onset of gelation, the secondary structure changes persist, but are



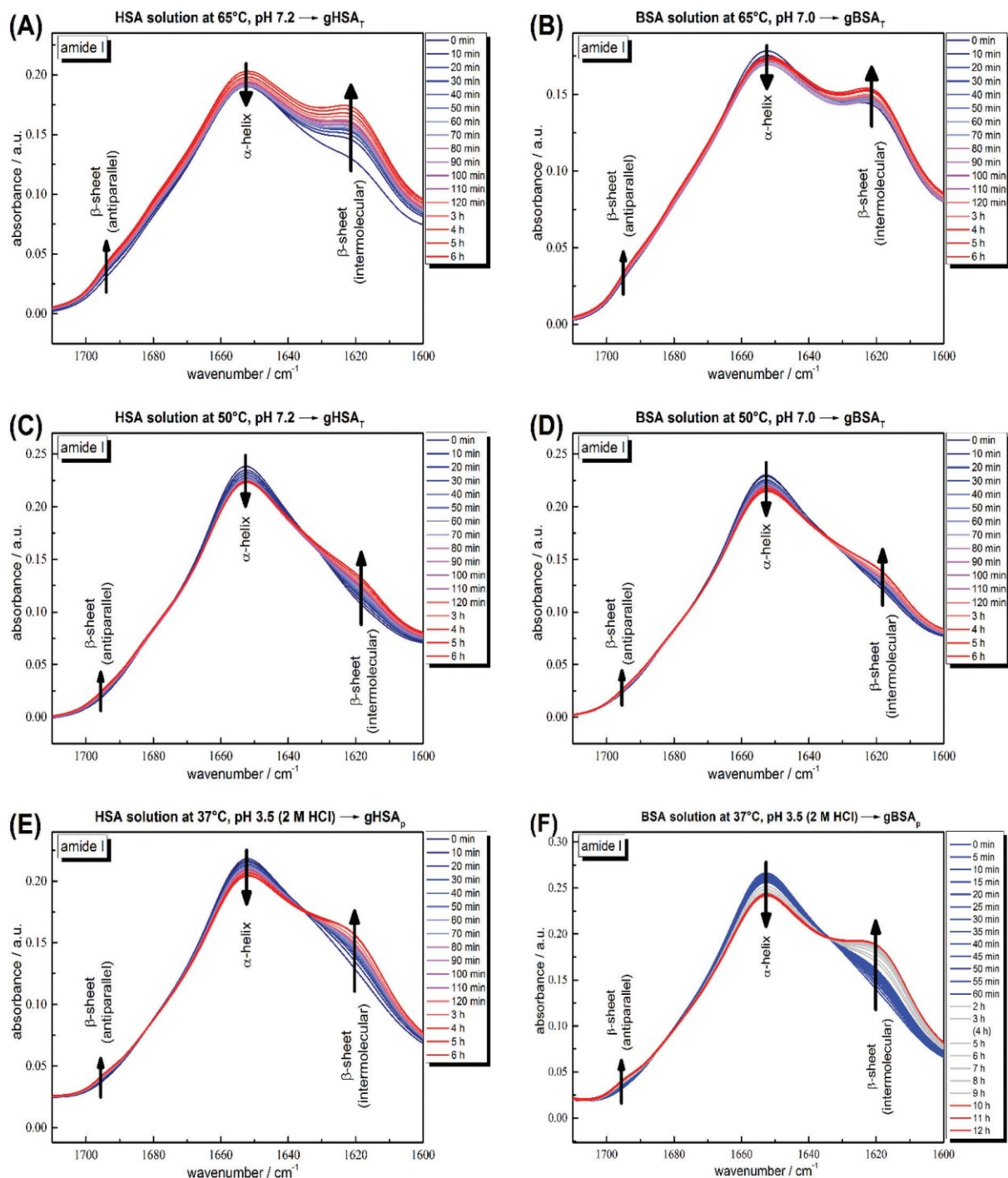


Fig. 4 Time-dependent ATR-IR measurements of 20 wt% (A) HSA precursor solution at 65 °C, pH 7.2 forming $gHSA_T(65,7.2,t)$, (B) BSA precursor solution at 65 °C, pH 7.0 forming $gBSA_T(65,7.0,t)$, (C) HSA precursor solution at 50 °C, pH 7.2 forming $gHSA_T(50,7.2,t)$, (D) BSA precursor solution at 50 °C, pH 7.2 forming $gBSA_T(50,7.2,t)$, (E) HSA precursor solution at 37 °C, pH 3.5 (2 M HCl used as an acid) forming $gHSA_p(37,3.5,t)$ and (F) BSA precursor solution at 37 °C, pH 3.5 (2 M HCl used as an acid) forming $gBSA_p(37,3.5,t)$. Band attributions are according to Clark *et al.*⁵²

slowed down (second time constant), probably due to hindered diffusion within the gel.

$$y \frac{1}{4} y_0 p A_1 1 - e^{-\frac{t}{\tau_1}} p A_2 1 - e^{-\frac{t}{\tau_2}} \quad \delta \rho$$

The time constants in Table 3 show the same trend as we observed in rheological characterization (see Table 2), *i.e.* both processes are faster at higher temperatures. However, these time constants are not characteristic numbers of the system, since they depend on the incubation time changes (in $gBSA_p(37,3.5,t)$).



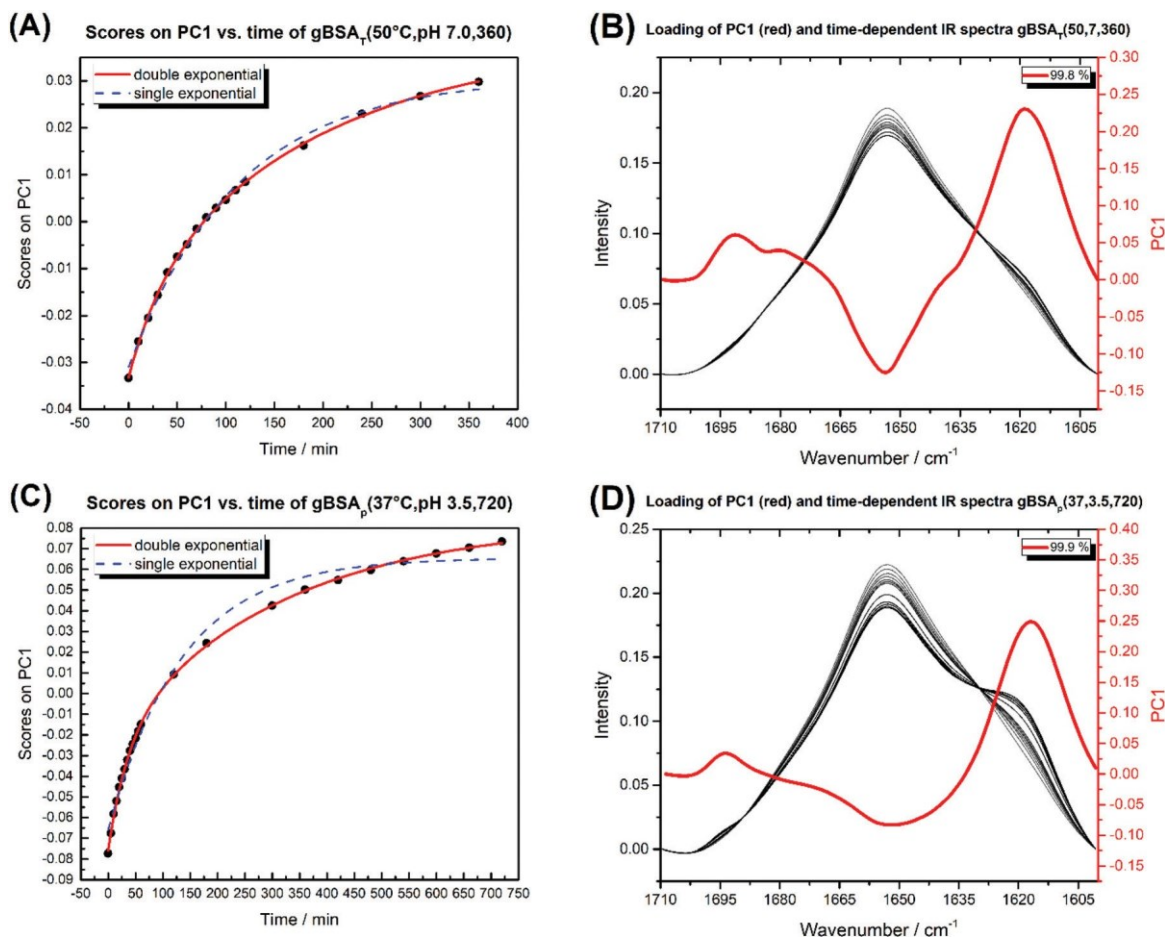


Fig. 5 (A) Diagram of PC1 scores against time for $gBSAT_{\tau}(50,7,t)$. (B) The time-dependent IR spectra of $gBSAT_{\tau}(50,7,t)$ (white to black) and the loading of PC1 in red. (C) Diagram of PC1 scores against time for $gBSA_p(37,3.5,t)$. (D) The time-dependent IR spectra of $gBSA_p(37,3.5,t)$ (white to black) and the loading of PC1 in red. The double and single exponential functions were fitted to PC1 scores vs. time. The obtained time constants are shown in Table 3.

Table 1 Comparison between G' and G'' values at different time scales in various gelation mechanisms of Fig. 2

Type	Temperature [°C]	pH	Fig. 2	15 min		60 min		120 min	
				G' [Pa]	G'' [Pa]	G' [Pa]	G'' [Pa]	G' [Pa]	G'' [Pa]
gHSAT	65	7	A	11 500	1220	27 300	2580	45 900	3980
gBSAT	65	7	B	12 000	715	16 300	309	19 500	568
gHSAT	50	7	C	0.00368	0.0492	0.00797	0.00328	0.0898	0.175
gBSAT	50	7	D	0.024	0.00865	0.0791	0.0619	34.7	7.62
gHSAp	37	3.5	E	1.74	1.03	141	46	742	130
gBSAp	37	3.5	F	123	46.8	3700	374	7160	479

$$gXSA_{\tau}(50,7,t) < gXSA_p(37,3.5,t) < gXSA_{\tau}(65,7,t)$$

Table 2 Relations between β -sheet/ α -helix ratio, gelation kinetics and mechanical properties

β -Sheet/ α -helix ratio

Gelation kinetics (from left to right: the incubation time needed shortens)

Mechanical properties (from left to right: the storage modulus increases)



To unravel similarities and differences between pH and temperature induced gelation processes we performed a simultaneous PCA on all three BSA as well as on all three HSA data-sets. In Fig. 6 we present the results of the gBSA analysis (for the gHSA analysis see Fig. S8†). Scores on PC2 are plotted against scores on PC1. Remarkably, we observe that in gXSA_T – regardless of the incubation temperature – PC2 is negligible. The gelation apparently follows the same mechanism at both

Table 3 Time constants (in minutes) of double exponential fitted curves on PC1 scores vs. time (Fig. 5)

	HSA			BSA		
	gHSA _T (65,7)	gHSA _T (50,7)	gHSA _p (37,3.5)	gBSA _T (65,7)	gBSA _T (50,7)	gBSA _p (37,3.5)
t_1	5.9	45	18	6	32	35
t_2	126	251	163	182	192	312

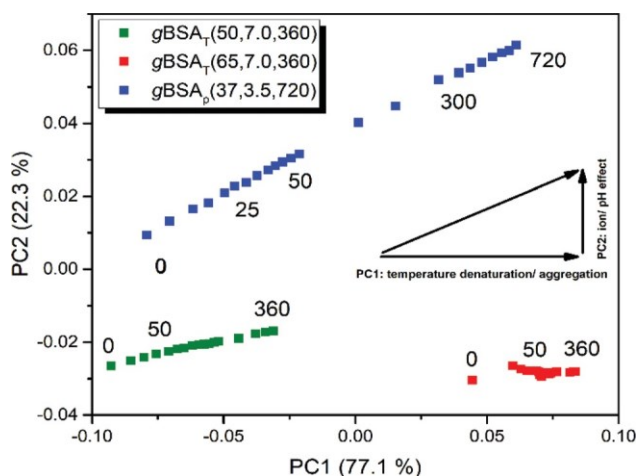


Fig. 6 Diagram of PC1 against PC2 scores during the gelation process of BSA. Blue squares depict the process of gBSA_p(37,3.5,720). The green and red squares depict the gBSA_T(50,7,360) and gBSA_T(65,7,360), respectively. All preparations were done on the ATR crystal. The PC2 component becomes relevant only for gBSA_p, where the pH was lowered to 3.5 by using 2 MHCl.

the investigated temperatures; however, the extent of the structural change described by PC1 is much higher at higher temperatures, as can be concluded from the higher scores on PC1. Interestingly, also gXSA_p reaches comparably high scores on PC1, even though the gelation is performed at low temperatures. In addition, PC2 plays a significant role (22% of total variance) in gXSA_p, *i.e.* it describes the differences in the gelation processes at neutral and acidic pH values. The main difference depicted by PC2 is a different content in β -turn structures, which is lower the higher the scores on PC2. This would imply a higher content in parallel β -sheets and un-

ordered structures in the gels formed at low pH value.

The pH value not only has an independent role in the gela-

tion process, but also it is an auxiliary factor for the role which temperature plays in the process; although the gXSA_p is being prepared at 37 °C the step changes of PC1 are far larger in gXSA_T prepared at 50 °C.

Fatty acid binding capacity of the hydrogels

The FA binding capacity of HSA and BSA in solution, including the dynamics of the bound FAs and also their distribution are known.^{5,54,55}

binding process and the bound states can be analyzed (see, *e.g.*, Akdogan *et al.*¹⁶ and Reichenwallner *et al.*⁵). BSA and HSA in their native isoform have also been found to feature 7 ± 1 long-chain fatty acid binding sites. In our experiments on the hydrogels and the gelation process, introducing amphiphilic spin-labeled FAs that are amenable to EPR spectroscopy is not as straightforward as for low-concentration solutions. We have tested the dynamics of the FAs for all three methods introduced in the Materials and Methods part for loading FAs into the hydrogel. Our results show that there are strong FA binding sites available inside the hydrogels, with certain differences in the final number of bound FAs. In the following, we describe EPR-spectroscopic results gained from the different methods of FA addition. Please note that the driving force for FA-binding to protein binding sites is the fact that the amphiphilic 16-DSA molecules partition between the more nonpolar/hydrophobic binding pockets and the surrounding aqueous solution with a strong preference for the protein-based pockets when available.

In Fig. 7(A) the spectra of our spin-probe FA, 16-DSA, dissolved in PBS buffer solution at 5 °C and 37 °C are shown; as expected the spectra reflect the freely tumbling FAs without protein. Fig. 7(B) and (C) show the spectral signatures of the individual 16-DSA fractions that contribute to the overall EPR spectrum. Spectra of the spin probes in polar/hydrophilic environments, in hydrophobic environments, and in micelles are shown in Fig. 7(B), while the spectra that show freely tumbling and strongly immobilized spin probes in FA binding sites of albumin are shown in Fig. 7(C). For a quantitative comparison, the simple rotational correlation time τ_c (the rotational correlation time is the average time it takes for a spin probe to rotate by one radian; in other words the time scale of individual stochastic fluctuations, which is calculated from the simulation parameter diffusion tensor D (rotational

p^{-1}
correlation time $\tau_c = \frac{1}{4} \frac{1}{\delta D_{xx}} (D_{yy} D_{zz} + 3))$, can be used to charac-

From CW EPR measurements, the long chain FA binding can be monitored quantitatively and even subtleties of the



terize the rotational reorientation, as shown in Table 4. Fig. 7 (D–F) display the spectra of 16-DSA that was introduced into the hydrogels through method (I). The results of (E) and (F) are comparable with the rheological characterization and IR spectra, as $gHSA_T(65,7)$ shows higher elasticity and a mechanically more robust gel; the FAs are also immobilized more strongly than in $gBSA_T(65,7)$; on the other hand, although there is no sign of freely tumbling FAs in $gHSA_T(65,7)$; less than 1% of FAs in $gBSA_T(65,7)$ are apparently unbound. This can be due to two reasons: smaller changes in the secondary structure of HSA during gelation (see the IR results) and/or the possibility that the hydrophobic regions of HSA are more

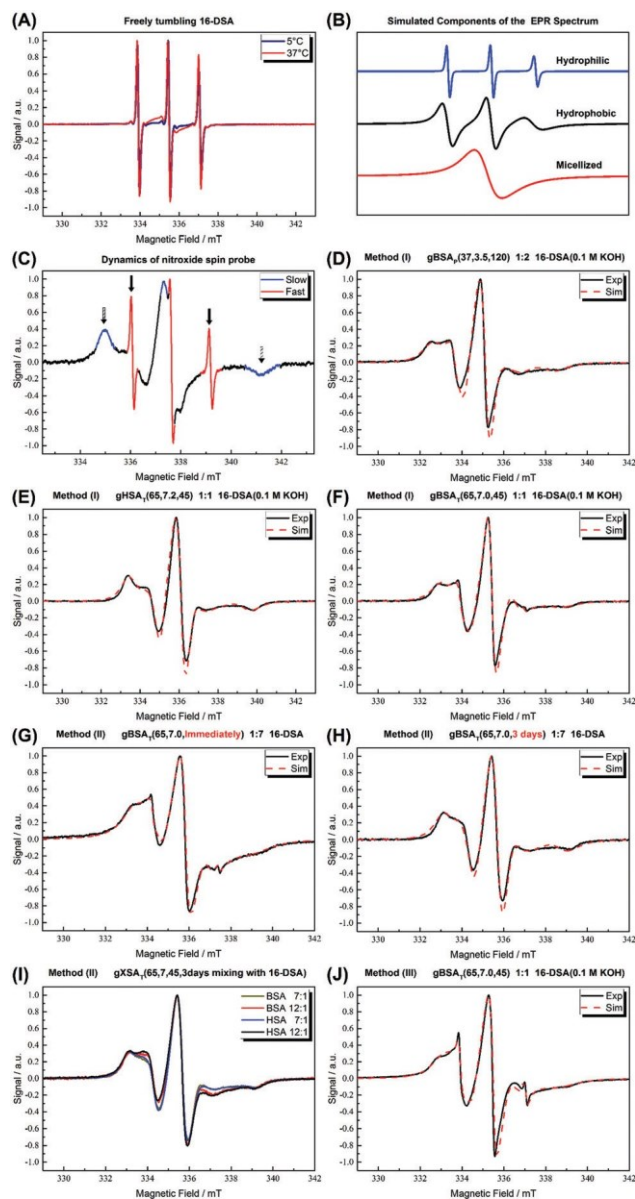


Fig. 7 (A) CW EPR spectra of 16-DSA in buffer solution at 5 °C and 37 °C are shown. As shown in ref. 5, the spectra are indicative of freely tumbling and micellized 16-DSA. (B) Simulated components of which the EPR spectra are composed. (C) Signatures of different regions of EPR spectrum for 16-DSA. (D) $gBSA_T(37,3.5,t)$ hydrogels at a 2 : 1 16-DSA : BSA molar ratio (method (I)). (E) $gHSA_T(65,7.2,t)$ hydrogels at a 2 : 1 16-DSA : HSA molar ratio prepared using method (1). (F) $gBSA_T(65,7.2,t)$ hydrogels at a 2 : 1 16-DSA : BSA molar ratio prepared using method (1). (G) $gBSA_T(65,7.0,t)$ prepared once after addition of 16-DSA due to method (2), FA : albumin molar ratios of 7 : 1 (F) $gBSA_T(65,7.0,t)$ prepared after letting the added 16-DSA be mixed with the precursor solution for 3 days due to method (2), FA : albumin

molar ratios of 7 : 1. (I) $gBSA_T(65,7.0,t)$ and $gHSA_T(65,7.0,t)$ hydrogels at high FA : albumin molar ratios of 7 : 1 and 12 : 1 (method (2)).

(J) $gBSA_T(65,7.0,t)$ prepared by method (3) where the 16-DSA solution is poured on the hydrogels prepared without 16-DSA, FA : albumin molar ratios of 1 : 1. The spectra were measured at 37 °C.

Table 4 Parameters of EPR spectra of Fig. 7

Figure	Fraction	Correlation time τ_c (ns)	Hyperfine splitting constant a (MHz)
D	93.6%	6.1	46.1
	6.4%	1.7	46.9
E	100%	8.9	45
F	99.3%	8.6	45.8
	0.7%	0.24	46.1
G	59.8%	4.5	44
	40%	14	45
H	0.2%	0.17	45.8
	100%	8.7	45.5
J	66.8%	11.9	45
	32%	4.9	42.8
	1.2%	0.17	46

easily reachable for FAs, as HSA is significantly more hydrophobic than BSA, indicated in the cumulative hydropathy index.¹⁶ Fig. 7(G) and (H) both show $gBSA_T(65,7)$ at 7 : 1 16-DSA : BSA ratio where the gels are prepared by method (II), and present the importance of mixing time. In Fig. 7(G), after introducing 16-DSA into the gel, the vials were put into the thermomixer for gel preparation; Fig. 7(H) shows the spectrum of 16-DSA in the hydrogel, in which the 16-DSA powder was simply added to the precursor solution, then shaken for 3 days and subsequently incubated in the thermomixer. Remarkably, it shows that almost 60% of 16-DSA shows intermediate rotational motion and only 40% are strongly bound to protein (immobilized). When the solution and FAs are mixed long enough all the FAs are bound to the BSA/HSA. In method (2), which gave the largest amount of immobilized 16-DSA molecules, as quantified from rigorous spectral simulations, the most striking finding spectroscopically is that regardless of the 16-DSA : albumin ratio, the spin-labeled FAs are all either strongly immobilized or at least intermediately immobilized (after a long enough mixing time), there is no sign of freely tumbling or micellized 16-DSA molecules. Both, the strongly and intermediately immobilized FAs, are spectral components that can be observed when studying FA-binding to BSA (or HSA) in low-concentration protein solutions. The strong rotational immobilization in BSA usually takes place in FA binding sites that can be found at the interfaces of α -helices.^{5,16,56} The intermediate-bound state(s), on the other hand, indicate more rotational freedom, which could stem from more transient attachment to BSA in water-swollen regions of the protein gels and that we could, *e.g.*, also identify in β -sheet structure forming elastin-like polypeptides.^{44,57} Finally, Fig. 7(J) shows the spectrum of $gBSA_T(65,7)$ in which 16-DSA are added into the gels through method (III).

Apparently, the 16-DSA molecules diffuse into the hydrogel and almost 67% of them are bound to protein-based binding sites and 32% form micelles (almost 1% are not bound and rotate freely). In addition, the value of the isotropic ^{14}N -hyperfine coupling of a nitroxide spectrum a_{iso} is indicative of the local polarity around the NO-group. High polarities lead to larger hyperfine coupling, while less polar environments shift



a_{iso} to lower values.^{43,57,58} All these quantitative results gained from rigorous simulation of the spectra are shown in Table 4. The preliminary results of EPR tests on the hydrogels using other spin-probes, namely TEMPO (214000 ALDRICH) and 4-hydroxy TEMPO benzoate (371343 ALDRICH), and their potential effect on the mechanical properties of the hydrogels are available in the ESI†

The EPR spectra thus also contain information comparable to those from ATR-IR experiments and rheological characterization, with the additional advantage of delivering these insights from a tracer molecule point of view and reflecting their interaction with the gel scaffolds. This might be of interest and direct use for applications in drug release.

A more detailed description of all these results, the specific conditions for each item, the role of time and mixing, the comparison between the spectra in solution and hydrogel state, and the diffusion of FAs into the hydrogels as observed in the FA addition method (3) are available in the ESI.†

Protein gelation as a process can be described as a phenomenon of protein aggregation in which the attractive and repulsive forces and the interactions between the polymer (protein) and the solvent, itself, and co-solutes are balanced so that a three-dimensional network or matrix forms. This matrix is able to trap or immobilize a large amount of solvent (water).⁵⁹

Since intermolecular contacts are pivotal for protein gelation, it is concentration dependent. There is a critical concentration for most globular proteins below which a gel network cannot form. This critical concentration is known as the least concentration endpoint (LCE).⁴⁹ It also includes differences in molecular properties such as net charge, molecular size, conformation and the number density of functional groups available for cross-linking and hence is protein-specific. Moreover, several extrinsic factors such as pH, ionic strength, incubation time, and temperature affect this value.

We have shown that thermally induced albumin hydrogels form at temperatures considerably below the denaturation temperature of serum albumin even at neutral pH values. In Fig. 8, we now summarize the combined macroscopic and nanoscopic insights gained into the gHSA_T and gBSA_T systems in approximated phase diagrams at different precursor solution concentrations and gHSA_p and gBSA_p phase diagrams at a fixed concentration, *i.e.* 20 wt% (3 mM) and different pH values and incubation times. These diagrams reflect the properties at a specific incubation time, which as described above is an important parameter in the parameter space of albumin gelation, of $t_i = 48$ hours. If the incubation time of these temperature-triggered gelation processes is varied, it can affect the shape of the phase diagrams drastically. Different types of gels shown in Fig. 8 are labeled according to their gelation kinetics and viscoelastic properties. In our categorization, gel type I represents gels that need several hours for formation and that have a $G' < 1000$ [Pa] even after 5 hours. Gel type II denotes the type of gel formed fast (in less than one hour) but with weak mechanical properties.

Gel type III has very strong mechanical properties and gelation happens very fast and their G' surpass 10 000 Pa after

1 hour. The rheological characterization (Fig. 2) suggests that gelation kinetics are dependent on both, temperature and pH value. We observe that in gXSA_p(37,3.5,120) the gelation starts earlier than in gXSA_T(50,7.0,120), despite the lower temperature and that it has a much higher storage modulus after the respective time periods. The PCA analysis of the FTIR spectra shows that at the molecular level we can observe the same trend, namely, the rate of change in the secondary structure of the protein follows the same trend as what we see at the macroscopic level (see Fig. 5, Fig. S3–S7 in the ESI†); however, in all cases the changes at the molecular level happen with a steep slope in the beginning of the gelation process and, depending on the preparation method, these changes become observable at the macroscopic level. One can even describe this as a two-stage process, with early fast formation of gel-point contacts (*e.g.* beta-sheet, or hydrophobic contacts, always from a highly concentrated solution) that have yet little effect on the mechanical, macroscopic properties. The contact formation slows down considerably in the second stage, when the solution has already turned considerably viscous, which slows down the new contact formation in the highly water-swollen sample. Further investigation provided a detailed view on how the pH value affects the gelation process of serum albumin. Interestingly, in the low-pH region of the gXSA_p diagrams in Fig. 8(C) and (D) we find a very delicate connection between the incubation time and the minimum temperatures needed to obtain gels. Moreover, pH 4.3 (acidic hydrogels forms below pH 4.3) is the pH value below which an abrupt transition between the so-called N form and F form of albumin occurs.^{60,61} This can thus be seen as the first step of protein denaturation that is necessary to form the electrostatically derived gels. The gels created at high pH-values (pH > 10.6) are not further investigated for their specific gelation kinetics and will be reported in a subsequent publication.

Considering the process of protein aggregation which leads to gel formation we can define a model process that involves an XSA transition state that is subsequently only then converted into intermolecular β -sheets when a concentration threshold is surpassed. Simplified, the gelation process of serum albumin can be seen as:



In this two stage scheme according to PCA analysis and IR results, the changes at the molecular level happen faster in the beginning of the gelation process (these changes are not observable macroscopically) until an intermediate state forms. Then on increasing the incubation time this intermediate state – by some local network formation – transforms into the gel state and from this stage on, we can observe hydrogel formation at the macroscopic level (see the Rheological characterization part).

To further substantiate this postulated process, we used a 5 wt% (0.75 mM) HSA/BSA precursor solution (below the LCE) to repeat all the IR-based experiments described above. Despite an, also in this case, observable reduction in α -helical content, there is no sign of intermolecular β -sheet formation.



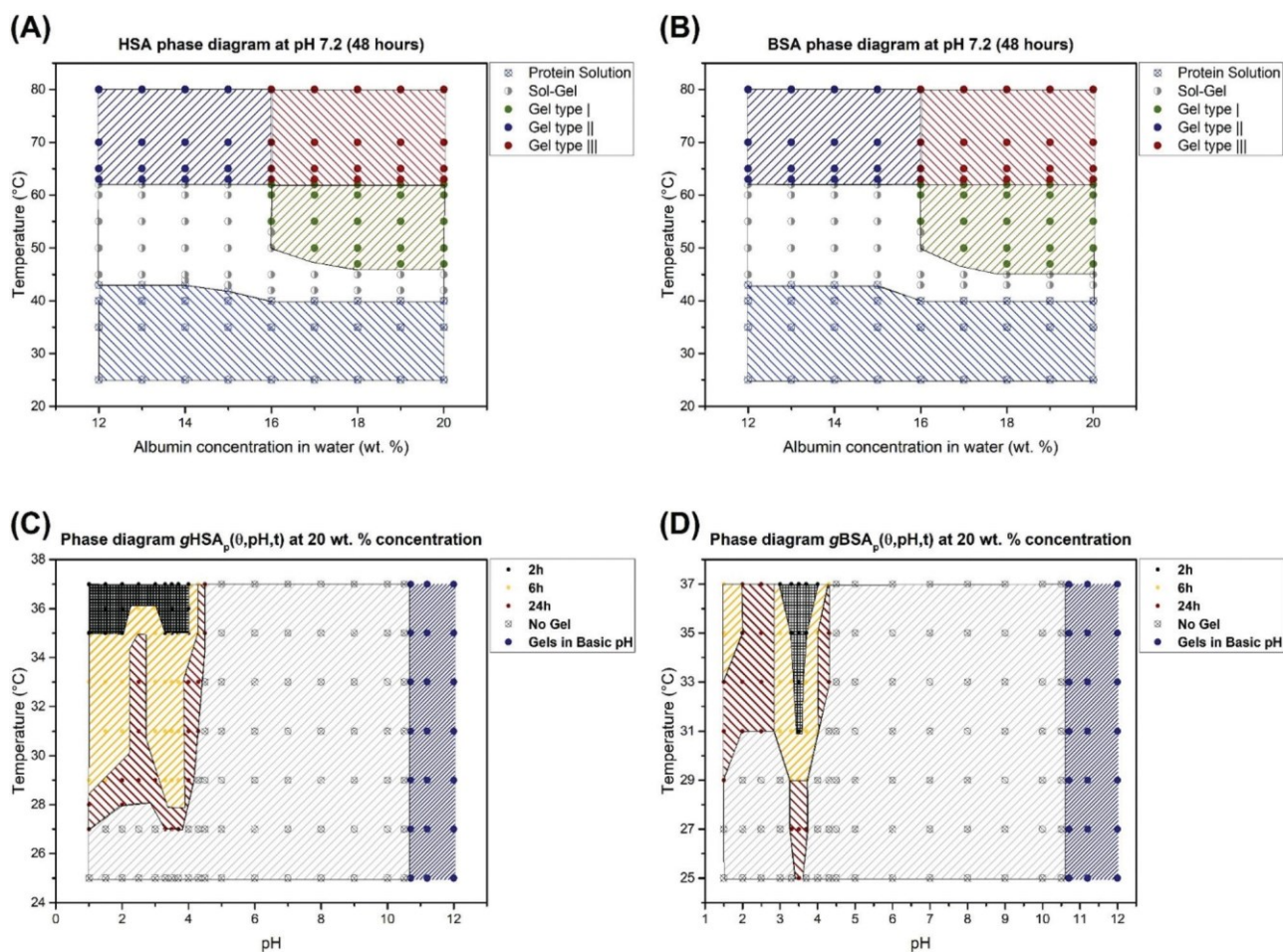


Fig. 8 (A) Phase diagram for human serum albumin-based gels after 48 hours based on different concentrations and temperatures. (B) Phase diagram for bovine serum albumin-based gels after 48 hours based on different concentrations and temperatures. These phase diagrams are valid only for the time scale of 48 hours. Changing this time may affect the shape of these phase diagrams. (C) Phase diagram for 20 wt% HSA solution at different pH values and incubation times. 2 h means that for gel formation after a maximum of 2 hours the gels form (according to the temperature and pH value), and the same applies for 6 hours and 24 hours showing the maximum time needed for obtaining hydrogels. Gels at high pH values ($\text{pH} > 10.6$) form in less than 2 hours at RT. (D) The same phase diagram for 20 wt% BSA solution.

The IR results back the speculation that the incubation time can affect the properties of the hydrogels in a non-trivial fashion. In Fig. 4(A) we observe that after two hours the trend of β -sheet formation at the cost of α -helix reduction is reversed; namely, the β -sheet content is reduced and a new structure (whether α -helix or random coil cannot be distinguished at ease) forms. This is even observable at the macroscopic level, in which the hydrogel structure is damaged in such a way that its water-holding capacity is diminished, see Fig. 2(A), and after almost 80 minutes there is a jump in the storage modulus, which is attributable to the loss of water and an increase in the protein concentration.

The TEM micrographs of the (produced from diluted precursor solutions) gel-state samples also support the idea that at the molecular level, β -sheet formation leads to fibrillar morphologies, as is well known from amyloid-forming proteins. pH-Induced gels show much smaller and less fibrillar structures that are rather reminiscent of larger networks.

From a thermodynamics point of view, there is an entropy gain during gel formation. The unfolding and rearrangement of the proteins from intra- to intermolecular interfaces is an entropy-driven process, in which the transfer of the nonpolar residues from the aqueous phase to the non-aqueous phase and the consequent release of water molecules from the hydration shells of these groups increase the overall entropy.⁴⁹ This process is affected by the intramolecular constraints and extensive segment–segment interactions in the folded state and particularly by covalent linkages such as the eight pertinent disulfide bonds in both BSA and HSA.⁶² In low-concentration solutions, one would summarize the conformational changes that happen even at human body- or room temperature under protein degradation – it is apparent that above a certain concentration threshold of the serum albumin solution, the equilibrium during the degradation is shifted to protein aggregation and/or gel formation, which can therefore take place at low temperatures, e.g. 37 °C when the gelation



incubation time increases, to *e.g.* 72 hours. Other factors like the pH value are auxiliary to this process, and may affect the gelation kinetics, LCE, *etc.*

The investigation of the FA binding capacity of the hydrogels shows that the FAs are bound inside the hydrogels. Depending on the method one uses to introduce the FAs into the hydrogels (see Fig. 7) the amount of FAs that can be bound by the hydrogels and also the strength of the binding sites differ. In method (2) in which the solid powder 16-DSA is added directly to the precursor solution, the largest amount of FAs is trapped inside the hydrogels. When one dissolves the FAs into the KOH and then adds this solution to the precursor solution of the hydrogel, at high albumin : FA ratios, first of all the overall concentration of the protein decreases, leading to mechanically weaker hydrogels until no hydrogels form at all. As described above, besides the 16-DSA molecules that are strongly immobilized, the intermediately immobilized FAs with more residual rotational mobility in the hydrogels are indicative of water-swollen nanoscopic regions, as evidenced by the higher a_{iso} values. The mesh size of the hydrogels and the nanoscopic water pools also play an important role. In method (2) we observe that the FAs do not form micellar aggregates when the mixing time is sufficient (see Fig. 7(G, H, I)), which indicates that the FAs are homogeneously spread all over the gel and there is just a few of them in each hydrophilic part. That is the reason why method (2) gives the possibility of loading even more than 7 FAs per protein in the hydrogels, information that again in the light of potential uses in controlled drug release is of high interest.

Conclusions

We have presented different synthetic methods for the preparation of HSA (for the first time) and BSA hydrogels and characterized and correlated their macroscopic and nanoscopic features. Our results considerably expand the range of thermally induced albumin hydrogels. We have shown that hydrogels can be formed at incubation temperatures significantly below the denaturation temperature of the protein. The critical role of the gelation incubation time in protein aggregation and gelation phenomena is discussed explicitly and the phase spaces of thermally induced and electrostatically triggered gels are explored in phase diagrams for HSA and BSA, based on temperature, concentration, pH and time.

Additionally, we were able to provide more details building on the pioneering work of Baler *et al.*²² on electrostatically triggered BSA hydrogels and their gelation mechanism. Changing the charge distribution on the BSA by changing the pH causes partial denaturation of the protein. Newly exposed hydrophobic areas and the presence of counter-ions facilitate the hydrogel formation of BSA at low temperature. We showed that the pH range is significantly broader than what is suggested and extended this research to HSA. The preliminary results of our experiments also suggest that the counter-ion not only affects the minimum protein concentration required for gela-

tion, but also affects the stability of the hydrogels, gelation kinetics, mechanical properties and, notably, the fatty acid (FA) binding capacity of the gels. On the other hand, regardless of the acids or bases used to change the pH of the protein solution, the pH range in which electrostatically induced hydrogels can, in principle, be formed is bound to below pH 4.3 and above pH 10.6.

Rheological characterization, a study of secondary structure changes of proteins during gelation *via* ATR-IR spectroscopy and an investigation of the FA binding capacity of the hydrogels by CW EPR spectroscopy together indicate a two-stage gelation process of hydrogel formation from this family of abundant biomacromolecules. We hope that this initial study, which connects the nanoscopic properties with the macroscopic features of the hydrogels leading to phase diagrams, will pave the way also for their exploration in applications such as controlled release of (bio-)molecules.

Conflicts of interest

There are no conflicts of interest to declare.

Acknowledgements

We thank Annekatrin Rother for recording the electron micrographs and Franziska Zeuner and Heike Schimm for technical support. This work was supported by the European Regional Development Fund (ERDF) and the Federal State of Saxony-Anhalt.

References

- 1 T. Peters Jr., in *All About Albumin*, Academic Press, San Diego, 1995, pp. 9–II, DOI: 10.1016/B978-012552110-9/50004-0.
- 2 Y. S. Day and D. G. Myszkka, *J. Pharm. Sci.*, 2003, 92, 333–343.
- 3 M. L. Ferrer, R. Duchowicz, B. Carrasco, J. G. de la Torre and A. U. Acuna, *Biophys. J.*, 2001, 80, 2422–2430.
- 4 E. Gianazza, M. Galliano and I. Miller, *Electrophoresis*, 1997, 18, 695–700.
- 5 J. Reichenwallner and D. Hinderberger, *Biochim. Biophys. Acta, Gen. Subj.*, 2013, 1830, 5382–5393.
- 6 M. J. N. Junk, H. W. Spiess and D. Hinderberger, *Angew. Chem., Int. Ed.*, 2010, 49, 8755–8759.
- 7 M. J. N. Junk, H. W. Spiess and D. Hinderberger, *J. Magn. Reson.*, 2011, 210, 210–217.
- 8 N. A. Peppas, J. Z. Hilt, A. Khademhosseini and R. Langer, *Adv. Mater.*, 2006, 18, 1345–1360.
- 9 B. V. Slaughter, S. S. Khurshid, O. Z. Fisher, A. Khademhosseini and N. A. Peppas, *Adv. Mater.*, 2009, 21, 3307–3329.
- 10 I. M. El-Sherbiny and M. H. Yacoub, *Global Cardiol. Sci.*



Pract., 2013, 2013, 316–342.

- 11 E. A. Foegeding, *Am. Oil Chem. Soc.*, 1989, 58, 185–194.
- 12 A. H. Clark, G. M. Kavanagh and S. B. Ross-Murphy, *Food Hydrocolloids*, 2001, 15, 383–400.
- 13 D. Seliktar and L. Oss-Ronen, *US 20110238000A1*, 2011.
- 14 Y. Sun and Y. Huang, *J. Mater. Chem. B*, 2016, 4, 2768–2775.
- 15 F. Iemma, U. G. Spizzirri, F. Puoci, R. Muzzalupo, S. Trombino and N. Picci, *Drug Delivery*, 2005, 12, 229–234.
- 16 Y. Akdogan, J. Reichenwallner and D. Hinderberger, *PLoS One*, 2012, 7, e45681.
- 17 J. D. Ferry, in *Advances in protein chemistry*, ed. M. L. Anson and T. E. John, Academic Press, 1948, vol. 4, pp. 1–78.
- 18 H. Jian, Y. L. Xiong, F. Guo, X. Huang, B. Adhikari and J. Chen, *Int. J. Food Sci. Technol.*, 2014, 49, 2529–2537.
- 19 X. D. Sun and R. A. Holley, *Compr. Rev. Food Sci. Food Saf.*, 2011, 10, 33–51.
- 20 J. I. Boye, I. Alli and A. A. Ismail, *J. Agric. Food Chem.*, 1996, 44, 996–1004.
- 21 D. C. Carter and J. X. Ho, *Adv. Protein Chem.*, 1994, 45, 153–203.
- 22 K. Baler, R. Michael, I. Szleifer and G. A. Ameer, *Biomacromolecules*, 2014, 15, 3625–3633.
- 23 S. Damodaran, *Interrelationship of molecular and functional properties of food proteins Food Proteins*, 1989.
- 24 N. Matsudomi, D. Rector and J. Kinsella, *Food Chem.*, 1991, 40, 55–69.
- 25 M. Paulsson, P. O. Hegg and H. B. Castberg, *J. Food Sci.*, 1986, 51, 87–90.
- 26 M. Yamasaki, H. Yano and K. Aoki, *Int. J. Biol. Macromol.*, 1990, 12, 263–268.
- 27 K. Baler, O. A. Martin, M. A. Carignano, G. A. Ameer, J. A. Vila and I. Szleifer, *J. Phys. Chem. B*, 2014, 118, 921–930.
- 28 A. Barth, *Biochim. Biophys. Acta, Bioenerg.*, 2007, 1767, 1073–1101.
- 29 A. Bouhekka and T. Bürgi, *Appl. Surf. Sci.*, 2012, 261, 369–374.
- 30 J. Kong and S. Yu, *Acta Biochim. Biophys. Sin.*, 2007, 39, 549–559.
- 31 R. Lu, W.-W. Li, A. Katzir, Y. Raichlin, H.-Q. Yu and B. Mizaikoff, *Analyst*, 2015, 140, 765–770.
- 32 S. Krimm and J. Bandekar, *Adv. Protein Chem.*, 1986, 38, 181–364.
- 33 H. Abdi and L. J. Williams, *Wiley Interdiscip. Rev.: Comput. Stat.*, 2010, 2, 433–459.
- 34 J. Shlens, 2014, arXiv preprint arXiv:1404.1100.
- 35 S. Dray, *Comput. Stat. Data Anal.*, 2008, 52, 2228–2237.
- 36 *Principal Component Analysis*, ed. I. T. Jolliffe, Springer New York, New York, NY, 2002, pp. 150–166, DOI: 10.1007/0-387-22440-8_7.
- 37 P. Robert, M. F. Devaux and D. Bertrand, *J. Near Infrared Spectrosc.*, 1996, 4, 75–84.
- 38 C. Schwiager and M.-H. Ropers, *Food Hydrocolloids*, 2013, 30, 241–248.



- 39 M. Kaupp, M. Bühl and V. G. Malkin, in *Calculation of NMR and EPR Parameters*, Wiley-VCH Verlag GmbH & Co. KGaA, 2004, pp. 1–5, DOI: 10.1002/3527601678.ch1.
- 40 D. Hinderberger, H. W. Spiess and G. Jeschke, *J. Phys. Chem. B*, 2004, 108, 3698–3704.
- 41 N. M. Atherton, *Principles of electron spin resonance*, Ellis Horwood, New York, revised edition, 1993.
- 42 M. J. N. Junk, W. Li, A. D. Schlüter, G. Wegner, H. W. Spiess, A. Zhang and D. Hinderberger, *Angew. Chem., Int. Ed.*, 2010, 49, 5683–5687.
- 43 D. Kurzbach, M. J. N. Junk and D. Hinderberger, *Macromol. Rapid Commun.*, 2013, 34, 119–134.
- 44 K. Widder, S. R. MacEwan, E. Garanger, V. Nunez, S. Lecommandoux, A. Chilkoti and D. Hinderberger, *Soft Matter*, 2017, 13, 1816–1822.
- 45 D. J. Schneider and J. H. Freed, in *Spin Labeling: Theory and Applications*, ed. L. J. Berliner and J. Reuben, Springer US, Boston, MA, 1989, pp. 1–76, DOI: 10.1007/978-1-4613-0743-3_1.
- 46 K. A. Earle and D. E. Budil, in *Advanced ESR Methods in Polymer Research*, John Wiley & Sons, Inc., 2006, pp. 53–83, DOI: 10.1002/047005350X.ch3.
- 47 S. Sugio, A. Kashima, S. Mochizuki, M. Noda and K. Kobayashi, *Protein Eng.*, 1999, 12, 439–446.
- 48 K. A. Majorek, P. J. Porebski, A. Dayal, M. D. Zimmerman, K. Jablonska, A. J. Stewart, M. Chruszcz and W. Minor, *Mol. Immunol.*, 2012, 52, 174–182.
- 49 S. Damodaran, *IFT Basic Symp. Ser.*, 1994, 9, 1–37.
- 50 P. D. Ross and A. Shrake, *J. Biol. Chem.*, 1988, 263, 11196–11202.
- 51 D. Charbonneau, M. Beauregard and H.-A. Tajmir-Riahi, *J. Phys. Chem. B*, 2009, 113, 1777–1784.
- 52 A. H. Clark, D. H. Saunderson and A. Suggett, *Int. J. Pept. Protein Res.*, 1981, 17, 353–364.
- 53 D. Kurzbach, V. S. Wilms, H. Frey and D. Hinderberger, *ACS Macro Lett.*, 2013, 2, 128–131.
- 54 S. Curry, P. Brick and N. P. Franks, *Biochim. Biophys. Acta, Mol. Cell Biol. Lipids*, 1999, 1441, 131–140.
- 55 V. A. Livshits and D. Marsh, *Biochim. Biophys. Acta, Biomembr.*, 2000, 1466, 350–360.
- 56 A. A. Bhattacharya, T. Grüne and S. Curry, *J. Mol. Biol.*, 2000, 303, 721–732.
- 57 D. Kurzbach, W. Hassouneh, J. R. McDaniel, E. A. Jaumann, A. Chilkoti and D. Hinderberger, *J. Am. Chem. Soc.*, 2013, 135, 11299–11308.
- 58 D. R. Kattinig and D. Hinderberger, *Chem. – Asian J.*, 2012, 7, 1000–1008.
- 59 R. H. Schmidt, *Gelation and coagulation Protein Functionality in Foods*, 1981.
- 60 W. Qiu, L. Zhang, O. Okobiah, Y. Yang, L. Wang, D. Zhong and A. H. Zewail, *J. Phys. Chem. B*, 2006, 110, 10540–10549.
- 61 J. Reichenwallner, C. Schwieger and D. Hinderberger, *Polymers*, 2017, 9, 324.
- 62 S.-H. Chong and S. Ham, *Chem. Phys. Lett.*, 2012, 535, 152–156.

Communication

The Effect of Ethanol on Gelation, Nanoscopic, and Macroscopic Properties of Serum Albumin Hydrogels

Seyed Hamidreza Arabi , David Haselberger and Dariush Hinderberger * 

Institut für Chemie, Martin-Luther-Universität Halle-Wittenberg, Von-Danckelmann-Platz 4, 06120 Halle, Germany; seyed.arabi@chemie.uni-halle.de (S.H.A.); david.haselberger@student.uni-halle.de (D.H.)

* Correspondence: dariush.hinderberger@chemie.uni-halle.de; Tel.: +49-345-552-5230

Academic Editor: Mircea Teodorescu



Received: 24 March 2020; Accepted: 16 April 2020; Published: 21 April 2020

Abstract: Serum albumin has shown great potential in the development of new biomaterials for drug delivery systems. Different methods have been proposed to synthesis hydrogels out of serum albumin. It has been observed that ethanol can also act as a trigger for serum albumin denaturation and subsequent gelation. In this study, we focus on basic mechanisms of the albumin gelation process at 37 °C when using the chemical denaturant ethanol. The temperature of 37 °C was chosen to resemble human body temperature, and as under physiological conditions, albumin is in a non-denatured N conformation. As established in our previous publication for the triggers of pH and temperature (and time), we here explore the conformational and physical properties space of albumin hydrogels when they are ethanol-induced and show that the use of ethanol can be advisable for certain gel properties on the nanoscopic and macroscopic scale. To this end, we combine spectroscopic and mechanically (rheology) based data for characterizing the gels. We also study the gels⁰ binding capacities for fatty acids with electron paramagnetic resonance (EPR) spectroscopy, which implies observing the effects of bound stearic acids on gelation. Ethanol reduces the fraction of the strongly bound FAs in bovine serum albumin (BSA) hydrogels up to 52% and induces BSA hydrogels with a maximum storage modulus of 5000 Pa. The loosely bound FAs in ethanol-based hydrogels, besides their relatively weak mechanical properties, introduce interesting new materials for fast drug delivery systems and beyond. **Keywords:** serum albumin; hydrogels; drug delivery; materials science; protein denaturation

1. Introduction

Serum albumin is the most abundant protein in vertebrate blood plasma with typical concentrations of 35–45 mg/mL (0.53–0.68 mM) [1]. It is essential for the oncotic pressure and serves as carrier for many

hydrophobic substances in the blood plasma [1]. It has the molar mass of approximately 66.000 Da [2]) and consists on average of 585 amino acids [3]. Due to its availability at high purity and relatively low price, serum albumin is used for many physicochemical and biochemical studies [3,4]. Human serum albumin (HSA) is mainly used for medical, metabolism and genetic research [3]. Bovine serum albumin (BSA) shares 75.52% of its primary structure with HSA [3]. It is used as a model protein for in vitro tasks [3]. In a previous study, we have shown that HSA and BSA both display a complex and rich phase behavior that includes very interesting methods pioneered by Baler et al. of achieving protein hydrogels based on thermal denaturation or triggering electrostatic interaction networks through changes in pH [5,6].

Serum albumin has shown promising properties to develop new biomaterials for drug delivery systems [5]. Through thermal or chemical methods and at the cost of loss of native α -helices in the structure, there is a potential to form intermolecular β -sheets leading to a cage-like structure in which

water or other molecules can be trapped [6]. The goal is to synthesize gels with high stability and biocompatibility, and the luxury of being able to tailor the properties based on certain requirements.

In our previous work [6], the properties of bovine, and for the first time human, serum albumin (BSA and HSA, respectively) gels generated through tuning of pH or temperature as established by Baler et al. [5] have been extensively studied. The incubation time of the gels has been introduced as an excellent parameter for fine-tuning of gel properties and the data were summarized in phase diagrams [6]. Starting from this point, in preliminary tests, gel formation has been observed in a mixture

with a wide variety of different BSA and ethanol concentrations after an incubation time of 16 h at 37 °C. To understand the properties of these hydrogels and their differences compared to hydrogels made based on other methods (pH- and temperature-induced), different aspects have been systematically investigated, namely (i) at which concentrations of bovine serum albumin and ethanol hydrogels form, (ii) how these different concentrations affect the mechanical stability of the gels, (iii) what molecular structure changes are observable depending on time, (iv) how stearic acids affect the gelation process, and (v) how the fatty acid (FA) binding capacity of the hydrogels changes. Fatty acids are chosen as there are seven FA binding sites in albumin that are known to stabilize the tertiary structure of individual albumin proteins [7,8].

To achieve this, the rheological properties during the gelation process are measured, the changes in secondary structure are characterized using their IR-spectroscopic signatures, and a nanoscopic view on the fatty acid (FA) binding capacity of albumin hydrogels by means of electron paramagnetic resonance (EPR) spectroscopy, both of which have been established before [6].

2. Results

The gelation experiments have been performed in several experimental setups, generally in a thermomixer (under shaking, see Materials and Methods). Gel formation has then also been studied in the rheometer for rheological experiments, in the IR spectrometer (ATR setup), and the EPR spectrometer during the respective spectroscopic measurements.

2.1. General Gelation Properties

As shown in Figure 1, a wide variety of the different BSA and ethanol concentrations displays a complex phase diagram after an incubation time of 16 h at a temperature of 37 °C. All gelation experiments were performed at a neutral pH (approximately 7.2), allowing an overall mild environment. This comes at the cost of mechanical stability and binding capacity compared to the other methods, putting more chemical or thermal stress on the protein solutions [6].

Figure 1 illustrates the property (ethanol mole fraction versus BSA mole fraction) space of samples prepared at 37 °C after an incubation time of 16 h. The mole fractions were used to remove the effect of volume dilution that would have to be taken into account for the concentrations. As mentioned above, there also seems to be a minimum amount of BSA needed for the gelation. Below this concentration (1.07 mM), the proteins cannot form enough cross-links to build a gel, potentially because of low probabilities for intermolecular secondary structure (β -sheet) formation. The absolute values (without ethanol) for gel formation have been extensively studied in a previous publication [6] to find the absolute minimum with ethanol; more experiments are needed and are beyond the scope of this study. Another interesting phenomenon can be observed by the addition of high amounts of ethanol. At molar fractions between 0.3 and 0.35 of ethanol, the obtained gels show a high turbidity. After adding more ethanol, only a turbid liquid is obtained. Nevertheless, above a molar fraction of 0.49, turbid gels can be observed again. The turbidity reflects the inhomogeneity of the gel structure.

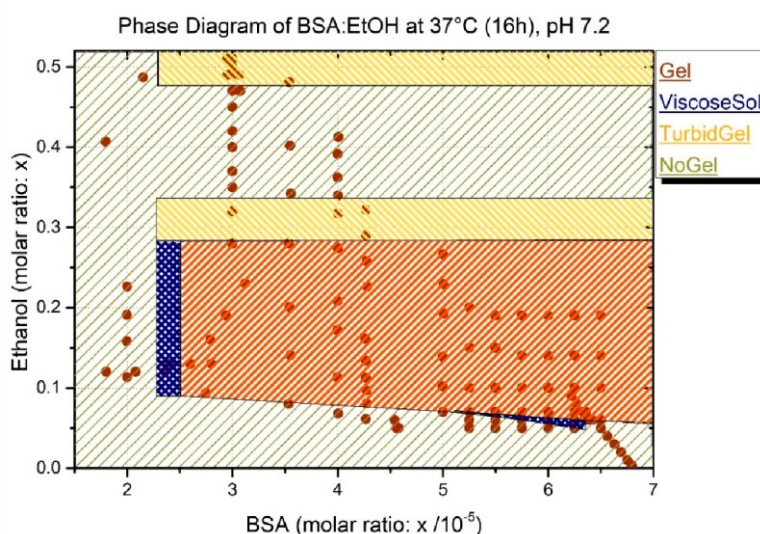


Figure 1. Phase diagram of bovine serum albumin (BSA) after 16 h at 37 °C (data points based on Table A1). ViscosSol refers to viscous solution but fall short of being a robust gel. Gel refers to clear gel which can be differentiated from turbid gels. NoGel refers to state like precursor solution (not viscous). Table A1 (see Appendix A), which shows the details of the exact albumin and ethanol concentration for each point shown in Figure 1. From these data, it is apparent that the formation of hydrogels using ethanol is correlated to both the concentration of ethanol and the concentration of BSA. The concentration of BSA can be in some cases lower (compared to samples where no gel formation is observed) where due to the presence of a higher amount of ethanol hydrogels form; yet, the BSA concentration should be above the threshold of 7.15 wt% (1.07 mM) for a three-dimensional gel to form. The results of the gelation in the thermomixer show that the minimum amount of ethanol cannot be trivially found and is not dependent on a certain amino acid to ethanol (AA/EtOH)-ratio. Gels were

e.g., formed with an amino acid to ethanol ratio of 1.9, but other samples did not form gels at a very high (AA/EtOH) ratio of 11.6.

2.2. Rheological Characterization

The combined results obtained from rheological measurements of the gelation process on the rheometer plate show that ethanol plays a significant role in increasing the gelation rate, even at low protein concentrations. As a reference, one can state that no gelation can be observed at 37 °C and neutral pH regardless of BSA concentration [5,6]. By setting the pH to more extreme values (lower than 4.2 or higher than 10.6), hydrogels form, as described by e.g., Baler et al. and us [5,6].

In the experiments presented here using ethanol, the gelation proceeds much faster at 37 °C and neutral pH than when the pH is lowered to 4.2 or lower (see (Figure 2) and (Figure A1)). The rate of ethanol-induced gelation is comparable with that of high pH value gelation processes. To translate the measured values of G^0 and G'' into a comprehensible concise graph, the measured points in the diagram of Figure 1 are classified as (i) gel, (ii) no gel, (iii) turbid gel, and (iv) viscous solution (the classification is based on the gel classification in ref. [6]).

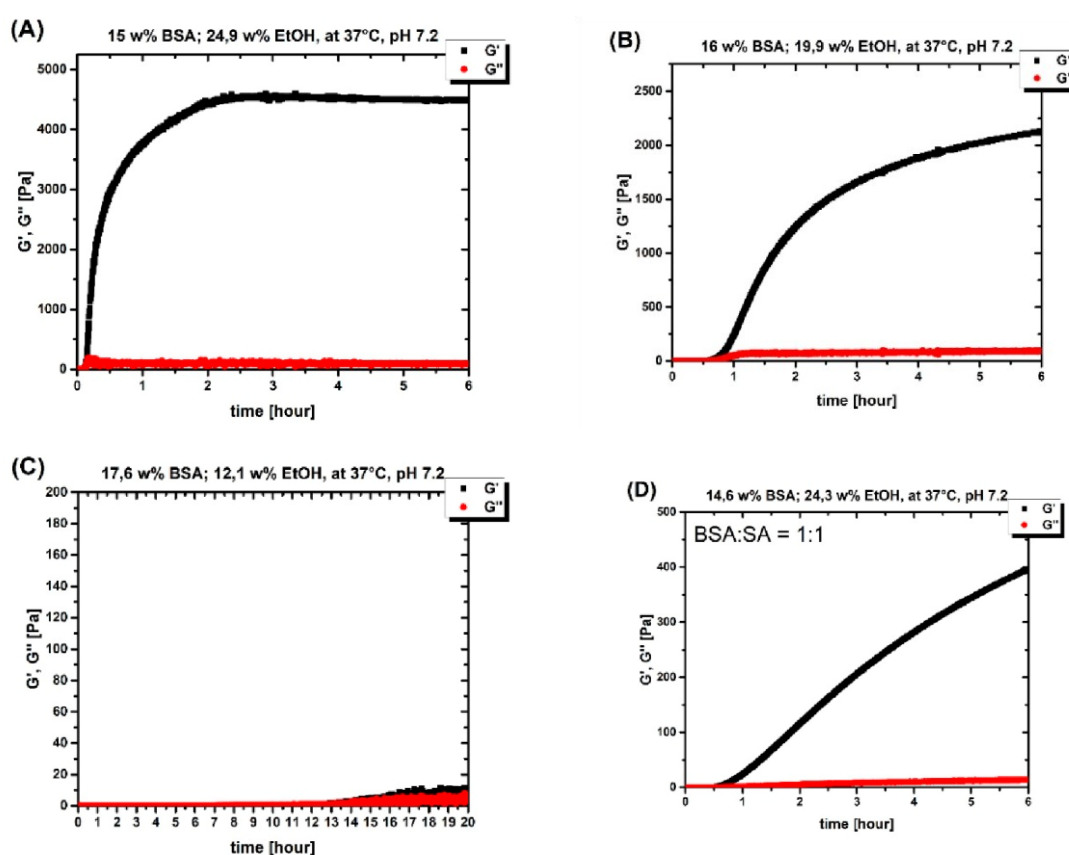


Figure 2. (A) 15 wt % (2.2 mM) BSA solution with 24.9 wt % EtOH at 37 °C on a rheometer plate for 6 h. (B) 16 wt % (2.4 mM) BSA solution with 19.9 wt % EtOH at 37 °C on a rheometer plate for 6 h. (C) 17.6 wt % (2.6 mM) BSA solution with 12.1 wt % EtOH at 37 °C on a rheometer plate for 20 h. (D) 14.6 wt % (2.1 mM) BSA solution with 24.3 wt % EtOH at 37 °C on a rheometer plate for 6 h with the BSA: stearic acid (SA) ratio of 1:1.

To elucidate the mechanical properties and the rate of gelation of the gels obtained from ethanol addition, the results are compared with the other hydrogels synthesized with other methods. Table 1 shows that the addition of ethanol, despite lower protein concentration, paves the way of gel formation to a more robust and more rapid gelation compared to the pH-induced method.

Table 1. The difference in mechanical properties and gelation rate at 37 °C between pH-induced and EtOH-mediated gelation.

Type	BSA Concentration	G ⁰ (Pa) *	G ⁰⁰ (Pa) *	Gelation Point
EtOH (25 wt%)	15 wt% (2.2 mM)	5000	150	8 min
pH induced ¹	20 wt% (3 mM)	900	130	45 min
Temp. induced	20 wt% (3 mM)	16000	300	1 min

To investigate how the addition of stearic acid (SA) affects the gelation properties, gels were made on the rheometer plate in the presence of SA at different BSA:SA molar ratios. Figure 2d shows the adverse effect of SA on the mechanical properties of the gel. The more SA present, the less robust the gel (see Figure A2). This observation is also made without ethanol (see [6]) and can be traced back to the stabilizing effect of bound SA on the tertiary structure of individual albumin molecules.

In addition, the denaturation temperature increases when SA ligands are bound [9].

As outlined above, to obtain more molecular/nanosopic insights into the macroscopic/rheological properties of the gel and the gelation processes, the gelation process at the molecular level using IR and continuous wave (CW) EPR spectroscopies was explored.

2.3. Infrared Spectroscopy (IR)

It has been shown [6] that the formation of intermolecular β -sheets at the cost of losing native α -helices leads to gel formation. This process is detectable by recording the spectra during gel formation on the crystal of an attenuated total reflection infrared (ATR-IR) spectrometer (A Bruker Tensor 27 FT-IR spectrometer equipped with a BioATRCell II and an LN-MCT photovoltaic detector and the OPUS Data Collection Program (all from Bruker, Ettlingen, Germany)) [6]. When ethanol and BSA concentrations are in the range where no gelation can be observed macroscopically (see Figure 1), there are also no significant time-dependent changes detectable in the IR spectra (Figure 3A). In contrast, in experiments showing gel formation macroscopically and in rheology, there is an obvious increase in intermolecular β -sheets at the cost of a decrease in native α -helices (Figure 3B).

¹ pH-induced gelation: the pH value set to 3.5 using 2M HCl (See ref. [6]), * the value of G⁰ and G'' after 2 h. In the EtOH-induced gelation, the G⁰ remains constant after 2 h; however, in pH-induced gelation, it increases up to 10,000 Pa. Temp. induced refers to temperature-induced gelation.

Furthermore, Figure 2 (see also Figure A3) illustrates the correlation between BSA and ethanol concentration; in Figure 2A, although the protein concentration is lower compared to Figure 2B, due to the higher ethanol concentration, gelation starts earlier and after six hours, the G⁰ (and the G', G'' difference) is higher. Figure 2C shows the importance of the role that EtOH plays, a higher BSA concentration results in no gelation after 20 h when the ethanol concentration was not high enough.

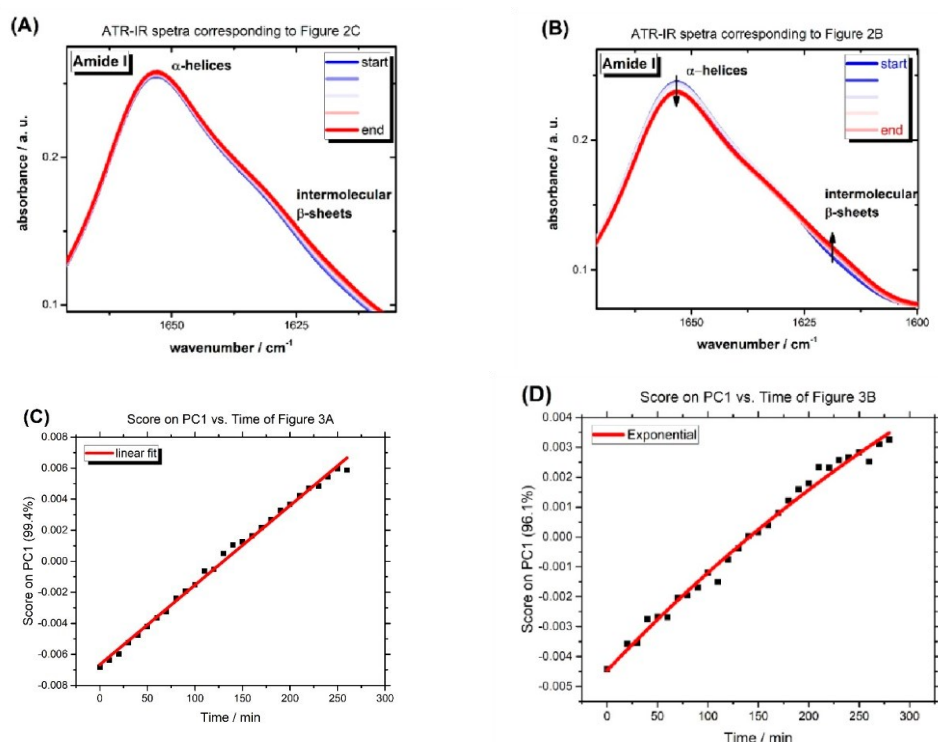


Figure 3. (A) Amide 1 band of 2.6 mM BSA solution with 12.1 wt % EtOH at 37 °C on ATR-IR crystal (BioATRCeIl), the same condition as Figure 2C, shows homogenous changes across all the amide 1 band and no gel formation. (B) Amide 1 band of 2.4 mM BSA solution with 19.9 wt % EtOH at 37 °C on ATR-IR crystal, the same condition as that in Figure 2B, shows an increase in the intermolecular β -sheet peak, whereas native α -helices of BSA are lost. In this case, gel formed on the spectrometer crystal. (C) PC1 scores vs. time regarding Figure 3A, (D) PC1 scores vs. time regarding Figure 3B. For more detailed information about PCA analysis, see ref. [6].

To find the correlation of the recorded IR spectra during the gelation, PCA (Principal Component Analysis) was applied to the spectral range of 1600–1700 cm^{-1} after the subtraction of a linear baseline and vector normalization of the spectra. In contrast to the linear changes in PC1 (first principal component), where more than the 95% of possible variance is detected, of Figure 3A versus time (see Figure 3C), Figure 3D shows exponential changes during the gel formation of Figure 3B. These results show that as long as no hydrogel formation takes place, changes on the nanoscopic level (secondary structure) are detectable, linear, and in all regions with identical effect, while concerted, yet strongly inhomogeneous changes during gel formation can be detected.

2.4. Electron Paramagnetic Resonance (EPR) Spectroscopy

The performed EPR spectroscopic measurements show the significance of ethanol concentration on the protein structure and the FA binding sites that are predominantly situated at the interfaces of α -helices (Figure 4a). For EPR spectroscopy, as generally established, stearic acids were employed that have an attached persistent nitroxide radical group, most often at position 16 of the alkyl chain (16-doxylstearic acid, 16-DSA) [5,7,10]. Generally, the EPR data indicate that when keeping the BSA and 16-DSA concentrations constant and merely increasing the amount of ethanol, fatty acids tumble much faster (see Table A2). This can be interpreted when one considers that for the amphiphilic 16-DSA molecules, ethanol in fact is a good solvent, and as such competes with binding to the—in water or buffer—much more favorable FA binding sites. Overall, the interactions between BSA and FAs are strongly weakened with significant amounts of ethanol present in the solutions/gels.

The comparison between (Figure 4B) with the EPR results obtained from other BSA hydrogels, synthesized by other methods, shows that the addition of ethanol results in weaker interaction between the BSA and FAs and consequently the faster tumbling of FAs. Accordingly, the results of EPR measurements reveal that the ethanol-induced gelation leads to a lower fatty acid binding capacity compared to other gelation methods [6]. They indicate that the amount of bound fatty acids relative to the amount of overall available fatty acids is decreasing with higher ethanol concentrations, but it does not change with higher fatty acid concentration in the tested concentration range, implying a thermodynamic equilibrium of bound and free fatty acids in the gelation process.

Table 2. Results of EPR samples of Figures 4 and A4.

Sample	Fraction of Bound Fatty Acid	Correlation Time τ_c (ns)	Fraction of Free Fatty Acid	Correlation Time τ_c (ns)
C	68%	5.28	32%	0.22
D	78%	5.28	22%	0.22
E	68%	5.28	32%	0.22
F	48%	5.28	52%	0.22

* Samples preparation of (A) and (B) are not simulated.

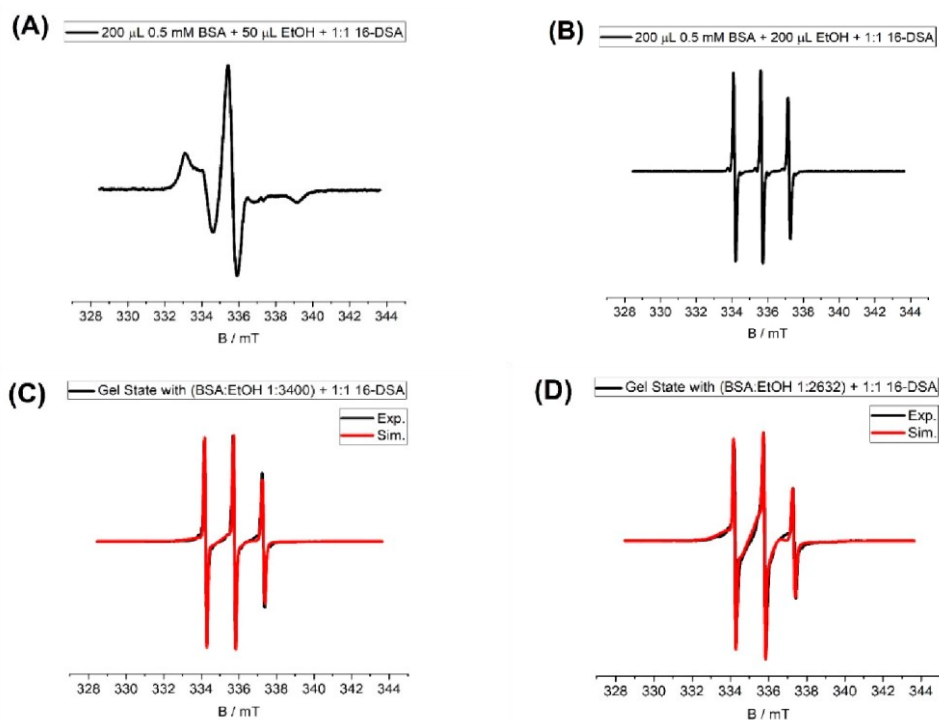


Figure 4. The samples are prepared based on Table A2. Electron paramagnetic resonance (EPR) spectra of (A,B) shows that the addition of ethanol dramatically weakens the interaction between protein and stearic acid. The data for (C,D) and Figure A4 are shown in Table 2.

3. Discussion

Our experiments show that the addition of ethanol results in gel formation at low temperature and neutral pH values. The correlation between ethanol and albumin concentration for gel formation is remarkable and detectable at macroscopic and molecular/nanoscale levels. These results are concisely summarized in the phase diagram of Figure 1. When the ratio between EtOH and BSA is

not in the range of gel formation, there is no sign of formation of intermolecular β -sheet (See Figure 3A). Although in ethanol-induced gels, the minimum concentration of albumin for gel formation is lower compared to the previously established pH-induced method, when the protein concentration is too low (below the gel formation threshold), the addition of EtOH cannot compensate for the low concentration of protein. On the other hand, when there is too much EtOH (see Figure 1) in the solution, it effectively denatures and solvates the proteins and as such has an adverse effect on the formation of the intermolecular β -sheet. Therefore, there is range of BSA:EtOH ratios, in which the formation of 3D-linked hydrogels of albumin molecules is possible. This cage-like network of protein is capable of holding water inside. As with temperature-induced gels, this comes at the cost of losing extensive amount of native α -helices in BSA (see Figure 3B). That means that the secondary structure of ethanol-induced hydrogels are comparable with temperature-induced ones.

Based on the rheological results, the mechanical properties of the gels are significantly poorer compared to pH-induced and temperature-induced hydrogels (see Table 1 and Figure 2). On the other hand, gel formation proceeds significantly faster in comparison to pH-induced hydrogels. These results are substantiated with EPR measurements; namely, the number of binding sites are remarkably reduced compared to other gelation methods, including temperature-induced methods [6]. Despite the strong denaturation of albumin during temperature-induced gelation, the resulting hydrogel is mechanically very robust (see ref. [6]), which can be concluded that although fatty acids will not be bound to hydrogel scaffold (protein wall), the FAs are rather trapped in strongly demobilized water phase of the hydrogels. Moreover, in the pH-induced method, despite lower rigidity (the mechanical properties are weak in comparison to temperature-induced gels), more of the native secondary structure of albumin is preserved, and that results in a relatively high number of available FA binding sites (see ref. [6]).

Hence, comparing the EPR and rheological results for the ethanol addition method and other methods shows that with ethanol addition, the protein has weaker interactions (less binding capacity) with Fas, and the water phase is less immobilized compared to the temperature-induced method.

This can be of interest for fast drug release systems.

We hope that this initial study, which connects the nanoscopic properties with the macroscopic features of the hydrogels leading to phase diagrams, will pave the way also for their exploration in applications such as the controlled release of (bio-)molecules.

4. Materials and Methods

4.1. Materials and Gel Preparation

Human (HSA) and bovine (BSA) serum albumin were purchased from the spin-labeled fatty acid 16-DOXYL stearic acid, 16-DSA (16-doxyl stearic acid, free radical, 253596, ALDRICH, Sigma-Aldrich Chemie GmbH, Schnelldorf, Germany). All chemicals and materials were used as received without further purification. Hydrogels were prepared in a thermomixer made by Halle University workshop (Halle, Germany).

4.2. Gel Formation

The precursor solutions were prepared by dissolving serum albumin (BSA) in water. The amounts were chosen based on the desired concentration. After two hours of stirring and the complete

dissolution of BSA in water, ethanol (EtOH) is added. The samples and the exact amount of each component are tabulated in Table A1.

4.3. Loading Stearic Acid (SA) into Gels

Stearic acid is dissolved first in 0.1 M KOH, and then it is added into the precursor solution of the gels. In these cases, the EtOH was added after the addition of the SA.

4.4. Rheology

Hydrogels have viscoelastic behavior under force load, i.e., the lattice stores the energy, which is retractable (elasticity), while some energy is dissipated. To describe this behavior, the storage- and loss-modulus are measured with an Anton Paar Physica MCR 301 rheometer (Anton Paar, Graz, Austria). The storage modulus represents the elastic portion (stored energy), and the loss modulus represents the viscous characteristics (energy dissipation). They are defined through Equations (1) and (2). For ideal elastic behavior, $G^0 \gg G''$, and for ideal viscous behavior, $G^0 \ll G''$.

$$\text{Storage Modulus } G^0 : \quad G^0 = \frac{\tau^A \cos \delta}{\gamma^A} \quad (1)$$

$$\text{Loss Modulus } G^{00} : \quad G^{00} = \frac{\tau^A \sin \delta}{\gamma^A} \quad (2)$$

τ/Pa = shear stress
 $\gamma/\%$ = deformation
 $\delta/^\circ$ = phase shift angle

In the gelation process, the values of G^0 and G'' are important. In the sol state, $G'' > G'$, at the gelation point, $G'' = G'$, and in the gel state, $G^0 > G''$. Based on the extent of the difference between G^0 and G'' , we define mechanically strong and weak hydrogels. These definitions all take the magnitude of G'' into account, which means that despite there being a large difference between G^0 and G'' , the mechanical properties may still be poor when G'' still is very high.

4.5. Infrared Spectroscopy (IR)

The secondary structure of proteins can be characterized using vibrational (infrared and Raman) spectroscopy. Infrared spectroscopy is based on the interaction of infrared radiation with molecules [10]. The IR radiation of certain wavelengths excite the vibrational modes of specific bonds whose wavelength and peak shape often depend on the local secondary structure. As a result, the IR absorption spectrum gives information on the secondary structure of the sample. The absorbance is plotted against the wavenumber (cm^{-1}). In the scope of our study, the amide I band (between 1600 and 1700 cm^{-1}) is the range of interest, since it shows the changes in the different secondary structures (α -helix, β -sheet, β -turn, and random coil) during the gelation [11]. The spectra were analyzed using Principal Component Analysis (PCA). PCA is a technique that transforms a number of possibly intercorrelated variables into a smaller number of orthogonal variables called principal components. This is to find trends and patterns in large datasets [10]. The goal is to de-correlate the original data by finding the directions along which the variance is maximized and then use these directions to define the new basis [10].

4.6. Electron Paramagnetic Resonance (EPR) Spectroscopy

Continuous wave (CW) EPR spectroscopy was used to investigate the fatty acid binding capacity of the hydrogels. By monitoring the changes in the dynamics of nitroxyl spin-labeled fatty acids (16-DOXYL stearic acid, 16-DSA, nitroxyl moiety at position 16 in the alkyl chain) during the presence and

absence of the protein and comparing these changes in the gel state (in which the protein is denatured to some extent) and native state (native BSA has 7 ± 1 fatty acid binding sites [8]),

we investigated the number of available FA binding sites of the gels. By simulating the spectra (using the EasySpin program package for MATLAB, in which the Schneider–Freed model of slow and intermediate rotational motion is implemented [12]), we can obtain information about the electronic and molecular structures, self-assembly, and dynamics of paramagnetic samples [7].

The CW EPR spectra were recorded using a MiniScope MS400 (Magnettech, Berlin, Germany) spectrometer working at the X-band (a microwave frequency of approximately $\nu = 9.4$ GHz and a magnetic field sweep of 15 mT centered at 340 mT).

Temperatures were adjusted with a Temperature Controller H03 (Magnettech) with an accuracy of approximately 0.2 °C. The exact frequency was recorded using a frequency counter (Racal Dana 2101, Neu-Isenburg, Germany). Absorption spectra were detected as a first-derivative spectra through field modulation with 100 kHz and an amplitude of x mT.

Author Contributions: Conceptualization, D.H. (Dariush Hinderberger); Data curation, S.H.A.; Formal analysis, S.H.A. and D.H. (David Haselberger); Funding acquisition, D.H. (Dariush Hinderberger); Investigation, S.H.A., D.H. (David Haselberger) and D.H. (Dariush Hinderberger); Methodology, D.H. (Dariush Hinderberger);

Project administration, D.H. (Dariush Hinderberger); Software, S.H.A.; Supervision, D.H. (Dariush Hinderberger); Validation, S.H.A. and D.H. (David Haselberger); Visualization, S.H.A. and D.H. (Dariush Hinderberger); Writing—original draft, S.H.A.; Writing—review & editing, D.H. (Dariush Hinderberger) All authors have read and agreed to the published version of the manuscript.

Funding: This work was supported by the European Regional Development Fund (ERDF) and the Federal State of Saxony-Anhalt.

Acknowledgments: We thank Heike Schimm for technical support.

Conflicts of Interest: The authors declare no conflict of interest.

Appendix A

Table A1. Samples and results after 16 h at 37 °C.

20 wt% BSA (μL)	EtOH (μL)	H ₂ O (μL)	w% BSA	w% EtOH	x BSA 10 ⁻⁵	x EtOH	EtOH AA	Result
200	1	0	19.92	0.39	6.8	0.002	0.05	-
200	2	0	19.84	0.78	6.79	0.004	0.1	-
200	5	0	19.61	1.93	6.75	0.01	0.24	-
200	10	0	19.24	3.8	6.69	0.02	0.48	-
200	15	0	18.88	5.59	6.63	0.03	0.73	-
200	20	0	18.54	7.31	6.56	0.04	0.97	-
200	25	0	18.2	8.98	6.5	0.05	1.21	-
200	32	0	17.76	11.21	6.42	0.06	1.55	-
200	33	0	17.7	11.52	6.41	0.06	1.6	-
200	34	0	17.63	11.83	6.4	0.06	1.65	-
200	35	0	17.57	12.13	6.39	0.06	1.7	-
200	36	0	17.51	12.44	6.38	0.06	1.74	-
200	37	0	17.45	12.74	6.36	0.07	1.79	h. v.
200	38	0	17.39	13.04	6.35	0.07	1.84	gel
200	39	0	17.33	13.33	6.34	0.07	1.89	gel
200	40	0	17.27	13.63	6.33	0.07	1.94	gel
200	45	0	16.98	15.08	6.27	0.08	2.18	gel
200	50	0	16.7	16.48	6.22	0.09	2.42	gel
200	134.8	6.2	13.06	34.03	5.25	0.2	6.53	gel

200	96.5	8.6	14.49	26.74	5.5	0.15	4.68	gel
200	101.1	16.6	14.3	26.92	5.25	0.15	4.9	gel
200	61.5	10.7	16.1	18.72	5.75	0.1	2.98	gel
200	64.3	18.5	15.95	18.84	5.5	0.1	3.12	gel
200	67.4	27	15.8	18.98	5.25	0.1	3.27	gel
200	28.3	5.8	17.99	9.79	6.25	0.05	1.37	-
200	29.4	12.7	17.92	9.83	6	0.05	1.43	-
200	30.7	20.2	17.84	9.91	5.75	0.05	1.49	-
200	32.2	28.4	17.75	10.01	5.5	0.05	1.56	-
200	33.7	37.4	17.65	10.07	5.25	0.05	1.63	-
200	40.2	2.1	17.26	13.57	6.25	0.07	1.95	gel
200	41.9	8.89	17.16	13.66	6	0.07	2.03	gel
200	43.7	16.24	17.06	13.75	5.75	0.07	2.12	h. v.
200	45.7	24.3	16.95	13.85	5.5	0.07	2.22	h. v.
200	47.9	33	16.82	13.96	5.25	0.07	2.32	h. v.
200	38.5	2.66	17.36	13.04	6.25	0.07	1.87	gel
200	40.1	9.44	17.27	13.12	6	0.07	1.94	gel
200	41.9	16.8	17.16	13.23	5.75	0.07	2.03	gel
200	43.8	24.8	17.05	13.32	5.5	0.07	2.12	h. v.
200	45.8	33.7	16.94	13.39	5.25	0.07	2.22	-
200	36.8	3.19	17.46	12.5	6.25	0.06	1.78	gel
200	38.3	9.98	17.37	12.58	6	0.06	1.86	h. v.
200	40	17.4	17.27	12.68	5.75	0.06	1.94	-
200	41.8	25.4	17.17	12.76	5.5	0.06	2.03	-
200	43.8	34.3	17.05	12.85	5.25	0.06	2.12	-
200	40.6	17.2	17.24	12.85	5.75	0.07	1.97	gel
200	41.2	17	17.2	13.03	5.75	0.07	2	gel
200	50.3	42.7	16.69	14.05	5	0.07	2.44	gel
200	47.2	33.2	16.86	13.77	5.25	0.07	2.29	gel
200	46.5	33.4	16.9	13.58	5.25	0.07	2.25	-
200 *	28.5	0	3.48	10.11	4.58	0.05	1.95	-
200 *	29.3	0	13.45	10.36	4.57	0.05	2.01	-
200 *	30	0	13.41	10.58	4.56	0.05	2.05	-
200 *	33.5	0	13.25	11.67	4.54	0.06	2.29	-
200 **	136.1	17.8	15.38	33.02	6.5	0.19	5.04	gel
200 **	141.6	24.5	14.87	33.23	6.25	0.19	5.25	gel

Table A1. Cont.

20 wt% BSA (μL)	EtOH (μL)	H ₂ O (μL)	w% BSA	w% EtOH	x BSA 10 ⁻⁵	x EtOH	EtOH AA	Result
200 **	147.5	31.8	14.36	33.42	6	0.19	5.48	gel
200 **	153.9	39.7	13.85	33.62	5.75	0.19	5.73	gel
200 **	160.9	48.3	13.32	33.83	5.5	0.19	6	gel
200 **	102	28.3	16.19	26.06	6.5	0.14	3.78	gel
200 **	106.2	35.4	15.66	26.25	6.25	0.14	3.94	gel
200 **	110.6	43.1	15.13	26.41	6	0.14	4.11	gel
200 **	115.4	51.6	14.59	26.57	5.75	0.14	4.29	gel
200 **	68	38.8	17.1	18.35	6.5	0.1	2.52	gel
200 **	70.8	46.4	16.54	18.48	6.25	0.1	2.63	gel
200 **	73.7	54.5	15.99	18.6	6	0.1	2.74	gel
200 **	34	49.3	18.11	9.72	6.5	0.05	1.26	-
200 **	46.3	45.5	17.73	12.95	6.5	0.06	1.71	gel
200 **	44.2	46.1	17.8	12.41	6.5	0.06	1.64	gel
90	84	110	6.76	24.89	2.36	0.12	9.05	h. v.
80	84	120	6.01	24.89	2.08	0.12	10.18	-
70	84	130	5.26	24.89	1.8	0.12	11.63	-
100	100	85	7.58	29.9	2.79	0.16	9.69	gel

100	115	70	7.67	34.8	2.94	0.19	11.15	gel
100	130	55	7.76	39.82	3.12	0.23	12.6	gel
100	162.2	51.8	7.15	45.74	3	0.28	15.72	gel
100	191.6	42.7	6.81	51.44	3	0.32	18.57	t. g.
100	206	38.2	6.65	54.05	3	0.35	19.97	t. g.
100	221	33.6	6.49	56.62	3	0.37	21.42	t. g.
100	235	29.1	6.36	58.95	3	0.4	22.78	t. l.
100	250	24.5	6.22	61.31	3	0.42	24.24	t. l.
100	265	20	6.08	63.54	3	0.45	25.69	t. l.
100	280	15.4	5.95	65.69	3	0.47	27.14	t. l.
100	294	10.9	5.83	67.66	3	0.5	28.5	t. g.
100	79	90.4	7.91	24.66	2.8	0.13	7.66	gel
100	85.1	103.6	7.39	24.8	2.6	0.13	8.25	gel
100	92.2	118.9	6.86	24.94	2.4	0.13	8.94	-
100	295	14.04	5.77	67.12	2.95	0.49	28.6	t. g.
100	305	10.9	5.69	68.45	2.95	0.51	29.57	t. g.
100	285	9.79	5.98	67.19	3.07	0.49	27.63	t. g.
100	289	12.72	5.87	66.92	3	0.49	28.02	t. g.
100	300	9.09	5.78	68.45	3	0.51	29.08	t. g.
100	182	0	8.21	58.95	4.00	0.413	17.67	-
100	173	3	8.35	56.99	4.00	0.392	16.80	-
100	160	7	8.57	54.12	4.00	0.362	15.53	-
100	150	10	8.76	51.83	4.00	0.340	14.56	-
100	140	13	8.95	49.43	4.00	0.317	13.59	t. g.
100	121	19	9.33	44.51	4.00	0.274	11.75	gel
100	92	28	9.97	36.19	4.00	0.208	8.93	gel
100	76	33	10.36	31.08	4.00	0.172	7.38	gel
100	50	41	11.08	21.86	4.00	0.113	4.85	gel
100	30	47	11.72	13.87	4.00	0.068	2.91	-
100	94	0	11.48	42.58	5.00	0.266	9.13	gel
100	81	4	11.91	38.06	5.00	0.229	7.86	gel
100	68	8	12.37	33.19	5.00	0.193	6.60	gel
100	49	14	13.10	25.32	5.00	0.139	4.76	gel
100	36	18	13.66	19.40	5.00	0.102	3.50	gel
100	360	20	4.95	70.30	2.58	0.526	34.95	-
100	270	14	6.12	65.14	3.08	0.470	26.21	-
100	240	0	6.91	65.44	3.54	0.481	23.30	t. g.
100	200	12	7.41	58.49	3.55	0.402	19.42	-
100	170	21	7.84	52.57	3.55	0.342	16.50	-
100	140	31	8.28	45.75	3.54	0.280	13.59	t. g.
100	100	43	9.01	35.56	3.54	0.201	9.71	gel
100	70	52	9.65	26.65	3.55	0.141	6.80	gel
100	40	62	10.33	16.31	3.53	0.080	3.88	gel

Table A1. Cont.

20 wt% BSA (μL)	EtOH (μL)	H ₂ O (μL)	w% BSA	w% EtOH	x BSA 10 ⁻⁵	x EtOH	EtOH AA	Result
100	200	131	5.14	40.59	2.00	0.226	19.42	-
100	169	141	5.34	35.62	2.00	0.191	16.41	-
100	140	150	5.55	30.64	2.00	0.158	13.59	-
100	100	162	5.87	23.14	2.00	0.113	9.71	-
100	60	100	8.09	19.14	2.75	0.093	5.83	gel
100	400	100	3.88	61.21	1.80	0.407	38.84	-
100	400	50	4.30	67.78	2.15	0.487	38.84	-
100	50	400	3.71	7.31	1.10	0.031	4.85	-
150	200	10	9.44	49.65	4.27	0.322	12.95	t. g.
150	180	16	9.74	46.11	4.27	0.290	11.65	t. g.

150	160	22	10.06	42.33	4.27	0.258	10.36	gel
150	140	28	10.40	38.29	4.28	0.226	9.06	gel
150	100	41	11.12	29.23	4.26	0.161	6.47	gel
150	83	46	11.47	25.04	4.27	0.134	5.37	gel
150	70	50	11.75	21.64	4.27	0.113	4.53	gel
150	60	53	11.98	18.91	4.27	0.097	3.88	gel
150	50	56	12.22	16.07	4.27	0.081	3.24	gel
150	38	60	12.50	12.49	4.27	0.061	2.46	-

* 25 w% stock solution was used. ** 15 % stock solution was used. h.v. refers to high viscosity solution; t.l. refers to turbid liquid (no gel, not viscous, but due to denaturation of proteins the solution is turbid); t.g. refers to turbid gel. - means no gel has been observed.

Table A2. EPR samples of Figures 4 and A4.

Sample	20 wt% BSA (μL)	EtOH (μL)	H ₂ O (μL)	26 mM SA (μL)	w% BSA	w% EtOH	x BSA 10 ⁻⁵	x EtOH	Ratio BSA:16 DSA
C	300	105	44.1	35	24.3	16.48	5	0.13	1:1
D	300	105	44.1	2*35	24.3	44.10	5	0.13	1:2
E	300	70	44.1	70	24.3	0	5	0.13	1:2
F	0	105	344	35	24.3	16.48	0	0.13	1:1

* Samples preparation of (A) and (B) are explained in their title.

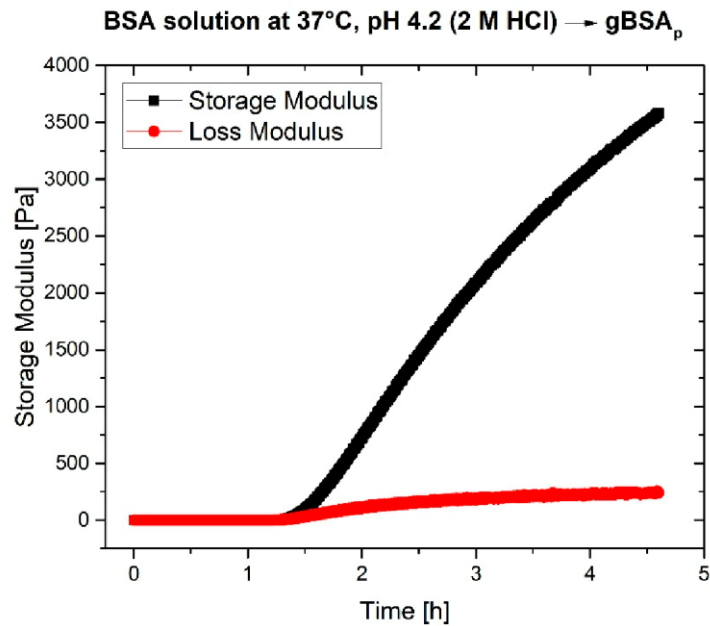


Figure A1. 3 mM BSA solution with no EtOH at 37 °C on rheometer plate. The pH is set to 4.2 by using 2M HCl.

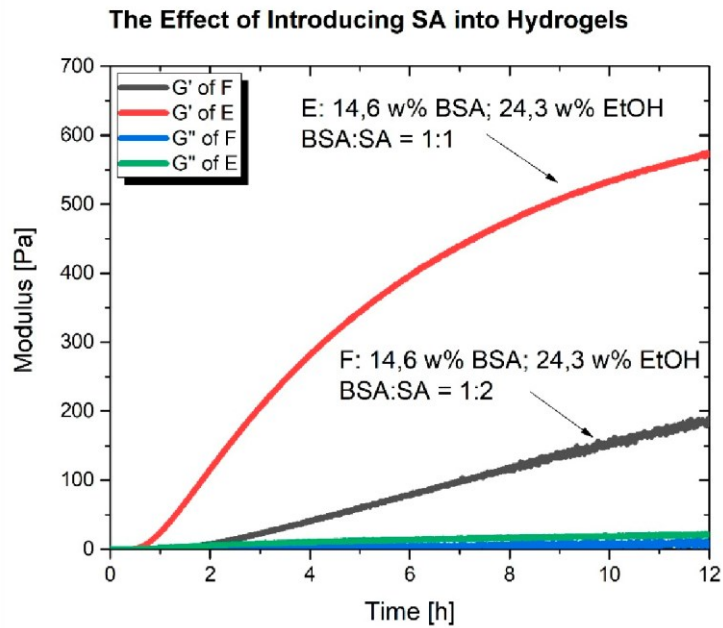


Figure A2. Addition of stearic acid (SA) into the precursor solution of the gels (2.1 mM BSA solution) leads to weakening the mechanical properties of the gels. The SA were dissolved in 0.1 M KOH prior to addition into precursor solution.

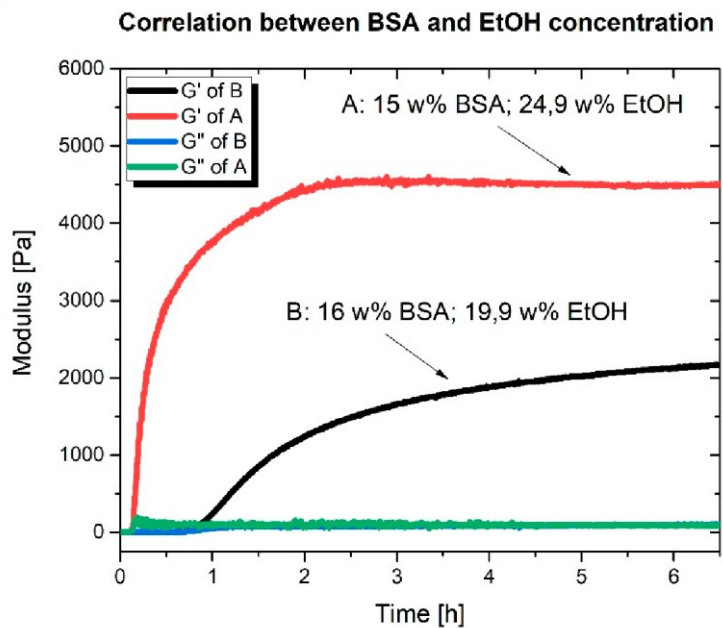


Figure A3. This figure illustrates that there is a correlation between ethanol and protein concentration. In A, although the BSA concentration is lower, due to the presence of more ethanol, a mechanically more robust gel is formed. In B, still a gel forms, but a higher concentration of BSA does not lead to a stronger gel structure, since the amount of ethanol is lower compared to A.

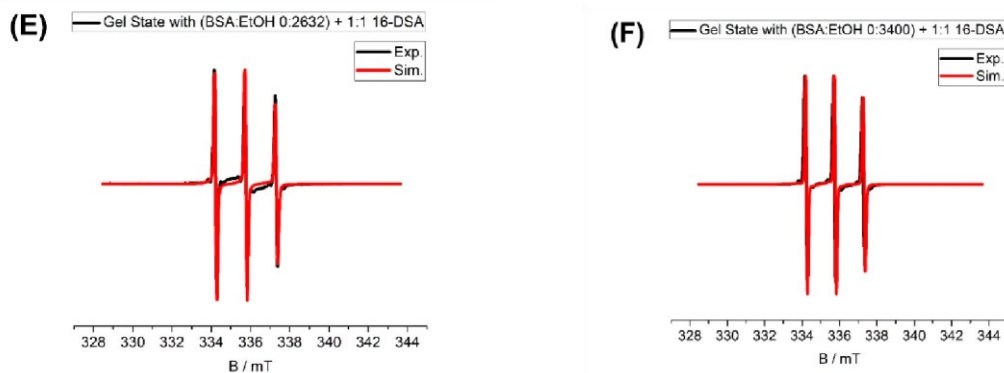


Figure A4. The samples are prepared based on Table A2. The data for (E,F) are shown in Table 2.

References

1. Minchiotti, L.; Galliano, M.; Kragh-Hansen, U.; Peters, T., Jr. Mutations and polymorphisms of the gene of the major human blood protein, serum albumin. *Human Mutation* **2008**, *29*, 1007–1016. [[CrossRef](#)] [[PubMed](#)]
2. Hirayama, K.; Akashi, S.; Furuya, M.; Fukuhara, K. Rapid confirmation and revision of the primary structure of bovine serum albumin by ESIMS and Frit-FAB LC/MS. *Biochem. Biophys. Res. Commun.* **1990**, *173*, 639–646. [[CrossRef](#)]
3. Peters, T., Jr. *All about Albumin: Biochemistry, Genetics, and Medical Applications*; Academic Press: Cambridge, MA, USA, 1995.
4. Ferrer, M.L.; Duchowicz, R.; Carrasco, B.; de la Torre, J.G.; Acuna, A.U. The conformation of serum albumin in solution: A combined phosphorescence depolarization-hydrodynamic modeling study. *Biophys. J.* **2001**, *80*, 2422–2430. [[CrossRef](#)]
5. Baler, K.; Michael, R.; Szeleifer, I.; Ameer, G.A. Albumin Hydrogels Formed by Electrostatically Triggered Self-Assembly and Their Drug Delivery Capability. *Biomacromolecules* **2014**, *15*, 3625–3633. [[CrossRef](#)] [[PubMed](#)]
6. Arabi, S.H.; Aghelnejad, B.; Schwieger, C.; Meister, A.; Kerth, A.; Hinderberger, D. Serum albumin hydrogels in broad pH and temperature ranges: Characterization of their self-assembled structures and nanoscopic and macroscopic properties. *Biomater. Sci.* **2018**, *6*, 478–492. [[CrossRef](#)] [[PubMed](#)]
7. Reichenwallner, J.; Hinderberger, D. Using bound fatty acids to disclose the functional structure of serum albumin. *Biochim. Biophys. Acta* **2013**, *1830*, 5382–5393. [[CrossRef](#)] [[PubMed](#)]
8. Akdogan, Y.; Reichenwallner, J.; Hinderberger, D. Evidence for Water-Tuned Structural Differences in Proteins: An Approach Emphasizing Variations in Local Hydrophilicity. *PLoS ONE* **2012**, *7*, e45681. [[CrossRef](#)] [[PubMed](#)]
9. Boye, J.I.; Alli, I.; Ismail, A.A. Interactions Involved in the Gelation of Bovine Serum Albumin. *J. Agric. Food Chem.* **1996**, *44*, 996–1004. [[CrossRef](#)]
10. Abdi, H.; Williams, L.J. Principal component analysis. *WIREs Computat. Stat.* **2010**, *2*, 433–459. [[CrossRef](#)]
11. Yang, H.; Yang, S.; Kong, J.; Dong, A.; Yu, S. Obtaining information about protein secondary structures in aqueous solution using Fourier transform IR spectroscopy. *Nat. Prot.* **2015**, *10*, 382–396. [[CrossRef](#)] [[PubMed](#)]
12. Schneider, D.J.; Freed, J.H. Calculating Slow Motional Magnetic Resonance Spectra. In *Spin Labeling: Theory and Applications*; Berliner, L.J., Reuben, J., Eds.; Springer US: Boston, MA, USA, 1989; pp. 1–76.

Sample Availability: Samples of the compounds showed in phase diagram (Figure 1) are available from the authors.



© 2020 by the authors. Licensee MDPI, Basel, Switzerland. This article is an open access article distributed under the terms and conditions of the Creative Commons Attribution (CC BY) license (<http://creativecommons.org/licenses/by/4.0/>).

Hydrogels from serum albumin in a molten globule-like state

Seyed Hamidreza
Volmer¹ |



Arabi | Behdad Aghelnejad² | Jonas
Dariush Hinderberger¹

¹Institut für Chemie, Martin-Luther-

Universität Halle-Wittenberg, Halle (Saale),
a protein, usually

²Département de chimie, École
is only present in a supérieure, PSL
preserved in the high
Université, Paris, France

Correspondence paramagnetic

Dariush Hinderberger, Institut für retains

Chemie, Martin-Luther-
Universität Halle-

Wittenberg, Von-Danckelmann-Platz
from MG-BSA Halle (Saale) 06120,
different (~0.2) pH units

Email:

halle.de

Funding information EPR-active stearic acid derivatives (16-DOXYL-stearic acid, 16-DSA), the MG-

Federal State of Saxony-Anhalt;
European

Abstract

Germany We demonstrate that a molten globule-like (MG) state of

normale described as a compact yet non-folded conformation that
University, Sorbonne narrow and delicate parameter range, is
concentration

environment of the protein hydrogel. We reveal mainly by means
of electron

resonance (EPR) spectroscopy that bovine serum albumin (BSA)

the known basic MG state after a hydrogel has been formed
from 20 wt%

4, precursor solutions. At pH values of ~11.4, BSA hydrogels made
Germany. remain stable for weeks, while gels formed at slightly

dariush.hinderberger@chemie.uni above and below the MG-state value
dissolve into viscous solutions. On the

contrary, when hydrophobic screening agents are added such as
amphiphilic,

Regional Development Fund State based hydrogel is the least long-lived, as
the hydrophobic interaction
of delicately exposed
hydrophobic patches of BSA
molecules is screened by the
amphiphilic molecules. These

bio- and polymer-physically unexpected findings may lead to new bio-compatible MG-based hydrogels that display novel properties in comparison to conventional gels.

KEYWORDS

albumin, ESR/EPR spectroscopy, fatty acids, hydrogels, hydrophobic effect, intermolecular interactions, ligand binding, molten globule, protein crowding, protein folding

1 | INTRODUCTION

Serum albumin is the most abundant protein in the circulatory system of a wide variety of organisms.¹ In addition to being the major transport protein for un-esterified fatty acids, it is also capable of binding reversibly an extraordinarily diverse range of metabolites, drugs and organic compounds and function as a carrier.²⁻⁴ This protein was and still is studied extensively concerning its structure and functionalities. Among others, electron paramagnetic resonance (EPR) spectroscopy has developed into a powerful analytical tool.^{5,6}

Developing new biocompatible materials which have an affinity towards therapeutic substances and can carry them inside a living organism is an attractive concept in

Seyed Hamidreza Arabi and Behdad Aghelnejad contributed equally to the biomedical sciences. Hydrogels based on proteins or this study. synthetic molecules are good candidates for this task

This is an open access article under the terms of the Creative Commons Attribution License, which permits use, distribution and reproduction in any medium, provided the original work is properly cited.

© 2020 The Authors. Protein Science published by Wiley Periodicals LLC on behalf of The Protein Society.

Protein Science. 2020;29:2459–2467.

wileyonlinelibrary.com/journal/pro | 2459

since one of their main common features is biocompatibility. Their high water content and soft nature make them similar to natural extracellular matrices and minimize tissue irritation and cell adherence.⁷ In addition, their capacity to embed biologically active agents in their water-swollen network makes them very attractive for controlled release of therapeutics.⁸ In a more general perspective, hydrogels are cross-linked networks made out of hydrophilic polymers, capable of retaining large amounts of water but yet remaining insoluble and maintaining their three-dimensional structures. The reason behind this insolubility is that the polymer is physically and/or chemically cross-linked.⁹⁻¹² Albumin hydrogels have previously been formed by thermal denaturation and chemical cross-linking.¹³⁻¹⁷ These hydrogel systems typically require either extensive protein denaturation (thermal) or chemical modification, which can hamper protein functionality and compromise biocompatibility. Another method called electrostatically triggered albumin self-assembly introduced by Baler et al.^{18,19} takes advantage of the fact that albumin has the ability to reversibly change its conformation when exposed to changes in solution pH while at least partly preserving secondary structure elements that may act as functional binding domains. We recently demonstrated that albumin hydrogels can in fact be formed well below their denaturation temperature if enough time is granted and explored the large pH range in which the hydrogels are formed. We also introduced supporting phase diagrams that precisely allow implementing hydrogels with specific properties on the nano- and macroscopic scales.¹⁹ A globular protein varies its tertiary structure under different solvent conditions. Native and fully denatured states are the most prominent ones. There is another important state that is thought to be the common intermediate in protein folding which is called molten globule (MG). Even four decades after its proposed discovery, the MG state of proteins still remains enigmatic.

There is substantial debate on its nature, ranging from MG states either reflecting a general intermediate in protein folding to being unique for every protein or simply a low-energy misfolded species. In this work, further complexity is added to the current discussion around MG states by demonstrating that molten globule-like state of protein, BSA, can be preserved in hydrogels, formed by the protein itself. In the context of our paper, one may define that molten globules are partially folded conformations of proteins that have near native compactness, substantial secondary structure, slowly fluctuating (little detectable) tertiary structure and an increased solvent-exposed hydrophobic surface area relative to the

native state.²⁰

2 | RESULTS AND DISCUSSION

In the following, the presence of the molten globule-like states both in acidic and basic pH ranges of bovine serum albumin (BSA) are investigated in high concentration environments with the help of continuous-wave electron paramagnetic resonance (CW EPR) spectroscopy. We first develop the spectroscopic analysis for a 5 wt% albumin solution (below the gel point) and then, for the first time, describe the same experiments performed with BSA hydrogels at high concentrations (20 wt%). We present evidence that the MG state observed in individual proteins persists in the gel state of the protein and in fact dominates its properties.

In case of human serum albumin (HSA), there is a molten globule state, which can be obtained under acidic conditions at pH 2.0.^{21,22} This state was recognized with the help of different techniques including far-UV and near-UV circular dichroism (CD), binding of

(8-anilinonaphthalene-1-sulfonic acid) ANS as a hydrophobic probe and viscosity measurements. In addition, Reichenwallner et al.²³ confirmed the presence of the known MG state at $\text{pH } 1.90 \pm 0.20$ by CW EPR spectroscopy on EPR-active stearic acid derivatives that bind to the protein. The first MG state of BSA that is well established was detected in alkaline BSA solutions at pH 11.2 and confirmed several times.^{24–26} Like in the mentioned case of HSA, the conclusion that BSA is present in an MG state was reached by analyzing far-UV and near-UV CD spectra. There are some experimental results that acknowledge the second potential MG state of BSA in the acidic pH range. One study has focused on the combined effects of concentration and pH on the conformational states of BSA by the means of small-angle X-ray scattering and came to the conclusion that there is in fact an acidic molten globule like state (pH 2.0).²⁷ Another independent research study came to a largely similar conclusion about the existence of the acidic MG like state for BSA. The method of choice was extrinsic and intrinsic protein fluorescence and it was reported that BSA assumes this conformation at pH 3.0.²⁸

Figure 1 displays the results in the basic pH range. Figure 1a presents a pH-dependent series of 16-DSA spectra in diluted 5 wt% albumin solutions. The isotropic hyperfine coupling constant (a_{iso}) peaks of freely tumbling 16-DSA appear from pH 11.29 onwards and the intensity of these peaks increases with increasing pH, while the broad spectrum of albumin bound 16-DSA (indicated by the apparent hyperfine coupling constant A_{zz}^0 in the spectra) decreases in intensity. As explained in detail in Reference 23, this is due to the protein changing into the so-called aged form of albumin, in which particularly the tertiary structure and parts of the secondary

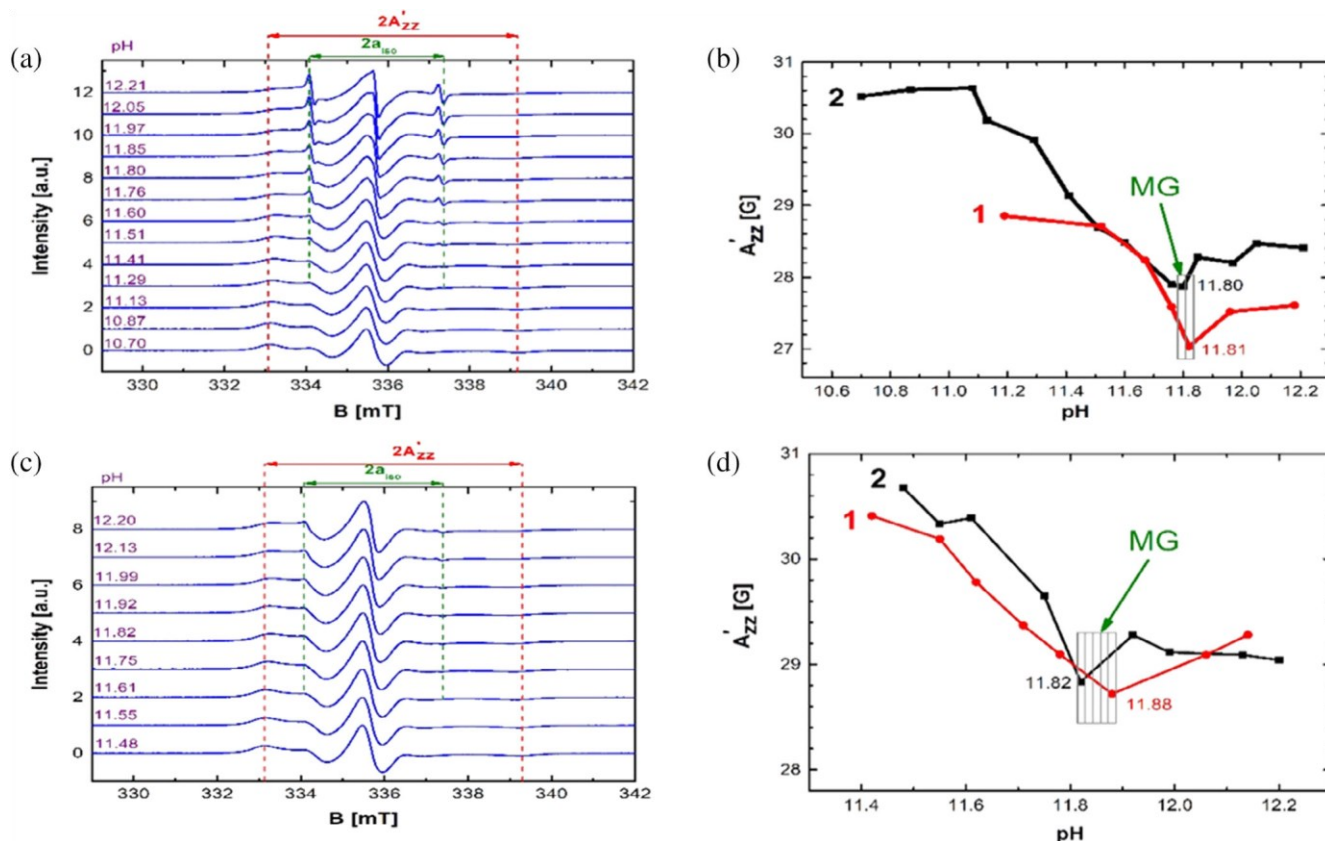


FIGURE 1 (a) EPR spectra of 16-DSA in diluted 5 wt% BSA solutions in the basic pH range at 20°C (1:1 ratio of BSA:16-DSA). (b) Dependence of A_{zz}^0 on pH in diluted BSA solutions in the basic pH range at 20°C (two independent measurement series). (c) EPR spectra of 16-DSA in 20wt% BSA hydrogels in the basic pH range at 20°C (1:1 ratio of BSA:16-DSA). (d) Dependence of A_{zz}^0 on pH in BSA hydrogels in the basic pH range at 20°C (two independent measurement series). Please note the difference in axis scaling between (b) and (d)

structure elements are largely dissolved, reducing the number of binding regions in the protein and leading to release of 16-DSA.²³

On the other hand, the value of apparent hyperfine coupling constant A_{zz}^0 is a spectroscopic determinant of the polarity of the molecular environment.²⁹ Polar environments lead to larger hyperfine splittings and reversibly, the hyperfine splittings are smaller in apolar surroundings.²⁹ One of the characteristics of the molten globule state is an increased solvent-exposed hydrophobic surface area. There is a higher accessibility to hydrophobic parts of the protein in this state. In this case, fatty acids can easily access and bind to these exposed areas. Now, because those spin probes reside longer times in apolar surroundings, the value of A_{zz}^0 decreases. Therefore, the point in Figure 1b in which A_{zz}^0 is at its minimum can be associated with the molten globule state.²³ Another aspect relating the minimum of A_{zz}^0 to the MG state is that the minimum of A_{zz}^0 also denotes the maximum rotational mobility of the spin probes. This stems from the fact that for fast and isotropic rotations of nitroxide spin probes, the apparent spectral separation of the outermost extrema (A_{zz}^0) converges towards its minimum value and approach the typical three-line pattern. Hence, when rotational mobility increases at the MG state, these spectral features move closer together, as it can be seen in Figure 1. It is widely accepted that the molten globule is a compact state with some fluctuating side chains. Here, the fatty acids interact with the exposed hydrophobic patches in the MG state, while conventionally their binding sites are rigid channels in the protein's interior, which gives them increased mobility. Two independent series of experiments were performed and reported in Figure 1b (first series is marked in red and the second one in black). It can be seen that both of them have a minimum at approximately pH 11.8. When considering that there is an uncertainty in the pH measurements (± 0.05) and apparent hyperfine coupling constant readouts, the fact that two

completely independent series of tests show two minima close to each other (within less than 0.1 pH units) reaffirms the notion that there is a molten globule like state at this point. The previously reported pH value for the basic BSA molten globule state is 11.2²⁴⁻²⁶ which is reasonably close to this research's finding. In another research work that used the CW EPR method, but with different buffer and protein concentrations, 11.8 was reported as the pH value, where the protein is in a molten globule like state.²³ For a more detailed quantitative description of the different 16-DSA binding and rotational motion modes, the reader is referred to Reference 23. The discrepancy in pH of the MG state (at pH 11.2 and 11.8 in EPR spectroscopy on 16-DSA) can be assigned to the presence of 16-DSA. We and others have previously shown that the presence of fatty acids stabilizes the native structure of albumin¹⁹ and thus seems to shift the molten globule state to slightly but significantly higher pH.

Figure 1c,d depicts the same pH-dependent series of 16-DSA EPR spectra, this time in BSA hydrogels made from 20 wt% precursor solutions. Tumbling of the spin probes is more restricted in hydrogels due to a denser protein environment than in solution. Unlike before, the freely rotating species are emerging at a higher pH of approximately 11.60 (instead of 11.30). Similar to the diluted experiments, there appears to be a drop in A_{zz}^0 , with a broad minimum centered at around pH 11.80 \pm 0.2 and a noticeable increase after that. It should be noted, though, that the drop in the apparent hyperfine coupling when increasing pH is much shallower than that observed for the dilute BSA solutions ($\Delta A_{zz}^0 \sim 2.0$ G in gels vs. ~ 3.0 G in dilute solution). These results suggest there could be a molten globule like state in the hydrogels. This further suggests that the functionality of the protein is mostly preserved during the electrostatically triggered method of the BSA gelation and even though the binding, configurations and even the macroscopic phase of the whole system is changed, the delicate state of the molten globule survived the process (see Figure S1 to compare the behavior of 16-DSA in presence and absence of protein in basic solution).

The same series of experiments have been conducted on the MG states acidic ranges (see Figure S2). In essence, we could not find experimental evidence that the acidic MG state can persist in BSA hydrogels. Hence, we here further focus on and elucidate the basic MG-state in BSA hydrogels.

As we know from our earlier studies,¹⁹ the effect of time on (basic and other) hydrogels is an important issue worth discussing. Therefore, one series of experiments was conducted in two stages. The first stage was performing EPR spectroscopy on the 16-DSA containing samples after the gelation started (denoted $t = 0$, in fact about 10 min after start of the gelation) and the second stage was the repetition of the same measurements after approximately 4 hr ($t = 4$ hr). The difference between these spectra revealed an unexpected characteristic (Figure 2c). It can be seen that after 4 hours the spectrum displayed a prominent change and A_{zz}^0 was decreased, that is, the outer extrema in the spectra moved closer to each other. This could be due to the fact that although at $t = 0$ the sample was, macroscopically seen, completely in the gel state, but the gelation process apparently was not completely finished and some sort of curing progressed slowly at the molecular level. This example was measured at pH 11.55, but all samples at different pH values showed these changes (Figure 2a). All the previous EPR measurements were performed at 20C. Switching to 37C reveals the effect of temperature on the gelation process (Figure 2b). After 4 hr the spectrum is identical to that measured at $t = 0$. This again proves the notion that temperature expedites the gelation process. Taking into account the time-dependent curing, the minimum apparent hyperfine coupling A_{zz}^0 in the pH-dependence can now clearly be ascribed to the pH region 11.80 \pm 0.2 and the ΔA_{zz}^0 also increases to ~ 2.5 G.

The CW EPR spectra strongly suggest that during and after the gelation process the albumin molecules persist in their MG state so that 16-DSA molecules can attach to the exposed hydrophobic

areas of the BSA-MG. This finding is remarkable, as in a 20 wt% protein solution that consequently gels, the system seems dominated by intermolecular contacts and extensive overlap between different albumin molecules. Yet, the presumably delicate MG state that energetically may be seen either as intermediate folding state or being a local energy (enthalpic and entropic) minimal state in these rather harsh conditions ($\text{pH} > 11$), seems robust enough to even persist the regime of strong intermolecular interaction posed by the gel state.

To further substantiate this remarkable EPR-derived conclusion, we expanded our research portfolio. As stated above, in literature there are different ways to verify the MG state in proteins. However, most of them are not applicable in this research work. IR spectroscopy cannot be used, as the pH range needed (above 10) is higher than the allowed pH limit of ATR-IR spectrometers' crystals. Moreover, viscosity measurements and rheological characterizations in general cannot be employed. Here, we are working with very high protein concentration and pH ranges. Accordingly, the gelation is a matter of seconds even at low temperatures (e.g., room temperature). Therefore, with these standard rheological methods it is almost impossible to get meaningful data of the initial stages of the gelation process. Furthermore, the data collected for low concentration media (Figure S4) show no substantial pH-dependent difference between the samples, making it unlikely to detect differences during the gelation process.

We aimed at exploring transmission electron microscopy (TEM) on lower concentration samples at pH 11.8

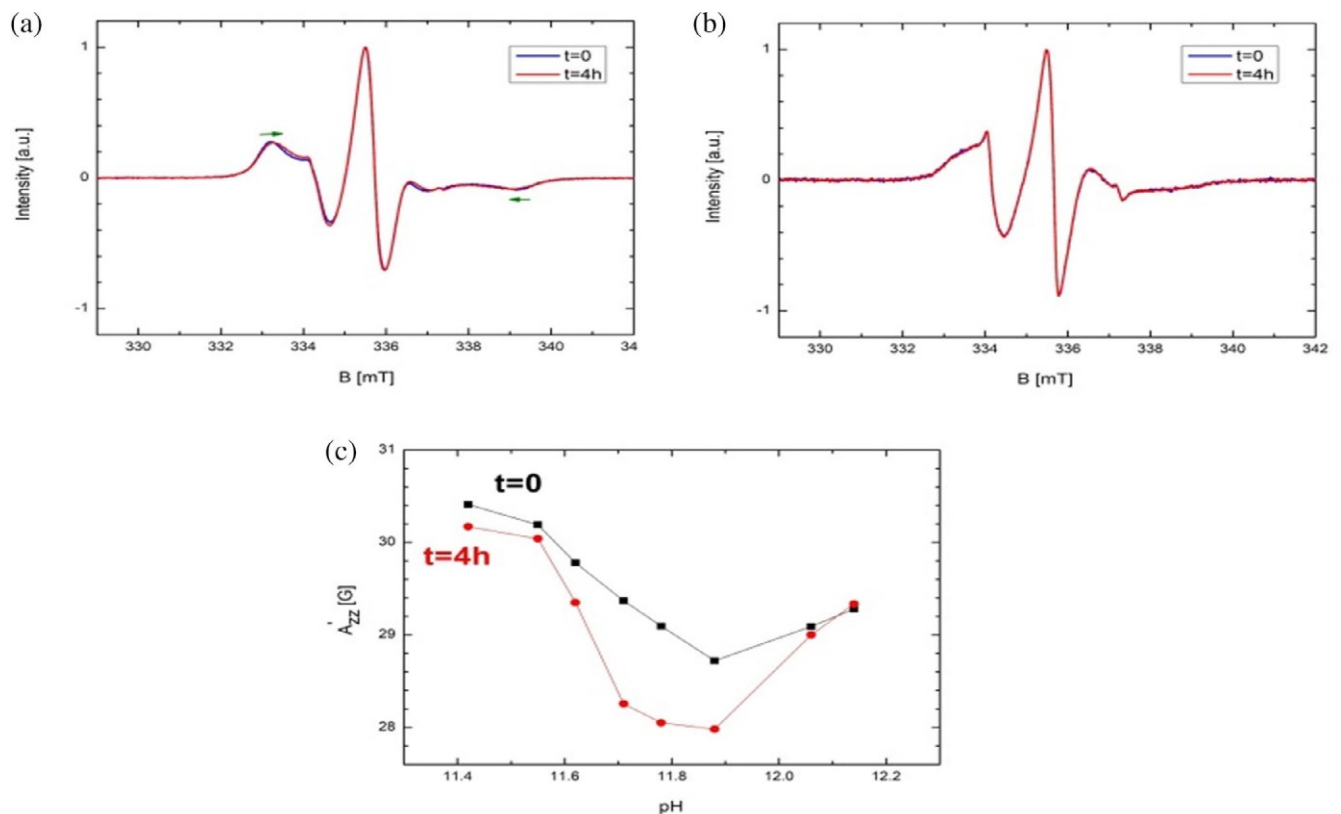


FIGURE 2 (a) EPR spectra of 16-DSA in 20 wt% BSA hydrogel with pH 11.55 at 20C (1:1 ratio of BSA:16-DSA). (b) EPR spectra of 16-DSA in 20 wt% BSA hydrogel with pH 11.5 at 37C (1:1 ratio of BSA:16-DSA). (c) Dependence of A_{zz}^0 on the pH at different times in 20wt% BSA hydrogels in the basic pH range at 20C

but the images are not conclusive and do not give additional information (Figure S3).

It may sound trivial, but one may also emphasize the importance of simple visual inspection of samples. In this case, we observed that the gelation process for all the samples (above a certain albumin concentration and pH value, based on previously reported phase diagram of albumin gelation, see Reference 19) took place in a few minutes. Astonishingly, when leaving the hydrogels (with or without 16-DSA) at RT for several weeks, we observed a seemingly paradoxical behavior of the gels. On the one hand, the hydrogels made in the presence of 16-DSA remained in gel state after at least 3 weeks with one remarkable exception, namely at pH ~11.65. In other words, the gels made at pH values only slightly (~0.2) above or below this value (between pH 11 and 12.2) all remain in a gel state (BSA:16-DSA ratio of 1:1) but the hydrogel made at pH 11.65 which initially and for up to 3 weeks was in the gel state turned into a viscous solution. Figure 3a,b illustrate this phenomenon. In Figure 3b the color change is noticeable. As Hall et al. showed the turbidity of protein solution increases as the aggregate size increases.³⁰ This indicates that there is protein aggregation at pH 11.65 in the solution and the 3D structure lost its water holding capacity and as a result it is not a gel anymore but only a cloudy solution, giving a darker, colloidal-like impression. On the other hand, all the hydrogels made without 16-DSA at all pH values above 11 turn into viscous solutions after several (at least two) weeks, with the exception of the hydrogel made at pH value '11.4 (without 16-DSA, Figure 3c,d, Table S1, and Video S1). Considering the known stabilization against denaturation of BSA due to presence of long-chain fatty acids like 16-DSA (e.g., Reference 19, 23) and comparing the values to the measured minimum of A_{zz}^0 in EPR spectroscopy, we can conclude that BSA molecules in the gel with 16-DSA at pH ~11.65 and in the gel without 16-DSA at pH ~11.4 are in the MG state. This would mean that the MG state does not only survive the gel-formation process and the gel state but it also seems to dominate the properties of the gel compared to non-MG state gels.

The clear deterioration of albumin without FAs in the non-MG state at high pH values, leads us to the conclusion, that the gelation process is likely kinetically controlled and that at the high pH values per se it is a rather thermodynamically unfavorable process. Only in the MG state the deterioration of the gelation network does not proceed.

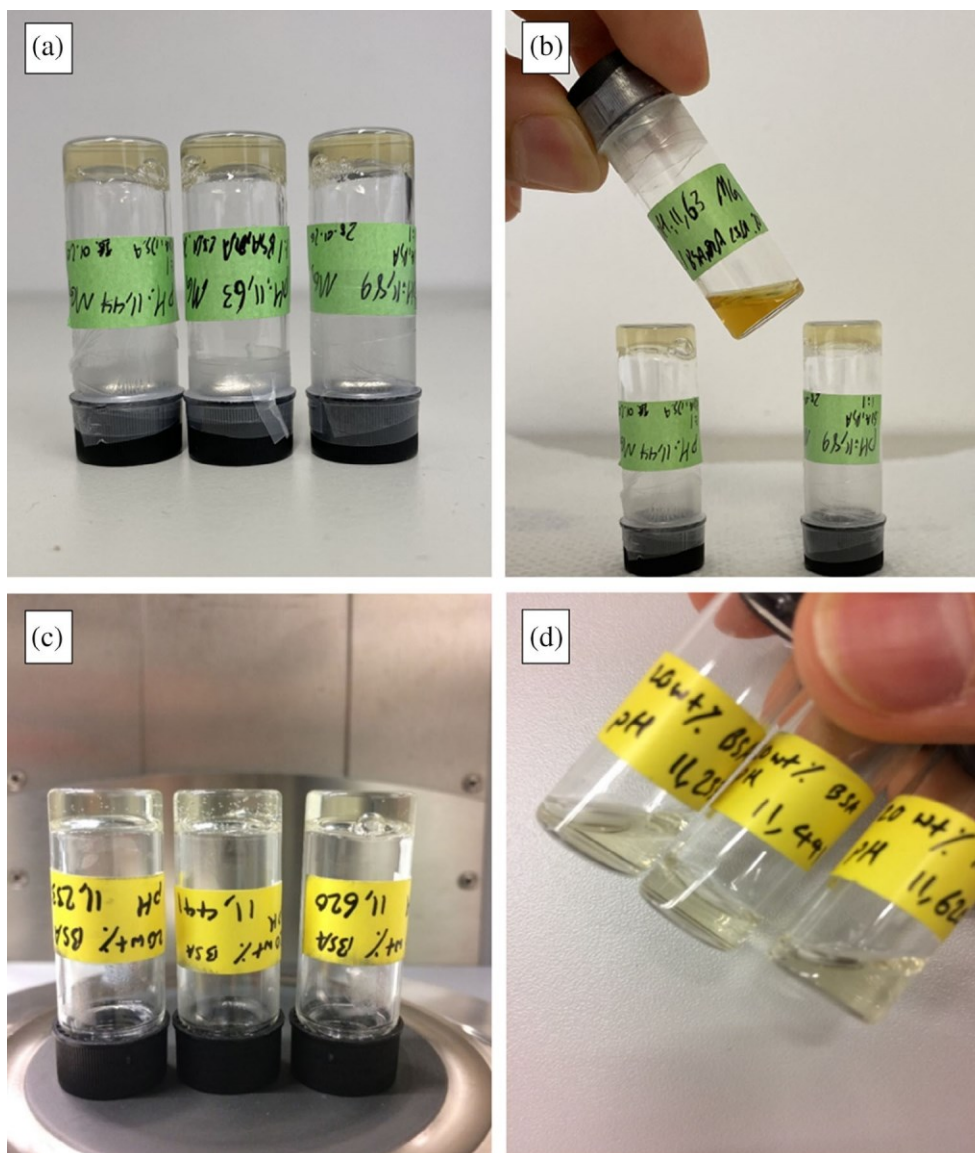


FIGURE 3 (a) 20 wt% BSA hydrogels with fatty acids (16-DSA) at \sim pH 11.233, 11.441, 11.626 at 20C (all the samples in gel state). (b) The same samples after 3 weeks (21 days) kept at RT. Only the sample with the pH value 11.65 turned into a viscous solution and lost its hydrogel 3D structure and water holding capacity, while at the other two pH values the gels remain intact. (c) 20 wt% BSA hydrogels without fatty acids at \sim pH 11.25, 11.45, 11.65 at 20C (all the samples in gel state). (d) The same samples after 3 weeks (21 days) kept at RT. Except for the sample with the pH value 11.45 the other turn into viscous solution and lost their hydrogel 3D structure and water holding capacity

One may interpret this on the molecular level as schematically shown in Figure 4. Serum albumin in the MG state has been shown to expose more hydrophobic areas to the solvent compared to its native state, where most of the hydrophobic areas are hidden inside the heart shaped protein. This may explain why gels made at the pH value where individual albumin molecules occupy the MG state persist in the gel state for weeks, while those at pH values even only slightly higher or lower than the MG pH at \sim 11.4 deteriorate with time (Figure 4c,d). Apparently, the compact MG state (one deals with a known basic contraction in albumins in the aged form above pH \sim 11) forms gels that are structurally stable.

However, when 16-DSA is introduced in the hydrogels, these FAs screen the hydrophobic intermolecular interactions between BSA molecules that is essential for keeping the three-dimensional scaffold of the gels.

In this case, the more exposed hydrophobic patches of BSA in the MG state can readily be targeted as loose attachment sites by amphiphilic 16-DSA molecules, which constitutes more favorable thermodynamic (entropy driven) state. Figure 4a shows that presence of 16-DSA might thus screen the hydrophobic interactions between individual BSA molecules in the MG state gels and destabilize the gel overall. This might explain the color change observable in Figure 3b as protein aggregates in a cloudy, nanocolloidal solution could lead to the observed darkening.

One may further conclude that when BSA is not in the MG state, residual classical binding sites for FAs are again available ($A_{zz}^0 \sim$ is larger again, indicating stronger immobilization) which may again stabilize secondary structure elements and such, indirectly, the gel. Amphiphilic FAs may also form hydrophobic bridges from the

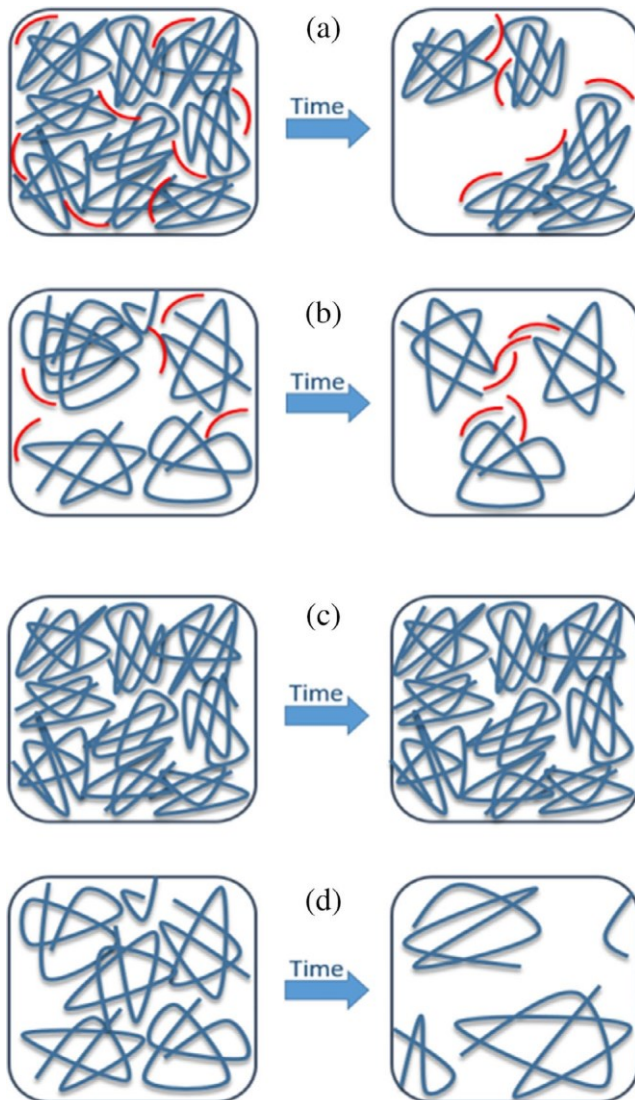


FIGURE 4 (a) Schematic suggested structure of the gels in compact MG state. 16-DSA (shown as red chains, the drawing is not to scale, for the sake of illustration 16-DSA molecules are drawn bigger compared to protein chains shown in blue) screening of the hydrophobic interactions between MG-BSA leads to destabilization of the gels in the MG-state. (b) Suggested structure of the gels, made at pH values where the MG state does not appear. In this state, due to presence of 16-DSA, the hydrogels show very high stability for several weeks. 16-DSA may act acts as secondary structure stabilizer and bridge BSA molecules to keep the 3D structure stable. (c) Suggested structure of the gels in the compact MG state without fatty acids. These gels remain in the stable gelstate for several weeks (thermodynamically stable) as BSA molecules can interact through their hydrophobic patches, which are presented on the outside in the MG state. (d) Suggested structure of the gels without fatty acids, made at pH values where the MG state does not appear. In this case although gels form initially (kinetically controlled), after several weeks the 3D structure of the gels is destroyed and its water holding capacity is compromised, such that a viscous solution ensues (thermodynamically controlled)

less exposed hydrophobic areas between BSA molecules and consequently stabilize these gels as shown in Figure 4b.

The MG state of the individual proteins is a thermodynamically stable (or metastable intermediate) conformational state.^{31,32} Serum albumin in the MG state has been shown to expose more hydrophobic areas to the solvent compared to its native state, where most of the hydrophobic areas are hidden inside the heart shaped protein. This may explain the contradictive behavior of the MG state gels. On the one hand, these exposed hydrophobic areas stabilize the gel for several weeks in contrast to other gels made with only slightly different pH values. On the other hand, they can destabilize the gel when the hydrophobic interaction is hampered and screened due to the presence of hydrophobic fatty acid chains.

As depicted schematically in Figure 4c, the increased long-term stability of MG-state hydrogels may thus on the molecular level be due to increased exposition of hydrophobic patches (as we see it in EPR spectroscopy; Figure 1).

Being compacted, the intermolecular network formation between individual albumins can take place despite the large negative charge that the molecules have at this pH (net charge around -80 , see Reference 23). The hydrophobic contacts persist while the large amounts of water and counterions entropically trapped in the gel lead to partial screening of the surface charges. This gel state is stable for weeks, similar to gels formed, for example, by thermal denaturation at native pH values.³³ Table S1 in the SM shows the concentration dependence of this process. As schematically illustrated in Figure 4d, at the pH-points above or below the MG state, the individual albumin molecules cannot form a stable gel that can persist longer than a few days. This indicates that thermodynamically the entropic trapping of water inside a protein network does not persist and only initially a kinetically trapped gel forms. The gel may break down because the molecules change their conformational states (they are not in the stable MG state), lose their relative compactness and cannot form the network through hydrophobic interactions. Instead, the large negative charge becomes relatively more important and likecharge repulsion leads to looser individual conformations and overall self-assembly.

This peculiar phenomenon cannot be seen in hydrogels synthesized in acidic pH ranges. Apart from the fact that gel formation in acidic ranges takes much longer (several hours compared to a few minutes in basic ranges), these hydrogels are water soluble before the leaching process¹⁹ and after the leaching, despite their enhanced mechanical properties.

3 | CONCLUSIONS

In conclusion, the existence of basic molten globule states for BSA hydrogels (and the non-existence in the acidic range hydrogels) has been shown with the help of CW EPR. This method takes advantage of the fact that there are more exposed hydrophobic patches in the MG state in comparison to the native or unfolded states that can then be detected by CW EPR spectroscopy on amphiphilic fatty acid derivatives (16-DSA). The MG state hydrogel without this fatty acid (pH 11.4) is the maximum stability point for the gel state (Figures 3 and S4) that can even be loaded with and manipulated by codissolved small molecules. Contrarily, the MG state hydrogel with fatty acid features the shortest stability time (at pH 11.6) and the hydrogels turn into viscous solution while the hydrogels made with slightly lower or higher pH values remain in hydrogels stated for several more weeks. The slight difference between these two values (11.4 and 11.6) can be traced back to the presence of 16-DSA in one of them which slightly shifts the pH in which MG state gel forms. These results are robustly confirmed with EPR spectroscopy.

To the best of our knowledge, the presence of the molten globule-state in the high-crowding environment of a hydrogel is proposed in the present research for the first time. Furthermore, we

made the observation (in independent measurements by different experimenters) of enhanced gel stability at the special pH value of the MG-state. These results indicate a new path for experimental studies of MG states in proteins (and their analysis from a “polymer under constraints” point of view) and given the broad spectrum of dynamic protein structures, reaching from globally folded via MG to intrinsically disordered states it may be of interest to test the persistence of many MG state proteins at high crowding conditions. By addition of equimolar amounts of other amphiphilic molecules like long-chain fatty acids, one may even apparently fine-tune of intermolecular interactions and thus the macroscopic gel properties. Even though the pH values needed for BSA MG hydrogels are too high to be of direct practical use, one may envisage new biocompatible materials (probably from proteins in MG states that are induced at less harsh conditions) with unique properties which can have practical use in biomaterials science such as in drug delivery applications and beyond. From a fundamental protein biophysical point of view, it is remarkable that the enigmatic molten globule state can apparently be very robust and not only persist in the high concentration environment of a hydrogel but even dominate the gels nanoscopic and macroscopic properties.

4 | MATERIALS AND METHODS

Our experimental strategy is based on co-dissolution of BSA and hydrophobic 16-DOXYL-stearic acid spin probes (also used before, e.g., in References 19, 23) to achieve a ratio of 1:1 c/c of 16-DSA and BSA. For each experiment, a certain amount of acid (2 M HCl stock solution) or base (2 M NaOH stock solution) was added to a previously prepared solution until the pH set point was reached (Orion Versa Star Pro pH Benchtop Meter). The gelation time was varied from 5 to 45 min in the basic pH range. For gelation in the acidic pH range, more time and higher temperature are required. Therefore, in this case they were first put in the capillaries and then the capillaries were incubated in a water bath at 37C for 20 hr. The prepared capillaries were placed in the resonator cavity of a Magnetech Miniscope MS 400 (Magnetech Berlin, now part of Bruker) benchtop EPR spectrometer (X-band range) and after reaching the desired temperature, the spectra were recorded.

The parameter used for EPR measurements included microwave frequency of approximately $\nu = 9.4$ GHz and a magnetic field sweep of 15 mT centered at 340 mT. Temperatures were adjusted with a Temperature Controller H03 (Magnetech) with an accuracy of 0.2C. The exact frequency was recorded using a frequency counter (Racal Dana 2101, Neu-Isenburg, Germany).

ACKNOWLEDGMENTS

We thank Heike Schimm (MLU) for technical support. This work was supported by the European Regional Development Fund (ERDF) and the Federal State of Saxony-Anhalt.

AUTHOR CONTRIBUTIONS

S. Arabi: Data curation; investigation; methodology; visualization; writing-original draft; writing-review and editing. Behdad Aghelnejad: Data curation; formal analysis; investigation; validation; visualization; writing-original draft; writing-review and editing. Jonas Volmer: Data curation; formal analysis; investigation; validation; writing-original draft. Dariush Hinderberger: Conceptualization; formal analysis; funding acquisition; investigation; methodology; project administration; resources; supervision; visualization; writing-original draft; writing-review and editing.

ORCID

Seyed Hamidreza Arabi  <https://orcid.org/0000-0003-4498-3427>

Dariush Hinderberger  <https://orcid.org/0000-0002-6066-7099>

REFERENCES

1. Carter DC, Ho JX. Structure of serum albumin. *Adv Protein Chem.* 1994;45:153–203.
2. Curry S, Mandelkow H, Brick P, Franks N. Crystal structure of human serum albumin complexed with fatty acid reveals an asymmetric distribution of binding sites. *Nat Struct Biol.* 1998; 5:827–835.
3. Peters T Jr. All about albumin: Biochemistry, genetics, and medical applications. Cambridge, Massachusetts, United States: Academic Press, 1995.
4. Hu YJ, Liu Y, Wang JB, Xiao XH, Qu SS. Study of the interaction between monoammonium glycyrrhizinate and bovine serum albumin. *J Pharm Biomed Anal.* 2004;36:915–919.
5. Junk MJN, Spiess HW, Hinderberger D. DEER in biological multi-spin-systems: A case study on the fatty acid binding to human serum albumin. *J Magn Reson.* 2011;210:210–217.
6. Schweiger A, Jeschke G. Principles of pulse electron paramagnetic resonance. Oxford, UK/New York: Oxford University Press, 2001.
7. Park H, Park K. Biocompatibility issues of implantable drug delivery systems. *Pharm Res.* 1996;13:1770–1776.
8. Buwalda SJ, Vermonden T, Hennink WE. Hydrogels for therapeutic delivery: Current developments and future directions. *Biomacromolecules.* 2017;18:316–330.
9. Vermonden T, Censi R, Hennink WE. Hydrogels for protein delivery. *Chem Rev.* 2012;112:2853–2888.
10. Peppas NA, Khare AR. Preparation, structure and diffusional behavior of hydrogels in controlled release. *Adv Drug Deliv Rev.* 1993;11:1–35.
11. Buwalda SJ, Boere KW, Dijkstra PJ, Feijen J, Vermonden T, Hennink WE. Hydrogels in a historical perspective: From simple networks to smart materials. *J Control Release.* 2014;190: 254–273.
12. Caló E, Khutoryanskiy VV. Biomedical applications of hydrogels: A review of patents and commercial products. *Eur Polymer J.* 2015;65:252–267.
13. Paulsson M, Hegg P-O, Castberg HB. Heat-induced gelation of individual whey proteins: A dynamic rheological study. *J Food Sci.* 1986;51:87–90.
14. Matsudomi N, Rector D, Kinsella JE. Gelation of bovine serum albumin and β -lactoglobulin; effects of pH, salts and thiol reagents. *Food Chem.* 1991;40:55–69.
15. Boye JI, Alli I, Ismail AA. Interactions involved in the gelation of bovine serum albumin. *J Agric Food Chem.* 1996;44:996–1004.
16. Iemma F, Spizzirri UG, Puoci F, et al. pH-sensitive hydrogels based on bovine serum albumin for oral drug delivery. *Intl J Pharm.* 2006;312:151–157.
17. Arabi SH, Haselberger D, Hinderberger D. The effect of ethanol gelation, nanoscopic, and macroscopic properties of serum albumin hydrogels. *Molecules.* 2020;25:1927.
18. Baler K, Michael R, Szeleifer I, Ameer GA. Albumin hydrogels formed by electrostatically triggered self-assembly and their drug delivery capability. *Biomacromolecules.* 2014;15: 3625–3633.
19. Arabi SH, Aghelnejad B, Schwieger C, Meister A, Kerth A, Hinderberger D. Serum albumin hydrogels in broad pH and temperature ranges: Characterization of their self-assembled structures and nanoscopic and macroscopic properties. *Biomater Sci.* 2018;6:478–492.
20. Dolgikh DA, Gilmanshin RI, Brazhnikov EV, et al. Alpha-Lactalbumin: Compact state with fluctuating tertiary structure? *FEBS Lett.* 1981;136:311–315.
21. Muzammil S, Kumar Y, Tayyab S. Molten globule-like state of human serum albumin at low pH. *Eur J Biochem.* 1999;266: 26–32.
22. Kumar Y, Tayyab S, Muzammil S. Molten-globule like partially folded states of human serum albumin induced by fluoro and alkyl alcohols at low pH. *Arch Biochem Biophys.* 2004;426:3–10.
23. Reichenwallner J, Oehmichen M-T, Schmelzer CEH, Hauenschild T, Kerth A, Hinderberger D. Exploring the pH-induced functional phase space of human serum albumin by EPR spectroscopy. *Magnetochemistry.* 2018;4:47.
24. Sen P, Ahmad B, Khan RH. Formation of a molten globule like state in bovine serum albumin at alkaline pH. *Eur Biophys J.* 2008;37:1303–1308.

25. Qu P, Lu H, Yan S, Lu Z. Influences of cationic, anionic, and nonionic surfactants on alkaline-induced intermediate of bovine serum albumin. *Intl J Biol Macromol.* 2010;46:91–99.
26. Qu P, Wang Y, Wu G, Lu Z, Xu M. Effect of polyethylene glycols on the alkaline-induced molten globule intermediate of bovine serum albumin. *Intl J Biol Macromol.* 2012;51:97–104.
27. Barbosa LR, Ortore MG, Spinuzzi F, Mariani P, Bernstorff S, Itri R. The importance of protein-protein interactions on the pH-induced conformational changes of bovine serum albumin: A small-angle X-ray scattering study. *Biophys J.* 2010;98:147–157.
28. Bhattacharya M, Jain N, Bhasne K, Kumari V, Mukhopadhyay S. pH-induced conformational isomerization of bovine serum albumin studied by extrinsic and intrinsic protein fluorescence. *J Fluoresc.* 2011;21:1083–1090.
29. Kurzbach D, Junk MJN, Hinderberger D. Nanoscale inhomogeneities in thermoresponsive polymers. *Macromol Rapid Commun.* 2013;34:119–134.
30. Hall D, Zhao R, Dehlsen I, et al. Protein aggregate turbidity: Simulation of turbidity profiles for mixed-aggregation reactions. *Analyt Biochem.* 2016;498:78–94.
31. Ferrer M, Barany G, Woodward C. Partially folded, molten globule and molten coil states of bovine pancreatic trypsin inhibitor. *Nat Struct Biol.* 1995;2:211–217.
32. Prajapati RS, Indu S, Varadarajan R. Identification and thermodynamic characterization of molten globule states of periplasmic binding proteins. *Biochemistry.* 2007;46:10339–10352.
33. Liu L, Li P, Asher SA. Entropic trapping of macromolecules by mesoscopic periodic voids in a polymer hydrogel. *Nature.* 1999;397:141–144.

SUPPORTING INFORMATION

Additional supporting information may be found online in the Supporting Information section at the end of this article.

How to cite this article: Arabi SH, Aghelnejad B, Volmer J, Hinderberger D. Hydrogels from serum albumin in a molten globule-like state. *Protein Science.* 2020;29:2459–2467. <https://doi.org/10.1002/pro.3976>

8 | References

1. Peppas, N.A., et al., *Hydrogels in Biology and Medicine: From Molecular Principles to Bionanotechnology*. Advanced Materials, 2006. **18**(11): p. 1345-1360.
2. Langer, R. and N.A. Peppas, *Advances in biomaterials, drug delivery, and bionanotechnology*. AIChE Journal, 2003. **49**(12): p. 2990-3006.
3. Vermonden, T., R. Censi, and W.E. Hennink, *Hydrogels for Protein Delivery*. Chemical Reviews, 2012. **112**(5): p. 2853-2888.
4. Peppas, N.A. and A.R. Khare, *Preparation, structure and diffusional behavior of hydrogels in controlled release*. Advanced Drug Delivery Reviews, 1993. **11**(1): p. 1-35.
5. Buwalda, S.J., et al., *Hydrogels in a historical perspective: From simple networks to smart materials*. Journal of Controlled Release, 2014. **190**: p. 254-273.
6. Gaharwar, A.K., N.A. Peppas, and A. Khademhosseini, *Nanocomposite hydrogels for biomedical applications*. Biotechnology and Bioengineering, 2014. **111**(3): p. 441-453.
7. Slaughter, B.V., et al., *Hydrogels in Regenerative Medicine*. Advanced Materials, 2009. **21**(32-33): p. 3307-3329.
8. Park, H. and K. Park, *Biocompatibility Issues of Implantable Drug Delivery Systems*. Pharmaceutical Research, 1996. **13**(12): p. 1770-1776.
9. Buwalda, S.J., T. Vermonden, and W.E. Hennink, *Hydrogels for Therapeutic Delivery: Current Developments and Future Directions*. Biomacromolecules, 2017. **18**(2): p. 316-330.
10. Peters Jr, T., *All about albumin: biochemistry, genetics, and medical applications*. 1995: Academic press.
11. Gianazza, E., M. Galliano, and I. Miller, *Structural transitions of human serum albumin: An investigation using electrophoretic techniques*. ELECTROPHORESIS, 1997. **18**(5): p. 695-700.
12. Ferrer, M.L., et al., *The Conformation of Serum Albumin in Solution: A Combined Phosphorescence Depolarization-Hydrodynamic Modeling Study*. Biophysical Journal, 2001. **80**(5): p. 2422-2430.
13. Hamilton, J.A., et al., *Interactions of myristic acid with bovine serum albumin: a ¹³C NMR study*. Proceedings of the National Academy of Sciences, 1984. **81**(12): p. 3718-3722.
14. Junk, M.J.N., H.W. Spiess, and D. Hinderberger, *The Distribution of Fatty Acids Reveals the Functional Structure of Human Serum Albumin*. Angewandte Chemie International Edition, 2010. **49**(46): p. 8755-8759.
15. Guizado, T.R.C., *Analysis of the structure and dynamics of human serum albumin*. Journal of Molecular Modeling, 2014. **20**(10): p. 2450.
16. Divsalar, A., et al., *Biological evaluation and interaction of a newly designed anti-cancer Pd(II) complex and human serum albumin*. Journal of biomolecular structure & dynamics, 2011. **29**(2): p. 283-96.
17. Reichenwallner, J. and D. Hinderberger, *Using bound fatty acids to disclose the functional structure of serum albumin*. Biochimica et Biophysica Acta (BBA) - General Subjects, 2013. **1830**(12): p. 5382-5393.
18. Akdogan, Y., J. Reichenwallner, and D. Hinderberger, *Evidence for Water-Tuned Structural Differences in Proteins: An Approach Emphasizing Variations in Local Hydrophilicity*. PLOS ONE, 2012. **7**(9): p. e45681.
19. Iemma, F., et al., *Radical Cross-Linked Albumin Microspheres as Potential Drug Delivery Systems: Preparation and In Vitro Studies*. Drug Delivery, 2005. **12**(4): p. 229-234.
20. Clark, A.H., G.M. Kavanagh, and S.B. Ross-Murphy, *Globular protein gelation—theory and experiment*. Food Hydrocolloids, 2001. **15**(4): p. 383-400.

21. Boresi, A.P. and R.J. Schmidt, *Advanced mechanics of materials*. 2003, New York: John Wiley & Sons.
22. Ward, I.M. and J. Sweeney, *Mechanical properties of solid polymers*. 2012: John Wiley & Sons.
23. Miller, F.P., A.F. Vandome, and M.B. John, *Hooke's Law*. 2010: VDM Publishing.
24. Rouxel, T., G.D. Soraru, and J. Vicens, *Creep viscosity and stress relaxation of gel-derived silicon oxycarbide glasses*. *Journal of the American Ceramic Society*, 2001. **84**(5): p. 1052-1058.
25. López-Guerra, E.A. and S.D. Solares, *Modeling viscoelasticity through spring-dashpot models in intermittent-contact atomic force microscopy*. *Beilstein J Nanotechnol*, 2014. **5**: p. 2149-63.
26. Pearson, K., *LIII. On lines and planes of closest fit to systems of points in space*. *The London, Edinburgh, and Dublin Philosophical Magazine and Journal of Science*, 1901. **2**(11): p. 559-572.
27. Hotelling, H., *Analysis of a complex of statistical variables into principal components*. *Journal of Educational Psychology*, 1933. **24**(6): p. 417-441.
28. Pedersen, M., *Functional analysis in applied mathematics and engineering*. 2018: CRC press.
29. Jolliffe, I.T. and J. Cadima, *Principal component analysis: a review and recent developments*. *Philosophical Transactions of the Royal Society A: Mathematical, Physical and Engineering Sciences*, 2016. **374**(2065): p. 20150202.
30. Deisenroth, M.P., A.A. Faisal, and C.S. Ong, *Mathematics for machine learning*. 2020: Cambridge University Press.
31. Abdi, H. and L.J. Williams, *Principal component analysis*. *WIREs Computational Statistics*, 2010. **2**(4): p. 433-459.
32. Geladi, P. and J. Linderholm, *Principal Component Analysis* ☆, in *Reference Module in Chemistry, Molecular Sciences and Chemical Engineering*. 2020, Elsevier.
33. Page, L., et al., *The PageRank citation ranking: Bringing order to the web*. 1999, Stanford InfoLab.
34. Schweiger, A. and G. Jeschke, *Principles of pulse electron paramagnetic resonance*. 2001: Oxford University Press on Demand.
35. Zavoisky, E., *Spin-magnetic resonance in paramagnetics*. *J Phys Ussr*, 1945. **9**: p. 211-245.
36. Moskowitz, B.M., *Fundamental physical constants and conversion factors*. *A Handbook of Physical constants*, 1995. **1**: p. 346-355.
37. Hunger, M. and J. Weitkamp, *In situ IR, NMR, EPR, and UV/Vis spectroscopy: Tools for new insight into the mechanisms of heterogeneous catalysis*. *Angewandte Chemie International Edition*, 2001. **40**(16): p. 2954-2971.
38. Sojka, Z. and M. Che, *EPR techniques applied to the study of chemistry and catalysis on oxide surfaces*. *Applied Magnetic Resonance*, 2001. **20**(3): p. 433-456.
39. Sahu, I.D. and G.A. Lorigan, *Site-directed spin labeling EPR for studying membrane proteins*. *BioMed research international*, 2018. **2018**.
40. Neese, F., *Quantum chemical approaches to spin-Hamiltonian parameters*. *Electron Paramagnetic Resonance*, 2007. **20**: p. 73-95.

9 | Eidesstattliche Erklärung

Ich erkläre hiermit an Eides statt, dass ich die vorliegende Arbeit selbständig und ohne fremde Hilfe verfasst, keine anderen als die von mir angegebenen Quellen und Hilfsmittel benutzt und die den benutzten Werken wörtlich und inhaltlich entnommenen Stellen als solche kenntlich gemacht habe. Weiterhin versichere ich, dass die vorliegende Arbeit keiner anderen Universität oder Hochschule vorgelegt wurde und ich mich zu keinem früheren Zeitpunkt um den Doktorgrad beworben habe.

Seyed Hamidreza Arabi, September 2023

SEYED HAMIDREZA ARABI

RESEARCH SCIENTIST

PERSONAL PROFILE

I am a research scientist in physical chemistry with professional knowledge of software development. I am also experienced in supervising and coordinating interdisciplinary projects.

EDUCATIONAL HISTORY

B.Sc. BioInformatik

Martin-Luther-University Halle-Wittenberg
September 2018 - present

- Overall GPA: 1.7

Ph.D. Physical Chemistry

Martin-Luther-University Halle-Wittenberg
January 2017 – Present

- Nanoscopic characterization of protein gels, in particular albumin-based Involved for Smart Drug Delivery Systems
- Dissertation Submitted

M.Sc. Polymer Materials Science

Martin-Luther-University Halle-Wittenberg
September 2014 – October 2016

- Overall GPA: 1.1
- MSc Thesis: 1.0

B.Sc. Chemical Engineering

Isfahan University of Technology
September 2008 – September 2013

- BSc Thesis: 16.5/20

WORK EXPERIENCE

Software Developer (Node.js)

Medizinische Fakultät der Martin-Luther-Universität
Halle, Germany | May 2020 – present

COMPUTER SKILLS

•••• JavaScript / TypeScript

•••• Node.js / Express.js

•••• React / Next.js

•••• SQL / PostgreSQL

•••• NoSQL / MongoDB / Mongoose

•••• Linux / Bash Script

•••• Docker

LANGUAGES

German: Fluent
(TestDaF: 19/20: C1.2)

English: Fluent
(TOEFL IBT: 90)

Persian: Native

LANGUAGES

German: Fluent
(TestDaF: 19/20: C1.2)

English: Fluent
(TOEFL IBT: 90)

Persian: Native

HOBBIES



Tennis



Hiking



Traveling



Swimming

WORK EXPERIENCE

Software Developer (Node.js)

Medizinische Fakultät der Martin-Luther-Universität
Halle, Germany | May 2020 – present

Full-Stack Web developer (Node.js)

DFG Research Training Group (RTG 2670, BEAM)
Halle, Germany | October 2020 – April 2021

- Web Application Developer (From Design to Deployment)
- [HTTPS://BEAM.UNI-HALLE.DE](https://beam.uni-halle.de)

Supervisor of Physical Chemistry Practicum

Martin Luther University of Halle-Wittenberg
Halle, Germany | April 2018 – April 2021

- For Master Students in Chemistry
- Fließkurven - Rotations-/Oszillations-Rheologie

Supervisor of Bachelor and Master Theses

Martin Luther University of Halle-Wittenberg
Halle, Germany | October 2018 – October 2021

- One Master Thesis in Polymer Materials Science
- Two Bachelor Thesis in Chemistry

Teacher Assistant in Physical Chemistry Module

Martin Luther University of Halle-Wittenberg
Halle, Germany | April 2017 – september 2018

- For Master Students in Polymer Materials Science

PUBLICATIONS (FIRST AUTHOR)

Biomaterials Science

Serum Albumin Hydrogels in Broad pH and Temperature Ranges: Characterization of Their Self-Assembled Structures, Nanoscopic and Macroscopic Properties

- <http://dx.doi.org/10.1039/C7BM00820A> | (2018)

MDPI Molecules

The Effect of Ethanol on Gelation, Nanoscopic and Macroscopic Properties of Serum Albumin Hydrogels

- <https://doi.org/10.3390/molecules25081927> | (2020)

Protein Science

Hydrogels from serum albumin in a molten globule-like state

- <https://doi.org/10.1002/pro.3976> | (2020)